TECHNISCHE UNIVERSITÄT MÜNCHEN

Physik-Department

Lehrstuhl für Funktionelle Materialien

Structure and transition behavior of novel thermo-responsive polymer films

Qi Zhong

Vollstädiger Abdruck der von der Fakultät für Physik der Technischen Universität München zur Erlangung des akademischen Grades eines

Doktors der Naturwissenschaften (Dr. rer. nat.)

genehmigten Dissertation.

Vorsitzender: Univ.-Prof. Dr. Martin Zacharias

Prüfer der Dissertation:

1. Univ.-Prof. Dr. Peter Müller-Buschbaum
2. Univ.-Prof. Dr. Christian Pfleiderer

Die Dissertation wurde am 20.11.2012 bei der Technischen Universität München eingereicht und durch die Fakultät für Physik am 10.12.2012 angenommen.

Abstract

In this thesis, thermo-responsive polymer films, consisting of poly(methoxydiethylenglycol acrylate) (PMDEGA) and poly(styrene-block-monomethoxydiethylenglycol-acrylate-block-styrene) (P(S-*b*-MDEGA-*b*-S)), are investigated. The focus is on the structure and the corresponding transition behavior. As probed with imaging and scattering techniques, although the films show homogeneous and smooth surfaces, they possess porous structure inside the films. Compared to the well studied poly(N-isopropylacrylamide) (PNIPAM) films, thin PMDEGA films show a higher lower critical solution temperature (LCST) and a broader transition region. The introduction of hydrophobic PS blocks shifts the LCST of thin P(S-*b*-MDEGA-*b*-S) films to a lower value, whereas the transition region is still broad. Under a sudden thermal stimulus the PMDEGA based thermo-responsive films react with a complex response, which is understood as shrinkage, reorganization and reswelling.

In dieser Arbeit werden thermoresponsive Polymerfilme, die aus Poly(Methoxydiethylen glycolacrylat) (PMDEGA) und Poly(styrol-block-monomethoxydiethylenglycolacrylat-block-styrol) (P(S-*b*-MDEGA-*b*-S)) bestehen, untersucht. Der Fokus liegt dabei auf ihrer Struktur und dem dazugehörigen Übergangsverhalten. Obwohl die Filme in abbildenden und Streutechniken homogene und glatte Oberflächen zeigen, besitzen sie eine poröse innere Struktur. Im Vergleich zu den ausgiebig untersuchten Filmen aus Poly(N-Isopropyl acrylamid) (PNIPAM), zeigen dünne PMDEGA Filme eine höhere untere kritische Entmischungstemperatur (LCST) und einen breiteren Übergangsbereich. Die Einführung hydrophober PS-Blöcke verschiebt die LCST dünner P(S-b-MDEGA-b-S) Filme zu niedrigeren Werten, während der Übergangsbereich unverändert breit bleibt. Das Antwortverhalten des Films auf eine plötzliche thermische Anregung ist komplex und wird auf Schrumpfen, Reorganisation und Wiederanschwellen zurückgeführt.

Contents

Chapter 1

Introduction

Among the wide categories of synthetic and natrual polymers, a special class of polymers possessing stimulus-responsive properties have attracted tremendous attention. Stimulus-responsive polymers show relatively abrupt, physical or chemical changes to a weak external stimulus such as temperature [1, 2], light [3, 4], or pH value [5, 6]. Due to this special property, there is a broad field of potential applications arising for these polymers [7, 8, 9, 10, 11, 12]. As the variation of temperature is easy to realize, the thermo-responsive polymers are of special interest among these stimulus-responsive polymers [13, 14, 15, 16, 17, 18, 19, 20, 21]. With a thermal stimulus, they can switch between an extended and a collapsed chain conformation. Thus the sample volume expereinces a strong change, accompaning with release of water [22]. Such a transition of polymers with a lower critical solution temperature (LCST) behavior is used in a large variety of applications. For instance, micro- and nanocontainers prepared by polymers with the LCST behavior can be used for delivery and release of active materials [23, 24]. By coating them on the surface, it is even possible to control the attachement or detachment of a sepcific cell in biotechnology [25, 26].

Among these thermo-responsive polymers, poly(N-isopropylacrylamide) (PNIPAM) is well known for its thermo-responsive behavior with a LCST at 32 °C in aqueous solution [2, 27, 28, 29, 30, 31, 32, 33, 34, 35, 36, 37]. When the temperature is below the LCST, the amide and ether groups of PNIPAM are generally considered to form hydrogen bonds with water. Due to this bound water, the volume of the polymers dramatically increases compared to the dry ones. When the temperature is raised to the LCST, new hydrogen bonds form between the amide and ether groups. Thus the former bound water is repelled from the film. The dehydration results in an abrupt phase transition from the swollen state to a collapsed state and induces the volume to shrink [38]. However, the LCST of

PNIPAM based thermo-responsive polymers is rather low, e.g. when comparing to human body temperature. Also for instance in some tropical countries, ambient temperature can easily reach the LCST of PNIPAM, thus confining the polymers to its collapsed state. For this reason, the switchable function of PNIPAM cannot be utilized. Hence, novel thermo-responsive polymers have been developed, such as poly(methoxydiethyleneglycol acrylate) (PMDEGA), ,which shows a LCST at about 39 °C, ensuring a broader application region. Moreover, by modification of both ends of a hydrophilic PMDEGA block with hydrophobic polystyrene (PS) blocks, an amphiphilic block copolymer P(S-*b*-MDEGA-*b*-S) is obtained. According to the chemical structure of P(S-*b*-MDEGA-*b*-S), it shows the ability to form self-assmbled micellar structure in solution. In addition, the introduction of the hydrophobic groups also influences the transition behavior of the PMDEGA based thermo-responsive polymers.

Until now, most of the work is focused on the bulk or the aqueous solution of thermo-responsive polymers [13, 39, 40, 41, 42] and thin films are only rarely investigated [43, 44, 45, 46]. However, instead of changing the volume in three dimensions (bulk or solution), thin films on a solid substrate can only change in one confined dimension, e.g. only the film thickness. Such change in film thicknesses is interesting for applications such as nano-switches or nano-sensors films [45].

Although thermo-responsive polymers are thoroughly investigated, many details about the swelling and the transition of thermo-responsive films in water vapor atmosphere are still not understood. Knowledge about the influence of the morphology - such as surface and internal structure - on the transition behavior are desired. Therefore, in this thesis, PMDEGA based thermo-responsive thin films are investigated. By spin-coating and solution casting, films in the nanometer range and films in the micrometer range are obtained, respectively. The morphology of these films is probed with imaging and scattering techniques (see figure 1.1). In particular, the following questions are addressed in this thesis: What is the surface and internal structures of such thin films? Is it possible to transfer micellar structure into thick films? How does the internal structure influence the swelling and the transition behavior? What is the role of the introduced hydrophobic groups in the swelling and the transition process? How does bound water change in the transition process?

As seen in figure 1.1, the thermo-responsive polymers PMDEGA and P(S-*b*-MDEGA-*b*-S) are firstly prepared as thin films (chapter 4 and chapter 5, respectively). The surface structure is investigated by optical microscopy and atmoic force microscopy. The vertical structure is meausred by grazing incidence small-angle X-ray scattering (GISAXS). The

swelling and transition behavior of the thermo-responsive films in the vapor atmosphere is probed with white light interferometry. In-situ neutron reflectivity measurements are performed to investigate the swelling behavior of thin films in D_2O vapor atmosphere and the responsive behavior of swollen films to an abrupt thermal stimulus. The variation of bound water in films with different thermal stimuli is measured by ATR-FTIR. Moreover, P(S-*b*-MDEGA-*b*-S) is also used to prepare thick films from different selective solvents (chapter 6). The related various internal structures are probed with SAXS measurements.

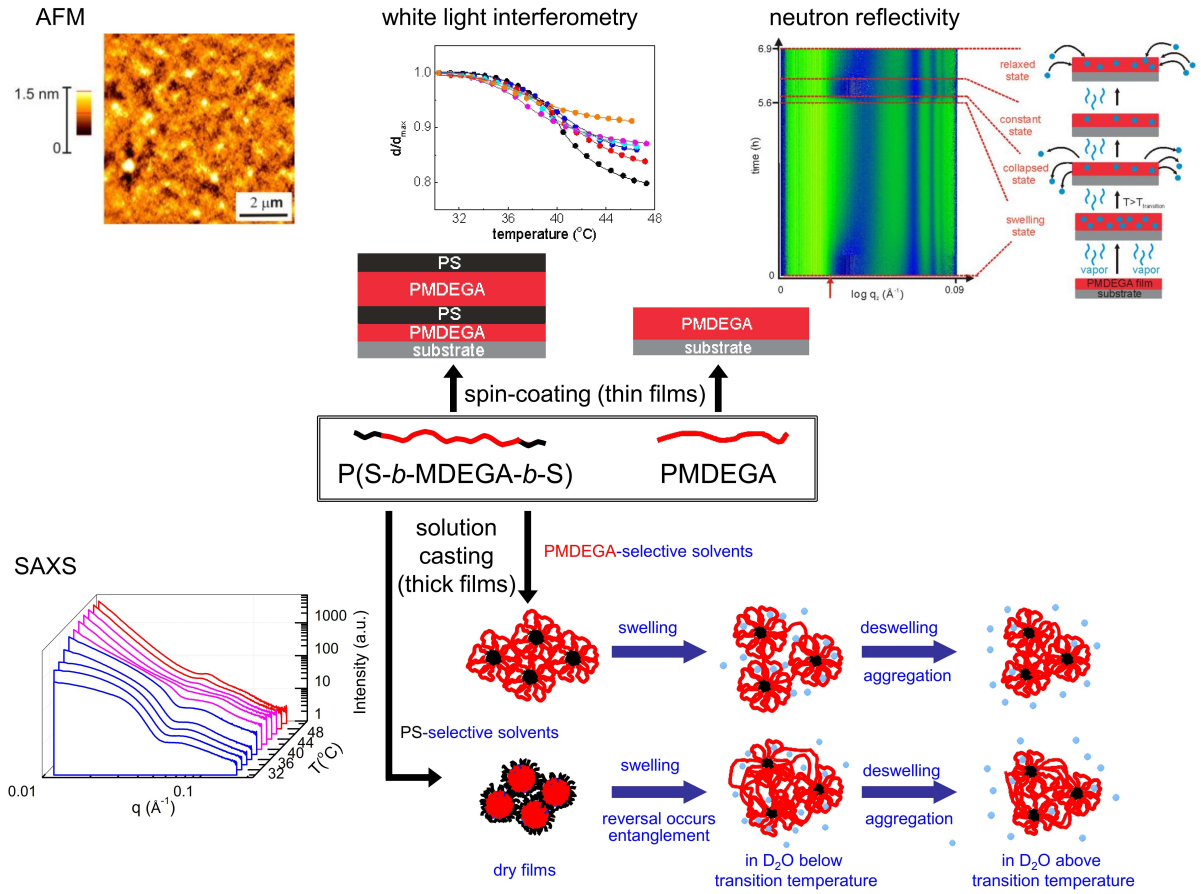

Figure 1.1: *Schematic illustration of the films prepared from PMDEGA based thermo-responsive hydrogels and the used characterization methods to investigate the morphology and transition behaviors of these films.*

To provide a background, the next chapter covers a short introduction to the theories related to block copolymers, phase separation and thermo-responsive polymers. The fundamentals of scattering methods applied in this thesis are also introduced. Afterwards, the sample preparation and the applied measurement methods are presented in chapter 3. In the mainpart of this thesis, the experimental results of thin PMDEGA films (chapter 4),

thin P(S-*b*-MDEGA-*b*-S) films (chapter 5) and thick P(S-*b*-MDEGA-*b*-S) films (chapter 6) are presented. Finally, a conclusion and outlook is given to complete this thesis (chapter 7).

Chapter 2

Theoretical background

2.1 Homopolymers and block copolymers

A homopolymer is a polymer consisting only one type of repeating units throughout the whole backbone without any branches [47]. Due to the different available monomers, molecular weight and weight distribution, homopolymers are formed in a large variety of plastic products and are widely used in our daily life. In order to extend the accessible polymers, different types of monomers are introduced into the backbone. These polymers containing different repeating units are called copolymers. According to the number of monomers introduced, as well as their ratio and position in the backbone, the copolymers can be devided as: (a) random copolymers, which consist of different repeating units with an arbitrary heterosequence, (b) alternating copolymers, in which the repeating units strictly alternate with each other, (c) graft copolymers, in which the backbone is composed of one kind of repeating units, whereas the side chains are formed by different repeating units, (d) block copolymers, in which two or more segments of pure repeating units are present (figure 2.1). Among these copolymers, block copolymers, especially the amphiphilic block copolymers, are of great interest due to their applications in separations [48], surface modifiers [49] and cosmetic products [50]. In this section, microphase separation of block copolymer is firstly introduced. Afterwards, the behavior of block copolymers in solution and on surfaces are discussed separately.

2.1.1 Microphase separation

Amphiphilic block copolymers are composed of at least two types of incompatible polymer blocks, which are covalently linked together. Generally, one block consisting of polar

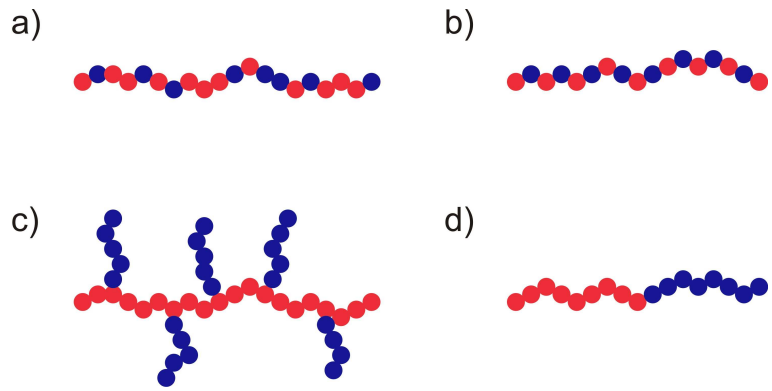

Figure 2.1: *Sketch of copolymers with different architectures: a) random copolymer, (b) alternating copolymer, (c) graft copolymer, (d) block copolymer.*

monomers is soluble in water, and named hydrophilic block. On the contrary, another block consisting of nonpolar monomers is insoluble in water, and named hydrophobic block. The amphiphilic block copolymers can be a diblock copolymer (AB) [51], triblock copolymer (ABA or ABC) [52], or even have a more complex structure such as ABCD or ABCA. Because the incompatible blocks are connected by covalent bonds, they can not separate into distinct macroscopic phases. Instead, they segregate into microdomains, which is called microphase separation, resulting in ordered structures with different morphologies (figure 2.2) [53].

The formation of these different morphologies is driven by an unfavorable mixing enthalpy coupled with a small mixing entropy. The microphase separation depends on three parameters [54]. The first one is the volume fraction of the blocks f. Considering a diblock copolymer AB, as there is only A and B components, $f_A + f_B = 1$. The second parameter is the total degree of polymerization N, where $N = N_A + N_B$. The third one is the Flory-Huggins interaction parameter χ_{AB}. It represents the degree of incompatiblility between A and B blocks, which is the driving force of phase separation. χ_{AB} is given by equation 2.1 [54, 55]:

$$\chi_{AB} = \frac{z}{k_B T}\left[\epsilon_{AB} - \frac{1}{2}(\epsilon_{AA} + \epsilon_{BB})\right]. \tag{2.1}$$

In equation 2.1, z is the number of nearest neighbours per repeating unit in the polymer. k_B is the Boltzmann constant, $k_B T$ is the thermal energy. ϵ_{AA}, ϵ_{BB} and ϵ_{AB} are the interaction energies per repeating unit of A-A, B-B and A-B, respectively [56]. Thus formation and stability of the ordered structure depends on the value of χN.

From figure 2.2, it is clear that the value of χN not only determines the formation of segregation, but also influences the degree of the segregation (sharpness of interface

between neighboring blocks). When χN is less than 10, the block copolymer exhibits only one phase. When χN is increased between 10 and 60, segregation can take place. Thus the interfaces between the neighboring blocks emerge (see the right side of figure 2.2). However, due to the weak segregation, there is still diffusion between the neighboring blocks, causing the interfaces to be broad. When χN is larger than 60, the segregation between the blocks is so strong that the sharp interfaces are observed. The pure subphases periodically repeat in space.

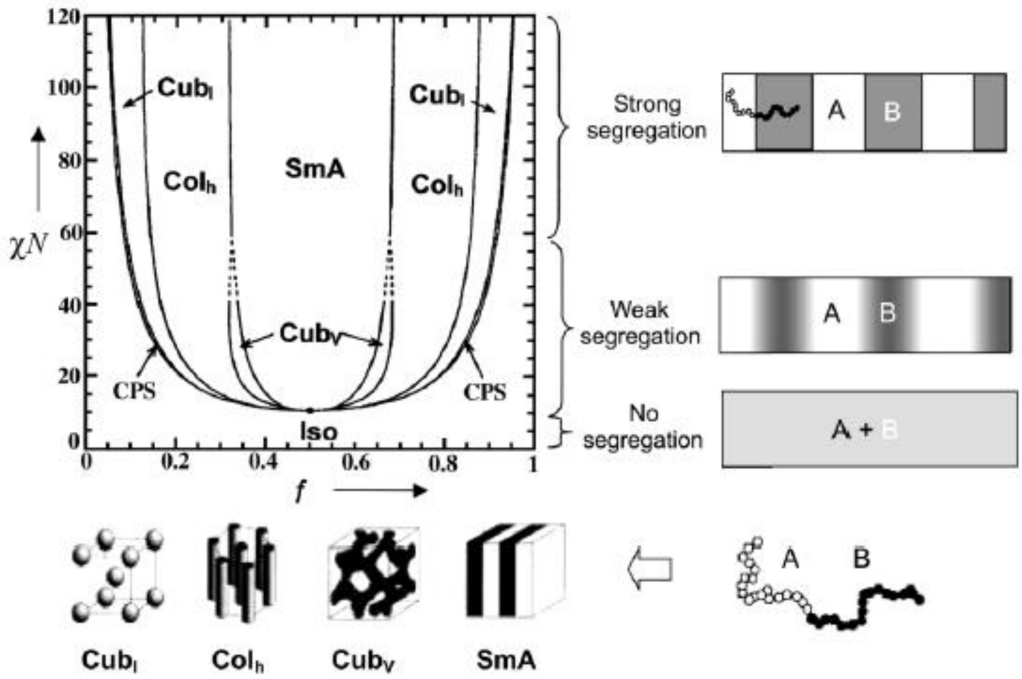

Figure 2.2: *Phase diagram of symmetric AB diblock copolymer. Cub_I denotes the arrangement of spherodic aggregates in a cubic lattice. CoI_h denotes the arrangement of columnar aggregates in a hexagonal 2D lattice. Cub_v denotes the interwoven network structure with cubic symmetry. SmA denotes the arrangement of alternating layers. CPS denotes the disordered arrangement of spheroidic aggregates. The structure of the mesophases are presented below the phase diagram. On the right side of the phase diagram, the strong-, weak-, and non-segregation of the intermaterial regime are exhibited by the sharpness of the interface. Images are taken from reference [57].*

In the discussion above, it is obvious that the value of χN can determine formation and degree of the subphase separation. If the value of χN is fixed, by changing the volume fraction of the blocks in the copolymer (f), the morphology of the subphase can be varied. For instance, in figure 2.2, when χN=40 and f=0.4, the ordered structure obtained is

lamellar (SmA). When f increases, the morphology switches to bicontinuous networks with a cubic symmetry (Cub_v), a hexagonal arrangement of infinite columns (CoI_h), the spheroidic aggregates organized in a cubic lattice (Cub_I) and a disordered arrangement of spheroids (I_{SO}) [57].

2.1.2 Block copolymers in solution

When solvent is introduced into amphiphilic block copolymers, the complexity of self-assembly in solution dramatically increases comparing to the self-assembly in bulk. For instance, when a diblock copolymer (AB) is placed into a solvent (S) - nonsolvent (N) mixture, there are 6 χ-parameters existing in the system (χ_{AB}, χ_{AS}, χ_{AN}, χ_{BS}, χ_{BN} and χ_{SN}) instead of one χ-parameter in bulk. Further increasing the components in solution induces more complexity in the self-assembly process.

The morphology of the amphiphilic block copolymers in solution can be influenced by several factors.

The first factor is the composition of copolymer. Similar to the copolymer in bulk, varying the composition (volume fraction of the blocks) affects the self-assembly in solution. For example, in the case of PS-*b*-PAA copolymer, when the PAA molar percentage decreases from 10.1 to 2.0 in DMF-water solution, the morphology changes from spheres, rods, vesicles to large compound micelles [56].

The second factor is the concentration of copolymer in solution. For instance, the morphology of copolymer PS_{190}-*b*-PAA_{20} in DMF-water solution varies from spheres to rods and vesicles, when the concentration increases from 1 to 3.5 wt% [58].

The third factor is the properties of solvents. As the solvent directly influences the dimension of the hydrophobic and hydrophilic domains in solution, the properties of the solvents play a important role in the formation of the morphology. For example, PS_{200}-*b*-PAA_{18} forms spheres in DMF-water solution. However, the morphology switches to large compound micelles in THF-water solution [59].

The fourth factor is the water content in solution. It is observed that when water is added into the copolymer solution, the copolymer always forms a spherical morphology first. This behavior is independent on the solvents used to prepare the solution. Then with the increase of the water content, the morphology varies from spheres to rods and vesicles [60, 61]. Besides these main factors mentioned above, temperature, polydispersities of copolymers and surfactants influence the morphology as well [62].

Figure 2.3 exhibits the transmission electron microscopy (TEM) micrographs and cor-

responding sketches of diverse morphologies formed from the amphiphilic block copolymers PS-*b*-PAA [63, 64]. In these graphs, the hydrophobic PS part is red, and the hydrophilic PAA part is blue. It is obvious that the amphiphilic block copolymer is able to form spherical micelles (figure 2.3a), rods (figure 2.3b), bicontinuous rods (figure 2.3c), small lamellae layers (figure 2.3d), large lamellae layers (figure 2.3e), vesicles (figure 2.3f), hexagonally packed hollow hoop (figure 2.3g) and large compound micelles (figure 2.3h).

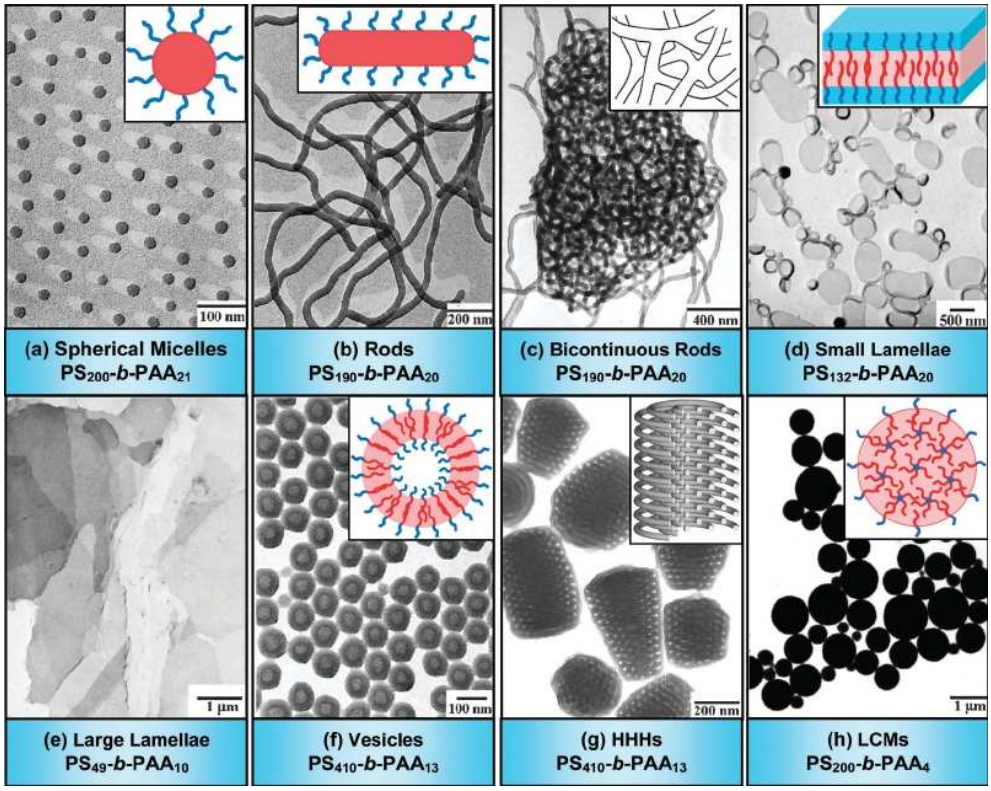

Figure 2.3: *Transmission electron microscopy (TEM) micrographs and corresponding sketches of diverse morphologies formed from the amphiphilic block copolymers PS-b-PAA. Images are taken from reference [64].*

2.1.3 Block copolymers on surface

In section 2.1.1, it is found that the bulk phase behavior of amphiphilic block copolymers (AB) depends on two factors. The first one is the interfacial tension between the two A- and B-rich microdomains. The second one is the entropic stretching energies of the two blocks [65]. The competition between these two factors determines the domain size. Additionally, the stretching energies of A and B blocks form a spontaneous curvature in

the interfaces. When the content of one component decreases, meaning A and B blocks become asymmetric, the morphology varies from lamellae, cylinders, to spheres [66].

When amphiphilic block copolymers are put onto a solid substrate, new parameters such as film thickness [67, 68] and interaction with the substrate are involved [69, 70, 71]. To address on the two new parameters mentioned above, the amphiphilic diblock copolymer AB with the same content is selected for discussion in this section. The morphology obatined from the copolymer is assumed to be lamellae.

When the amount of the amphiphilic diblock copolymer used for the sample preparation is small, the film obtained is ultrathin, meaning that the thickness (D) is even less than the lamellar period (L_0). As a consequence, only the vertical lamellar structure is predicted [72] and observed [67] (see figure 2.4a). Under this condition, the interaction with the substrate is not the dominant factor.

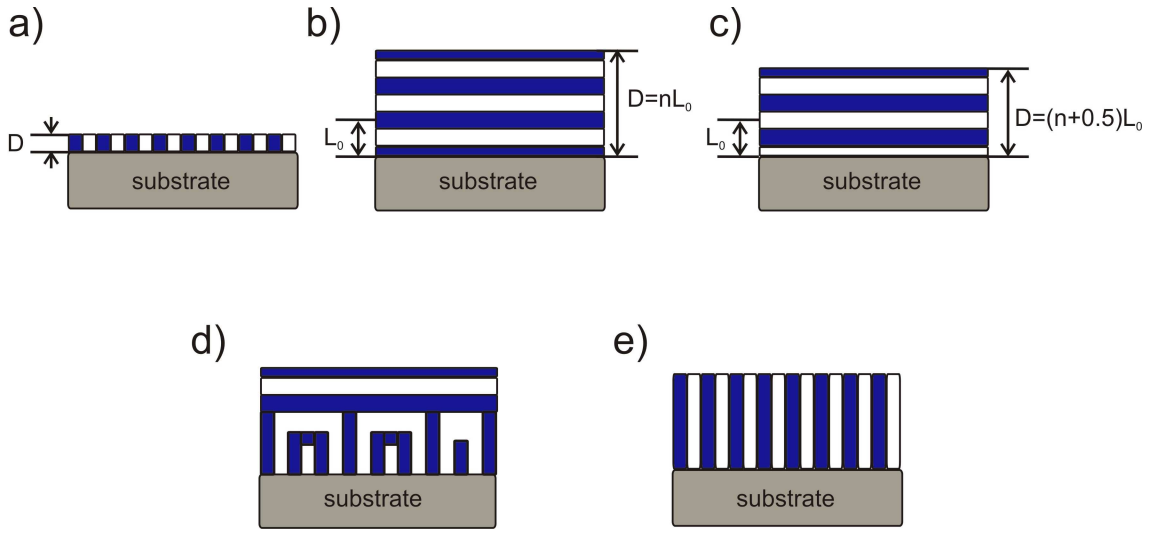

Figure 2.4: *Sketch of amphiphilic block copolymer films on a soild substrate with lamellar structure in different conditions. (a) ultrathin film with thickness D less than the lamellar period L_0, (b) thin film with a symmetric boundary condition, (c) thin film with an asymmetric boundary condition, (d) thin film with one nonpreferential and one preferential interface condition, (e) thin film with the nonpreferential condition.*

When the film thickness D is much larger than L_0, the interaction with the substrate becomes the dominant factor [73, 74]. For instance, when a symmetric PS-*b*-PMMA film is placed on a solid substrate which contains random copolymer brushes rich in PS, the PS blocks segregate to the film/substrate interface. Because the surface energy of PS is lower than PMMA, PS blocks also segregate to the film/air interface. Therefore, it

results in a horizontal lamellar structure with symmetric wetting (figure 2.4b) [71, 75, 76]. On the contrary, if the substrate is modified by random copolymer brushes rich in PMMA, then segregation of PMMA on the film/substrate interfaces takes place. It still forms the horizontal lamellar structure, but with asymmetric wetting (figure 2.4c). Further modifying the substrate with random copolymer to a condition that the interfacial interaction is balanced, meaning the substrate exhibits no preferential to either PS or PMMA, the resulting lamellar structure is a mixture of horizontal and vertical (figure 2.4d). If both interfaces (film/substrate and film/air) are modified to nonpreferential, a completely vertical structure is achieved (figure 2.4e). As a consequence, the modification of the interface can easily result in films with different morphologies.

2.2 Thermo-responsive polymers

Stimuli-responsive polymers are defined as polymers which undergo relatively large and abrupt, physical or chemical changes in response to small external changes [77]. These responses of polymers attract more and more attentions due to their applications in the fields of biology [7, 78, 79], medicine [80, 81, 82] and sensor technology [8, 83, 84, 85]. Among stimulus-responsive polymers, as the variation of temperature is easy to realize, the thermo-responsive polymers are considerably investigated [20, 86, 87, 88, 89, 90]. In this section, phase separation, transition behavior and effects influencing the transition behavior of thermo-responsive polymers are discussed.

2.2.1 Phase separation of thermo-responsive polymers

When a neutral linear polymer is dissolved in a solvent, the excluded volume interaction and the elastic force determine the swelling of the polymer [91, 92, 93]. When the thermal energy (k_BT) of the repeating units in the polymer is very high, the excluded volume interaction dominates over the attraction between the repeating units. Therefore, the polymer can swell in the solvent. But it should be noted that the former case is only suitable for the thermodynamically good solvent, meaning that the conformation of the linear polymer is a very loose extended coil. There are two limitations for the extension of the polymer chains. The first one is the C-C covalent bonds. The second one is the entropy of the coil, which decreases when the coil swells in solvents. The total internal energy of the segmental interactions, indicating the excluded volume effect, can be described as a

power series of the segment density ρ (equation 2.2) [93]:

$$U = VkT\left(\rho^2 A_2 + \rho^3 A_3 + \cdots\right). \tag{2.2}$$

In equation 2.2, A_2 is the second osmotic virial coefficient of expansion. It is used to describe the thermodynamic quality of the solvent to the polymer, which depends on temperature and interaction potential between the segments [93]. When $T = T_\theta$, the conformation of polymer is an ideal Gaussian coil, and the repeating units in the chains can be described as an ideal gas (connected in a chain). The molecules of gas do not interact with the polymer. Therefore, when $A_2 = 0$ and the molecular weight of the polymer is infinitely high, the polymer solution is in the θ condition [94].

When the temperature is cooling below T_θ, the coil-to-globule transition of a single polymer chain in organic solvents can be described by the mean-field theory [95]. Because the thermal energy of repeating units becomes lower than the minimum of the potential related to the van der Waals interactions, the solvent switches from the thermodynamic favorable to thermodynamic unfavorable ($A_2 < 0$). Thus, the former swollen repeating units start to separate from the solvent. Condensation sets in. It should be noted that this transition taking place at T_θ is strictly only valid for the polymers with infinite molecular weight. For real polymers with finite molecular weight, this transition occurs at a temperature lower than T_θ [96, 97, 98]. To determine the value of A_2 in an experiments, light scattering and osmotic pressure measurements are usually applied.

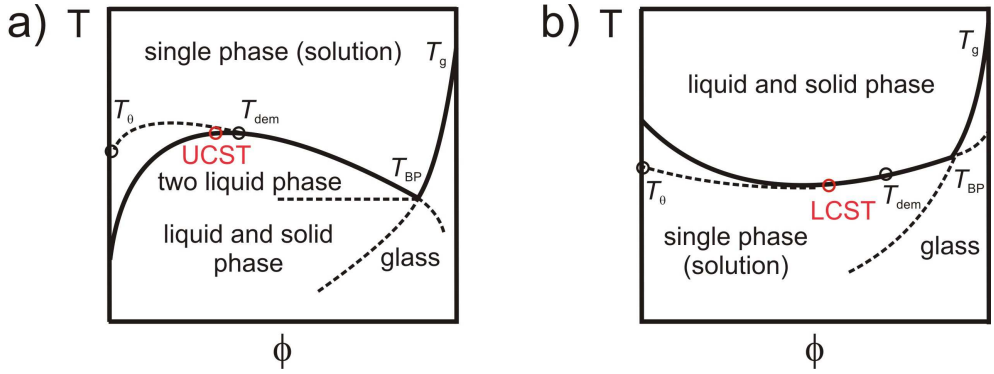

Figure 2.5: *Sketch of phase diagram for polymer solution with (a) upper critical solution temperature (UCST) behavior and (b) lower critical solution temperature (LCST) behavior. T_{dem} is the demixing temperature, T_θ is the theta temperature, T_g is the glass transition temperature and T_{BP} is the temperature corresponding to the Berghmans point.*

Figure 2.5a shows a typical upper critical sloution temperature (UCST) phase transition behavior (PS in cyclohexane), which is described above [99, 100, 101, 102, 103, 104].

When the temperature is above the critical solution temperature, the polymer is miscble with the solvent. The solution is homogeneous and transparent. When the temperature is below the critical solution temperature, the polymer and solvent are phase-separated. Thus the solution turns into turbid. In contrast, figure 2.5b presents a different type of phase separation (PNIPAM in water). When PNIPAM is dissolved in water, due to the introduction of water, hydrogen bonds are formed between the chains and water. Moreover, as there are hydrophobic groups in PNIPAM, hydrophobic interaction also exists in the system. Thus, these interactions are dominant to the swelling of the polymer instead of the van der Waals interaction. The phase transition is changed, which can be described by a phase diagram with a lower critical solution temperature (LCST). It exhibits single phases in solution at low temperature. When the temperature increases above the LCST, the polymer will become immisible to the solvent (water) and the phase separation takes place. The detail about the theory for swelling and transition process of the polymers with LCST will be discussed in the next section.

2.2.2 Transition behavior of thermo-responsive polymers

As mentioned in section 2.2.1, the LCST transition behavior is attributed to the favor of internal energy. When a water-soluble neutral polymer, containing both hydrophilic and hydrophobic groups, dissolves in water, the hydrophilic groups interact strongly with the water molecules and form hydrogen bonds. The formation of hydrogen bonds is the initial driving force for dissolution. Simultaneously, the hydrophobic groups do not like water. Thus they interfere the association of the polymer with water. But at lower temperature, the attraction between the hydrophilic group and water is much stronger than the repulsion between the hydrophobic groups and water. Therefore, the polymer dissolves in water. Additionally, the water surrounding the hydrophobic groups organizes itself and forms an ordered hydration layer. This behavior is called “hydrophobic effet” [89, 105, 106, 107, 108], which can help to minimize the contact surface between the hydrophobes and water. However, this state is entropically unfavourable and unstable [109, 110]. By increasing the temperature, the dominant force in the system is changed. Therefore, the solubility of the polymer is also changed and precipitation occurs.

Because PNIPAM is a typical and the most investigated thermo-responsive polymer with LCST behavior [2, 27, 28, 29, 30, 31, 32, 33, 34, 35, 36, 37], the transition behavior of PNIPAM is discussed here as a example. The amide groups (N-H) and ether groups (C=O) in PNIPAM can form hydrogen bonds with water (C-O$\cdots$$H_2O$, N-H$\cdots$$OH_2$). With

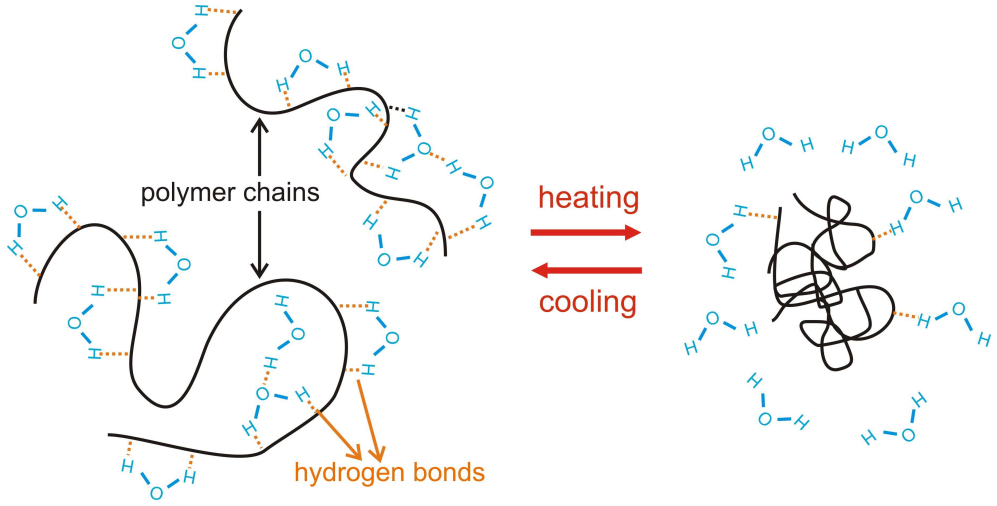

Figure 2.6: *Sketch of the swollen and collapsed thermo-responsive polymer chains below and above LCST.*

infrared spectroscopy, it is found that besides the intermolecular hydrogen bonds mentioned above, there are also the intramolecular hydrogen bonds formed between the amide groups and ether groups (C-O···N-H) [38, 42, 111, 112, 113]. At lower temperature, the intermolecular hydrogen bonds are dominant ones, thus PNIPAM is able to dissolve in water (see figure 2.6). However, the hydrophobic effect increases with temperature. When the temperature increases above the LCST, the intramolecular hydrogen bonds between hydrophobic part of the polymer chains are more favored [114]. Thus, the bound water are released and the polymer chains collapse (see figure 2.6). During the heating process, the negative change of the entropy is larger than the enthalpy of the hydrogen bonds, therefore the change in the free energy of the mixing is positive. This change results in the phase transition of the thermo-responsive polymer (see figure 2.5b).

Besides the hydrogen bonds discussed above, the cooperation of bound water also contributes to the transition of PNIPAM [115]. The PNIPAM chains are in the coiled state before being immersed in water. After being placed in water, the water molecules (blue circles in figure 2.7) start to connect with the amide groups or ether groups by hydrogen bonds. These water is called bound water. Whereas the other water molecules are called free water. The bound water causes a slight displacement of the isopropyl group on side chain. This displacement results in an easier formation of the second hydrogen bond on the neighboring position. Thus, a series of bound water is formed along the swollen chains. Simultaneously, the residual chains still stay in the coiled state, which is marked by grey circles in figure 2.7. When the temperature is heated up to the LCST, the

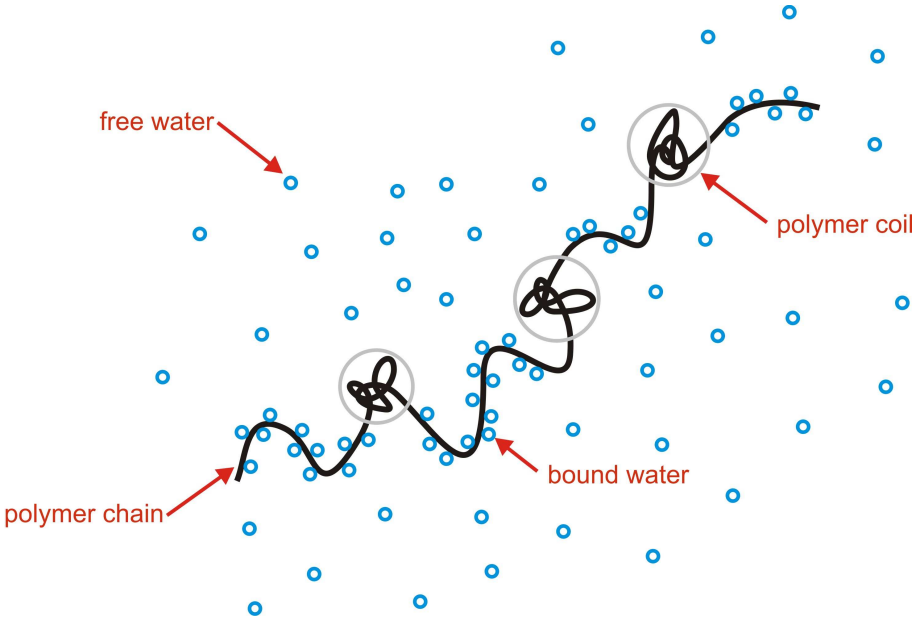

Figure 2.7: *Sketch for the cooperation of the bound water in PNIPAM solution.*

detachment of one bound water induces the easier detachment of the neighboring bound water. Therefore, similar to a zip, a series of bound water is released from the polymer chains. This cooperation results in the sharp transition behavior of PNIPAM [115].

2.2.3 Effects influencing transition behavior of thermo-responsive polymers

The transition behavior of thermo-responsive polymer can be influenced by several effects. In this section, PNIPAM is taken as an example to discuss the effects that influence the transition behavior.

The influence of molecular weight

Many investigations have been done about the influence of molecular weight on the transition behavior of PNIPAM. It is reported that the variation of molecular weight does not influence the transition temperature [116, 117, 118]. On the contrary, it is also observed that in some cases, the transition temperature shows a decreasing tendency when the molecular weight of PNIPAM increases [119, 120]. For instance, when the molecular weight of PNIPAM is smaller than 50,000 g/mol, the LCST is changed by 1 °C during the decrease of the molecular weight. Whereas the LCST stay constant when the molecular weight of PNIPAM is above 50,000 g/mol [120]. The reason for the contrary results may

be attributed to the different end-group structures in PNIPAM being present in these investigations.

The influence of end groups

As mentioned above, due to the incorporation of specific end-groups during the polymerization of PNIPAM, these end-group influence the transition behavior of PNIPAM. For instance, PNIPAM ended with the pyrenyl group shows a strong aggregation when the temperature increases. Thus the LCST even decreases from 32 °C to 22 °C [121]. In contrast, PNIPAM ended with amide end group exhibits a LCST of 45 °C (molecular weight 3,000 g/mol) [122]. However it should be noted that this end-group effect is most promient for PNIPAM with low molecular weight. When the molecular weight is increased, as the relative concentration of the end-group is reduced, the influnce of the end-group to the transition behavior is alleviated [120, 123]. For example, when the molecular weight of PNIPAM ended with amide end group is 3,000 g/mol, the LCST is 45 °C. If the molecular weight increases to 16,300 g/mol, the LCST drops to 34 °C [122].

The influence of hydrophobic and hydrophilic modifications

The transition behavior of PNIPAM can be easily modified by introduing hydrophobic or hydrophilic groups into the PNIPAM chains. For instance, when hydrophobic groups are introduced into PNIPAM, the LCST drops [124]. As discussed in section 2.2.2, the phase transition is realized by switching from the hydrophilic interaction to the hydrophobic interaction. The hydrophobicity of the copolymer is increased when the extra hydrophobic groups are introduced into the chains, the LCST shifts to lower values. Additionally, the higher the hydrophobic content in the copolymer, the lower the LCST [13]. However, when hydrophilic groups are introduced into PNIPAM, the result obtained is reversed. Due to the higher hydrophilic content in the copolymer, the switching from the hydrophilic interaction to hydrophobic interaction is hindered, inducing the LCST to shift to higher temperatures [40].

Furthermore, the position of the hydrophobic groups or the hydrophilic groups introduced influences the LCST as well. For example, when only one end side of the PNIPAM chain is copolymerized with hydrophobic groups, the copolymer will form core-shell micelles in water. The hydrophobic groups form the core, while the PNIPAM chains form the shell with a brush-like corona structure [39, 125]. If both ends of the PNIPAM chain are copolymerized with hydrophobic groups, core-shell micelles are still obtained in water,

but the shell part exhibits a flower-like structure instead of the brush-like corona [126]. Because the formation of the micelles increases the apparent molecular weight, the different kinds of micelles formed in the solution will further reduce the mixing entropy of the polymer chains. Thus, it favors the phase separation and shifts the LCST to lower value.

2.3 Scattering methods

For thermo-responsive polymer films, the internal structure is not only important for applications [13, 127], but also strongly influences the swelling and transition behavior [128]. X-ray and neutron scattering methods have proved to be powerful techniques to investigate the internal structure of thermo-responsive polymers [20, 37, 126, 129]. The most fundamental difference between X-ray and neutron scattering is the interaction mechanism of the incident radiation with the sample. X-rays are scattered by electrons around the atomic nucleus, whereas neutrons are scattered by the nucleus itself. The energy of an X-ray beam is given by $E = hc/\lambda$. Because neutrons have a mass (m $= 1.674\times10^{-27}$ kg), the energy of neutrons is calculated via $E = h^2/2m\lambda^2 = m\nu^2/2$. Thus, if X-ray and neutron have the same wavelength, it is obvious that X-ray contains much higher energy than neutron. For this reason, neutron has much less radiation damage effect than X-ray, which is suitable for the sensitive samples such as polymers. Secondly, due to the fact that the scattering of neutrons is from the nucleus. It introduces a large contrast between ^{1}H and ^{2}H, which is widely used for labelling in polymers and biology. In this section, the basic principle for elastic scattering is troduced firstly (section 2.3.1). Afterwards, the mainly applied scattering techniques, including X-ray reflectivity (XRR) and neutron reflectivity (NR), are discussed in section 2.3.2 and 2.3.3, respectively. In order to probe the internal structure in thick polymer films, small angle scattering (SAS) is introduced in section 2.3.4. Finally, grazing incidence small-angle X-ray scattering (GISAXS) is discussed in section 2.3.5 to measure the vertical and lateral structure in thin polymer films.

2.3.1 Basic principle

As mentioned above, X-ray and neutron scattering are the main methods used to investigate internal structure of films. Thus, the principles of X-ray elastic scattering are discussed in this section.

For an electromagnetic plane wave, the electric field vector $\vec{E}(\vec{r})$ can be described by

equation 2.3:

$$\vec{E}(\vec{r}) = \vec{E}(0)exp(i\vec{k}_i \cdot \vec{r}). \tag{2.3}$$

In equation 2.3, $\vec{E}(0)$ is the amplitude and polarization of the electromagnetic wave. $\vec{k}_i$ is the wavevector and $\vec{r}$ is the position vector. When the electromagnetic wave impinges into a medium characterized by an refraction index $n(\vec{r})$, the propagation of the wave is described by the Helmholtz equation (equation 2.4):

$$\Delta\vec{E}(\vec{r}) + k^2 n^2(\vec{r})\vec{E}(\vec{r}) = 0. \tag{2.4}$$

In equation 2.4, k is the modulus of the wavevector $\vec{k}_i$, which can be calculated by $k = 2\pi/\lambda$. λ is the wavelength of the incident X-ray. The refraction index n is described by equation 2.5 [130]:

$$n(\vec{r}) = 1 - \delta(\vec{r}) + i\beta(\vec{r}). \tag{2.5}$$

The dispersion term $\delta(\vec{r})$ and absorption term $\beta(\vec{r})$ in equation 2.5 can be calculated by equation 2.6 and 2.7, respectively.

$$\delta(\vec{r}) = \frac{\lambda^2}{2\pi} r_e \rho(\vec{r}) \sum\nolimits_{j=1}^{N} \frac{f_j^0 + f_j'(E)}{Z}. \tag{2.6}$$

$$\beta(\vec{r}) = \frac{\lambda^2}{2\pi} r_e \rho(\vec{r}) \sum\nolimits_{j=1}^{N} \frac{f_j''(E)}{Z} = \frac{\lambda}{2\pi}\mu_(\vec{r}). \tag{2.7}$$

In equation 2.6 and 2.7, r_e is the classical electron radius and $\rho(\vec{r})$ is the electron density. f_j is the forced oscillation strength of the electrons of each single atom, which can be calculated by $f_j^0 + f_j'(E) + if_j''(E)$. Z is the total number of electrons, which is obtained from $\sum_j Z_j$, in which Z_j is defined as the number of electrons of each component in material. $\mu(\vec{r})$ is the linear absorption coefficient. When the incident angle α_i (defined as the angle between the incident X-ray beam and the interface) and exit angle α_f (defined as the angle between the exit X-ray beam and the interface) are very small, f_j^0 is closed to Z_j.

Furthermore, when the medium is homogeneous, the refractive index can be simplified by equation 2.8.

$$n = 1 - \frac{\lambda^2}{2\pi} r_e \rho + i\frac{\lambda}{2\pi}\mu. \tag{2.8}$$

From equation 2.8, the dispersion term $\delta = \lambda^2 r_e \rho/2\pi \approx 10^{-5} - 10^{-6}$. As the dispersion term is very small, the refractive index $|n|$ is only slightly smaller than 1. It induces one

special property of X-ray or neutron. When the incident angle α_i is smaller than the critical angle $|\alpha_c|$, the total reflection takes place. α_c is given by equation 2.9:

$$cos\alpha_c = n = 1 - 2\delta. \tag{2.9}$$

Because δ is in the order of $10^{-5} - 10^{-6}$, it is clear from equation 2.9 that α_c is also very small. Therefore, $cos\alpha_c$ can be further replaced by $1 - {\alpha_c}^2$. Finally, equation 2.9 can be reformatted to:

$$\alpha_c = \sqrt{2\delta} = \lambda\sqrt{r_e\rho/\pi} \tag{2.10}$$

Thus total reflection can only take place when the incident angle is very small. When the incident angle increases, the beam penetrates into the sample and the reflected intensity dramatically decreases.

2.3.2 X-ray reflectivity (XRR)

XRR on semi-infinite substrate

In section 2.3.2, the principle of X-ray scattering is introduced. For X-ray reflectivity, the specular scattering is measured as a function of the incident angle $|\alpha_i|$. The example of a semi-infinite substrate is sketched in figure 2.8.

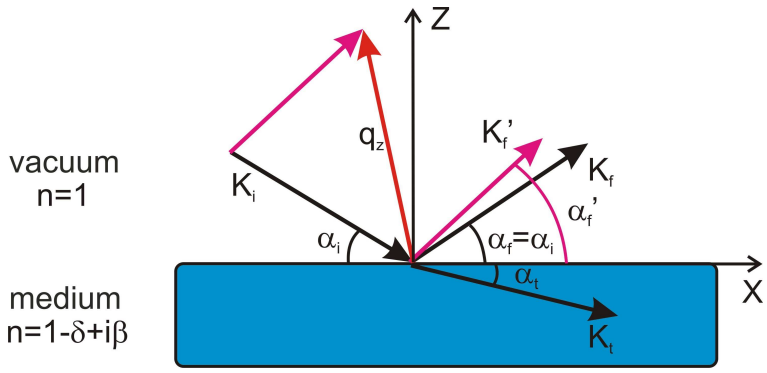

Figure 2.8: *Basic principle of X-ray specular scattering. An X-ray beam with incident wave vector $\vec{K}_i$ impinges the surface of medium with an incident angle α_i. One part of the wave is scattered with wave vector $\vec{K}_f$ at the angle of α_f. If $\alpha_f = \alpha_i$, the specular reflectivity is obtained. Another part of the wave is transimitted into the medium with wave vector $\vec{K}_t$ at the angle of α_t.*

Because $\alpha_i = \alpha_f$, the scattering vector is normal to the sample surface ($q_x = q_y = 0$). There is only the Z component of the scattering vector left, which is given by equation

2.11:

$$q_z = \vec{k}_f - \vec{k}_i = (\frac{2\pi}{\lambda} sin\alpha_f) + (\frac{2\pi}{\lambda} sin\alpha_i). \tag{2.11}$$

As $\alpha_i = \alpha_f$, equation 2.11 can be rewritten to equation 2.12:

$$q_z = \vec{k}_f - \vec{k}_i = \frac{4\pi}{\lambda} sin\alpha_i. \tag{2.12}$$

In figure 2.8, the incident, reflected and transmitted waves are expressed by $\vec{E}_i(\vec{r}) = a_i exp(i\vec{k}_i \cdot \vec{r})$, $\vec{E}_f(\vec{r}) = a_f exp(i\vec{k}_f \cdot \vec{r})$ and $\vec{E}_t(\vec{r}) = a_t exp(i\vec{k}_t \cdot \vec{r})$, respectively. The amplitude a and the wave vector $\vec{k}$ satisfy equation 2.13 and 2.14.

$$a_i + a_f = a_r. \tag{2.13}$$

$$a_i\vec{k}_i + a_f\vec{k}_f = a_r\vec{k}_r. \tag{2.14}$$

From Fresnel formulas [131], the reflection and transmission coefficient can be obtained (see equation 2.15 and 2.16):

$$r_F = \frac{\vec{k}_i - \vec{k}_t}{\vec{k}_i + \vec{k}_t}. \tag{2.15}$$

$$t_F = \frac{2\vec{k}_i}{\vec{k}_i + \vec{k}_t}. \tag{2.16}$$

Thus, the intensities of the reflected and transmitted X-ray wave are $R_F = |r_F|^2$ and $T_F = |t_F|^2$, respectively.

XRR on multilayers

Until now, the discussion is based on a semi-infinite medium only. But in reality, more complex scenarios are likely. Therefore, the scattering from all interfaces should be taken into consideration. Figure 2.9 exhibits the scattering of a incident wave impinging a medium with *N+1* layers and N interfaces [131, 132, 133, 134, 135]. Position Z_1 is defined as 0 position, then the others position Z_j are less than 0. The layer between the position Z_{j-1} and Z_j is defined as the j_{th} layer. The thickness of j_{th} layer (d_j) can be calculated from $Z_j - Z_{j-1}$. n_j denotes as the refractive index of each layer, which is given by equation 2.9. $k_{i,j}$ and $k_{f,j}$ are the incident and reflected wave vector in the j_{th} layer, respectively. T_j and R_j are the amplitude of the transmitted and reflected wave.

Before the incident wave ($k_{i,1}$) impinges the medium at position Z_1=0, the transimitted amplitude $T_1 = 1$. After the impingement, R_1 is the reflected wave from the first interface, and T_2 is the transmitted wave into the second layer. According to the literature from Parratt [135], the reflected wave and the transmitted wave in the j_{th} layer are given by R_j and T_j, respectively. Then the ratio of R_j and T_j in the j_{th} layer can be calculated from equation 2.17 [136]:

$$X_j = \frac{R_j}{T_j} = exp(-2ik_{z,j}z_j)\frac{r_{j,j+1} + X_{j+1}exp(2ik_{z,j+1}z_j)}{1 + r_{j,j+1}X_{j+1}exp(2ik_{z,j+1}z_j)}. \tag{2.17}$$

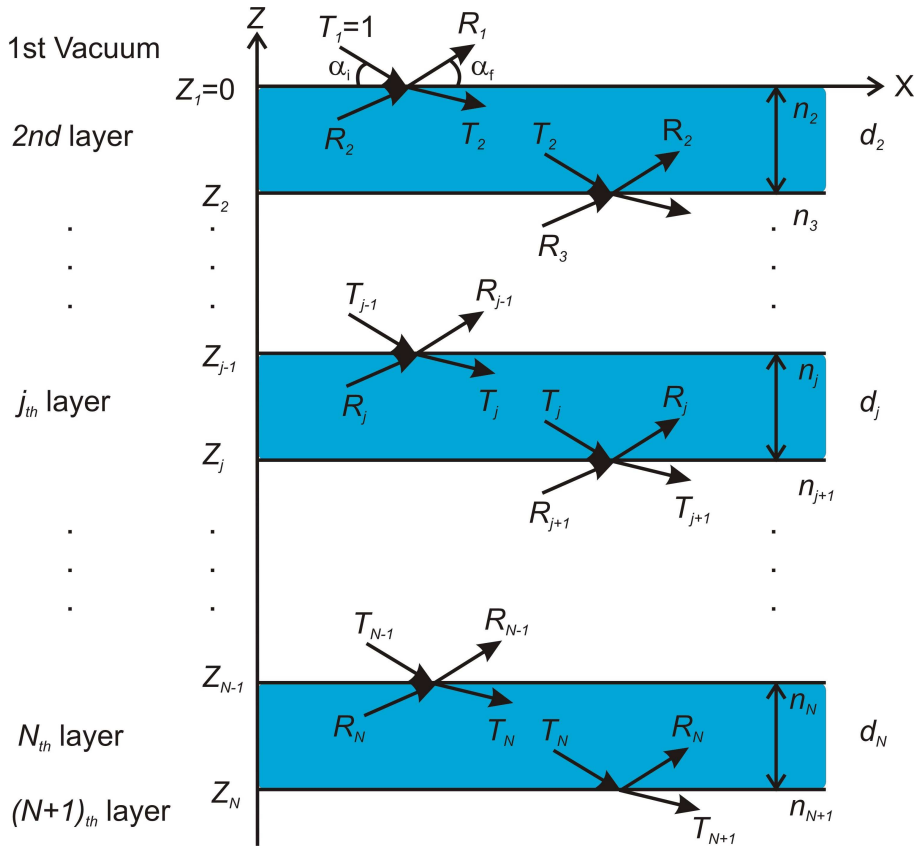

Figure 2.9: *Scattering of an incident wave impinges a medium which contains N+1 layers and N interfaces. The first layer is vacuum (top), and the (N+1)th layer is the substrate. For reflectivity, the incident angle (α_i) is equal to the exit angle (α_f). The amplitude of the incident wave (T_1) is normalized to 1.*

In equation 2.17, the Frensnel coefficient of the j_{th} interface $r_{j,j+1}$ can be given by $k_{z,j} - k_{z,j+1}/k_{z,j} + k_{z,j+1}$. While $k_{z,j} = k(n_j^2 - cos^2\alpha_i)^{1/2}$ is the z component of the wave vector in j_{th} layer. It is assumed that the substrate is so thick that the X-ray can not penetrate it. Therefore, R_{N+1}=0 and $X_{N+1} = R_{N+1}/T_{N+1} = 0$. From equation 2.17, the

reflected intensity R can be obtained as equation 2.18:

$$R = |X_1|^2 = |R_1|^2. \tag{2.18}$$

Influence of roughness in XRR

Until now, by switching the medium from single layer to mutilple layers, it is closed to the reality. However, the medium with ideally flat interfaces does not exist. There is always a roughness presented. To describe the surface roughness, the root mean square roughness τ_{rms} is applied, which is given by equation 2.19 [137]:

$$\tau_{rms}^2 = \frac{1}{N}\sum_{i=1}^{N}(Z_i - Z)^2. \tag{2.19}$$

In equation 2.19, N is the number of data points, Z_i is the surface level on the i point and Z is the mean surface level, which is given by equation 2.20:

$$Z = \frac{1}{N}\sum_{i=1}^{N}Z_i. \tag{2.20}$$

By using the Névot-Croce factor, which is described by an expotential function, to correct the Fresnel reflection coefficients, the surface roughness can be taken into consideration. However, the limit of this correction is that the roughness can not be larger than the thickness of the layer. More detail about the influence of the roughness to the X-ray reflectivity scattering can be found in literature [136].

XRR curve of thin PMDEGA film

Figure 2.10 shows a representative XRR curve of a thin PMDEGA film on a silicon substrate. It is clear that when the incident angle is very small (q_z is small), due to the total reflection of the X-ray beam ($\alpha_i < \alpha_c$), the intensity of the reflectivity stay constant. When α_i increases to a critical value, which is equal to the critical angle of the component (PMDEGA or Si), the minimum of the reflectivity appears (marked by the black arrow in the curve). Further increasing α_i to a large value, the oscillation of the reflectivity (Kiessig-fringes) occurs. From the distance between the neighboring fringes (Δq_z), the film thickness d can be approximated by $d \approx 2\pi/\Delta q_z$. Moreover, the amplitude of the oscillation is related to the roughness, indicating that the amplitude dramatically decreases when the roughness of the surface increases. Using software such as Parratt32, the XRR curve can be fitted. The film thickness, roughness and density profile can be obtained from the fits.

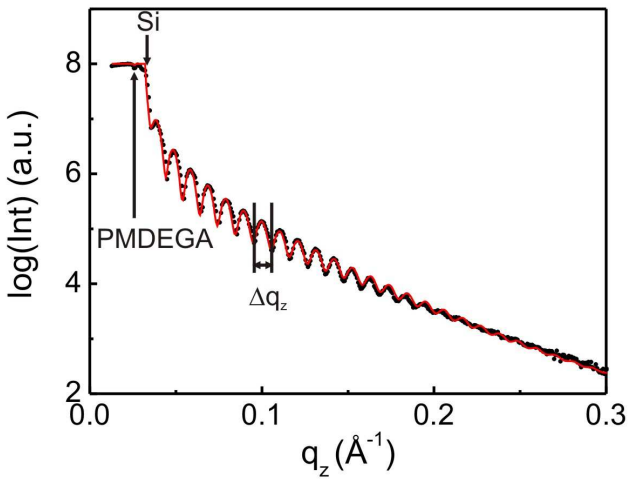

Figure 2.10: *Representative XRR curve of the PMDEGA film on the silicon substrate together with fit.*

2.3.3 Neutron reflectivity (NR)

Due to the large scattering contrast between ^{1}H and ^{2}H, neutron reflectivity is widely applied in the field of polymer and biology by selectively labelling a certain component of the sample with deuterium.

As the polymers are non-magnetic material, the optical indices can be introduced into neutron reflectivity, which is similar to X-ray reflectivity discussed above [134]. In vacuum, the energy of neutrons is described by equation 2.21:

$$E_0 = \frac{\hbar^2 {k_0}^2}{2m} = \frac{h^2}{2m\lambda^2}. \tag{2.21}$$

Without magnetic field, the Schrödinger equation is given by equation 2.22:

$$\frac{\hbar^2}{2m}\frac{d^2\psi}{dr^2} + [E_0 - V]\,\psi = 0. \tag{2.22}$$

In equation 2.22, ψ is the neutron wave function, $\hbar$ is the Plank's constant and m is the mass of neutron. V is the mean potential in the medium, which can be achieved by the integration of the Fermi pseudo-potential (equation 2.23).

$$V = \frac{1}{\nu}\int V(r)d^3(r) = \frac{2\pi\hbar^2}{m}b\rho. \tag{2.23}$$

Equation 2.22 can be further rewritten to:

$$\frac{d^2\psi}{dr^2} + k^2\psi = 0. \tag{2.24}$$

where $k^2 = 2m/\hbar^2 [E_0 - V]$. Thus, the refractive index of neutrons is defined as:

$$n^2 = \frac{k^2}{k_0^2} \approx 1 - \frac{\lambda^2}{2\pi}\rho b. \tag{2.25}$$

where ρ is the coherent scattering length and b is the number density. Thus, ρb is the scattering length density. As the neutron adsorption for most elements is very small, the imaginary part of the refractive index can be neglected. As a consequence, n can be further rewritten:

$$n \approx 1 - \frac{\lambda^2}{2\pi}\rho b = 1 - \delta. \tag{2.26}$$

2.3.4 Small-angle scattering (SAS)

Small-angle scattering (SAS) is a powerful scattering technique to investigate structured materials [138]. SAS contains small-angle X-ray scattering (SAXS) and small-angle neutron scattering (SANS) [139, 140]. As SAXS and SANS share the same basic principle, the later discussion is only focused on the SAXS technique. Figure 2.11 shows a sketch of typical setup for the SAXS measurement. After the X-ray beam is produced by the source, it first goes through the monochromator and slits. Then, the X-ray beam with a single wavelength is elastically scattered by the sample. Finally, the scattered beam is recorded by a detector. By analyzing the scattering pattern, the information about the size, the shape and the correlation in the sample can be obtained.

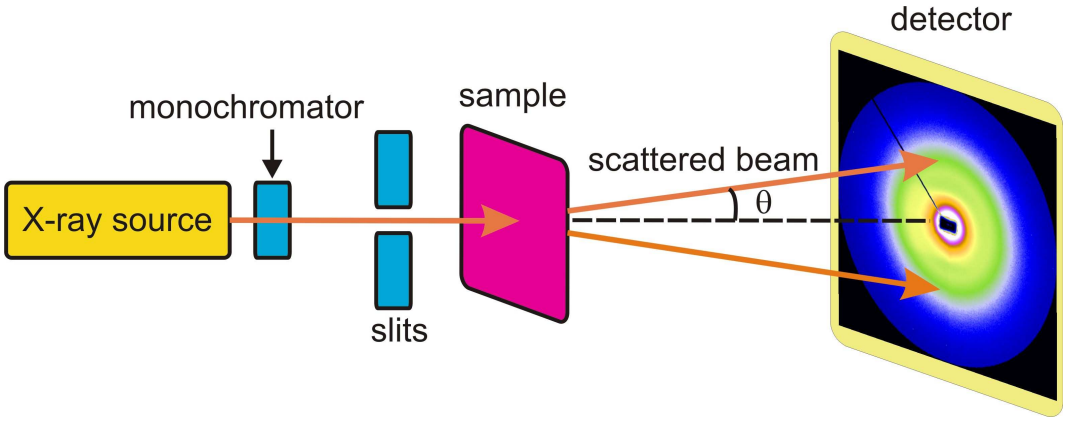

Figure 2.11: *Sketch of typical setup for SAXS measurement.*

Radius of gyration

First of all, an important parameter in small-angle scattering is introduced before the calculation of the scattering intensity of a single particle. The radius of gyration (R_g) is

used to describe the size of the polymer, and is given by equation 2.27:

$$R_g = \frac{\int \Delta\rho(r_i) {r_i}^2 dV_i}{\int \Delta\rho(r_i) dV_i}. \tag{2.27}$$

From equation 2.27, R_g of the solid sphere with radius R and the solid ellipsoid of half axes a, b and c is given by $\sqrt{\frac{3}{5}}R$ and $\frac{1}{\sqrt{5}}(a^2+b^2+c^2)^{1/2}$, respectively.

Form factor

In order to describe the scattering from a single particle, the form factor *P(q)* is introduced into the calculation, which depends on the size and the shape of the particles. For instance, some particles with electron density ρ_p and volume V_p are dispersed homogeneously in a diluted solution. The electron density of the solvent is ρ_s (see figure 2.12).

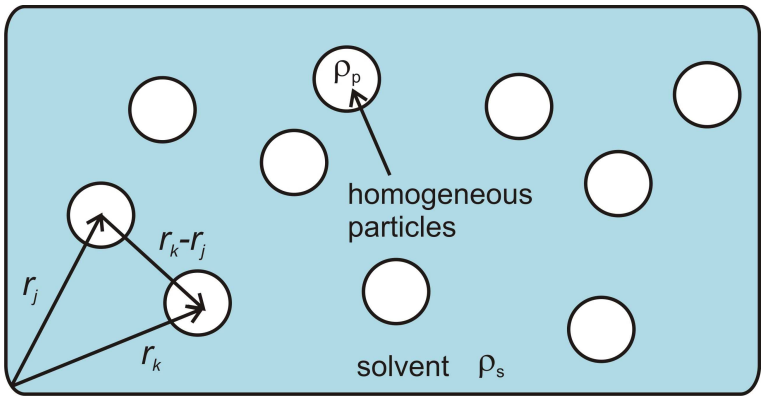

Figure 2.12: *Sketch of homogeneous particles with electron density ρ_p and volume V_p dispersed in the solvent with electron density ρ_s.*

Then the scattered intensity *I(q)* can be calculated from equation 2.28:

$$I(q) = \frac{d\sum(q)}{d\Omega} = \frac{N}{V}(\rho_p - \rho_s)^2 V_p^2 \left| \frac{1}{V_p} \int \rho(r) e^{-iqr} dr \right|^2. \tag{2.28}$$

In equation 2.28, V is the illuminated volume and V_p is the volume of the particle. $\rho(r) = \rho_p - \rho_s$ is the difference of the electron density (SLD) between particle and solvent, which is usually named scattering contrast. Thus, the form factor can be defined as equation 2.29:

$$P(q) = \left| \frac{1}{V_p} \int \rho(r) e^{-iqr} dr \right|^2. \tag{2.29}$$

Particularly, the form factor $P(q)$ for a monodisperse spherical particle with a core-shell structure can be described by equation 2.30:

$$P\left(q\right)=\frac{1}{V_{sh}}\left[\frac{3V_{co}\left(\rho_{co}-\rho_{sh}\right)j(qr_{co})}{qr_{co}}+\frac{3V_{sh}\left(\rho_{sh}-\rho_{so}\right)j(qr_{sh})}{qr_{sh}}\right]^{2}. \tag{2.30}$$

The form factor is normalized by the volume of the shell V_{sh}. In equation 2.30, V_{co} and V_{sh} are the volume of the core and the shell, respectively. Both of them can be calculated by equation 2.31.

$$V_i=\frac{4}{3}\pi r^3. \tag{2.31}$$

In order to define the core and the shell in the micelle, the difference of SLD between the core and the shell $(\rho_{co}-\rho_{sh})$ is multiplied. Similarly, $(\rho_{sh}-\rho_{so})$ is multiplied to define the contrast of the shell and the solvent. In equation 2.30, j is the first order Bessel function, as expressed in equation 2.32.

$$j(x)=\frac{sinx-xcosx}{x^2}. \tag{2.32}$$

Porod law

The porod law is usually used to describe the slope of the plot (lnI_q as a function of lnq). It shows the interface and fractal dimension of the scattering particles. For instance, the porod law is expressed with the Porod amplitude K, and the Porod exponent α (equation 2.33) [141].

$$P_{Porod}(q)=\frac{K}{1+0.22(qr)^{\alpha}} \tag{2.33}$$

For $\alpha=4$, the cluster exhibits a smooth surface. For $\alpha<4$, the surface is rough, and $\alpha>4$, the surface displays a scattering length density gradient [126].

Structure factor

From the discussion above, when the solution is dilute, the scattering intensity is dominated by the sum of scattering from each independent particles. Further increasing the concentration of the particles above a critical value, the particles are so close to each other that they can feel the existence of the neighboring particles. Thus the interaction between particles should be taken into consideration (see figure 2.12). In the case that all of the particles are monodisperse spheres, the intensity can be calculated by:

$$I(q)=\frac{d\sum\left(q\right)}{d\Omega}=n\left\langle\left|F_k(q)\right|^2\right\rangle\left\{1+\left\langle\sum_{k=1}^{N}\sum_{j=1,j\neq k}^{N}e^{-iq(r_k-r_j)}\right\rangle\right\}. \tag{2.34}$$

In equation 2.34, r_k and r_j are the mass center of particle k and j, respectively (figure 2.12). The term $\left\langle |F_k(q)|^2 \right\rangle$ is the form factor of the particles, while the term $\left\{ 1 + \left\langle \sum_{k=1}^{N} \sum_{j=1, j\neq k}^{N} e^{-iq(r_k - r_j)} \right\rangle \right\}$ corresponds to the dispersion of the particles in solution. This dispersion is related with the interaction between neighboring particles. Therefore, it is defined as the structure factor $S(q)$. Then equation 2.34 can be simplified to equation 2.35:

$$I(q) = \frac{d\sum(q)}{d\Omega} = nP(q)S(q). \tag{2.35}$$

Particularly in the case of simple hard sphere interaction, *S(q)* is given by:

$$S(q) = \frac{1}{1 + 24\eta G(2qr)/2qr}. \tag{2.36}$$

The structure factor *S(q)* is determined by the radius of the hard-sphere r and the volume fraction η. r describes the distance between the neighboring hard spheres, and η is the proportion of the occupied hard-sphere volume to the total volume, indicating the packing density. In equation 2.36, the function *G(x)* is given by equation 2.37:

$$\begin{aligned} G(x) = \alpha \frac{sinx - xcosx}{x^2} + \beta \frac{2xsinx + (2 - x^2)cosx - 2}{x^3} \\ + \gamma \frac{-x^4 cosx + 4\left(3x^2 - 6cosx + (x^3 - 6x)sinx 2xsinx + 6\right)}{x^5}. \end{aligned} \tag{2.37}$$

where the factors α, β and γ are defined in equation 2.38:

$$\begin{aligned} \alpha &= \frac{(1 + 2\eta)^2}{(1 - \eta)^4} \\ \beta &= \frac{-6\eta(1 + \eta/2)^2}{(1 - \eta)^2} \\ \gamma &= \frac{\alpha\eta}{2}. \end{aligned} \tag{2.38}$$

Combining these three components together, the total intensity of the scattering is obtained, which is given by:

$$I(q) = P(q)S(q) + P_{Porod}(q) + bg. \tag{2.39}$$

In equation 2.39, the last term *bg* denotes the incoherent background in the measurements.

2.3.5 Grazing incidence small-angle X-ray scattering (GISAXS)

Grazing incidence small-angle X-ray scattering (GISAXS) is an investigation method, which is simialr to SAXS. Instead of transmitting through the sample as in SAXS measurements, the X-ray beam hits the sample surface at a very small incident angle ($< 1\ °$) in GISAXS measurements. The specular and diffuse scattering are recorded by a 2D detector. Due to the diffuse scattering monitored, in GISAXS lateral structure inside the film are probed. Moreover, because the X-ray beam impinges the surface at a very small angle, the information about the surface structure is also achievable. The setup for GISAXS measurement is shwon in figure 2.13.

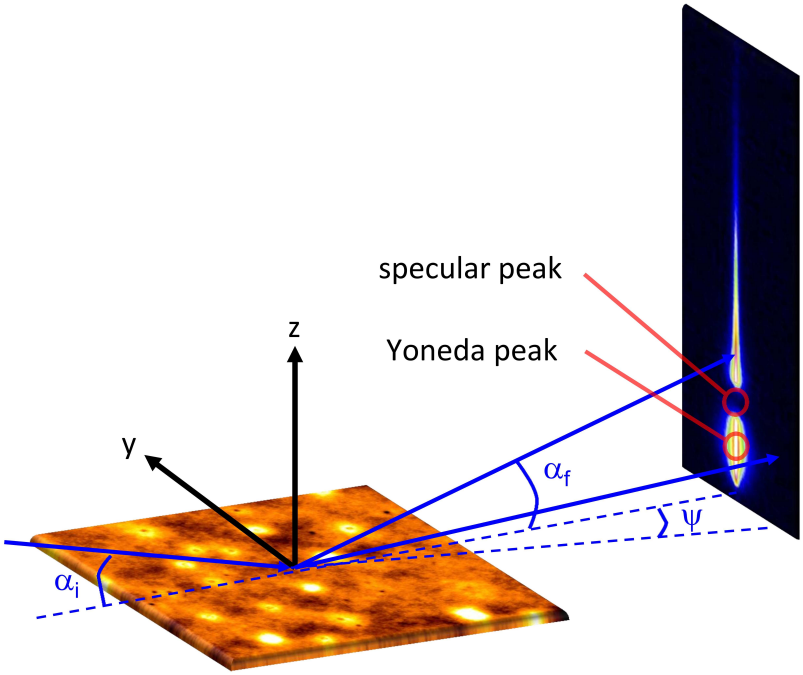

Figure 2.13: *Sketch of typical setup for GISAXS measurement.*

As seen in figure 2.13, a thin PMDEGA film is placed horizontally. The incident angle is fixed at α_i. The component of the diffuse scattering vector $\vec{q}$ in x-, y-, z-plane can be described by equation 2.40:

$$\begin{aligned} q_x &= \frac{2\pi}{\lambda}(cos(\psi)cos(\alpha_f) - cos(\alpha_i)) \\ q_y &= \frac{2\pi}{\lambda}(sin(\psi)cos(\alpha_f)) \\ q_z &= \frac{2\pi}{\lambda}(sin(\alpha_i) + sin(\alpha_f)). \end{aligned} \tag{2.40}$$

where α_f and ψ are the exit angle and out-of-plane angle, respectively.

If $\psi = 0$, the scattering is denoted as the in-plane scattering, which is usually used to investigate the vertical structure of the sample. When $\alpha_i = \alpha_f$, the corresponding reflected intensity maximum is called specular peak (see figure 2.13), which is normally shielded by a beamstop to avoid damage to the detector. When $\alpha_i = \alpha_c$, in which α_c is the critical angle of material, the maximum of the characteristic diffuse scattering intensity is named Yoneda peak (see figure 2.13). When $\alpha_i > \alpha_c$, the incident beam penetrates the film. Due to the interference between the interfaces, such as the top interfaces between the air and the film, or the bottom interface between the film and the substrate, there is a resonance diffuse scattering (RDS) in the scattering plane on the detector. By an analysis of the modulations between Yoneda peak and specular peak, the information about the correlation of the interfaces can be gained [142, 143].

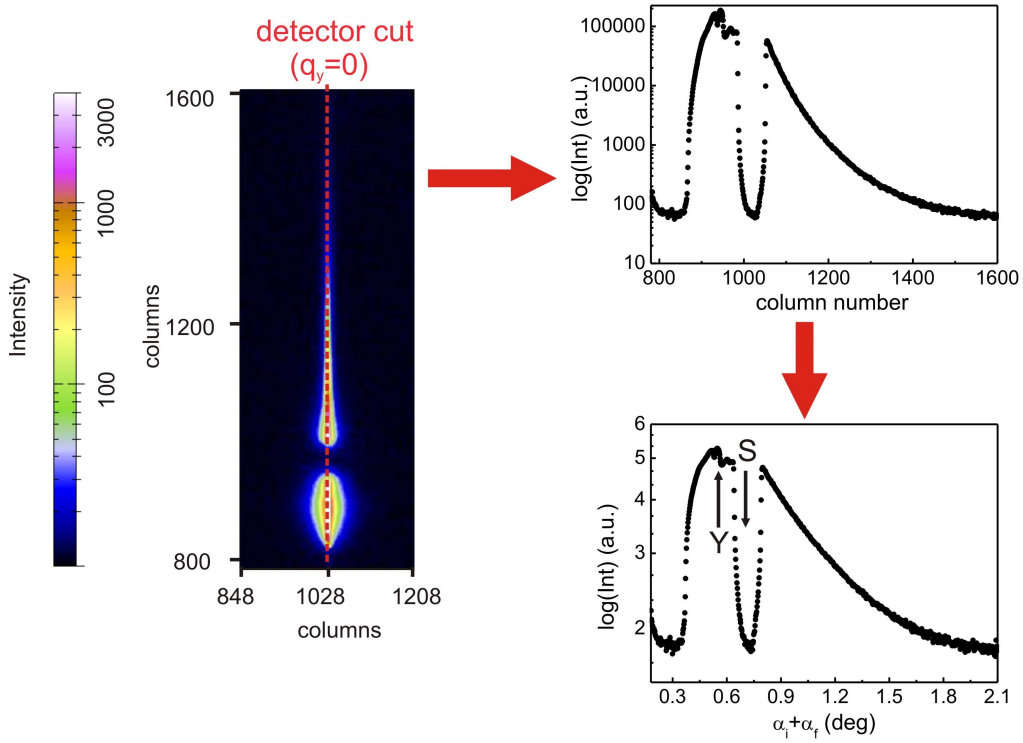

Figure 2.14: *Sketch of the detector cut for GISAXS measurement.*

For instance, figure 2.14 shows a 2D scattering image of thin PMDEGA film. By making a vertical cut on $q_y = 0$ ($\psi = 0$) and integrating the intensity over this region, the intensity can be plotted as a function of the piexl number of the 2D detector. By converting the piexl number to the sum of the incident and exit angle, the final curve,

named “detector cut” is obtained for thin PMDEGA film. Specular peak (S) and Yoneda peak (Y) are observable in this profile. If there is a multilayer structure formed in thin PMDEGA film, due to the correlation between the different interfaces, a modulation of the intensity should be observed between specular peak and Yoneda peak. However, to thin PMDEGA film, the modulation is not observed, which is attributed to the low glass transition temperature (T_g) of PMDEGA. As T_g = -50 °C, the PMDEGA chains sustain high mobility in the film, indicating that the chains can slowly rearrange themselves. Therefore, the possible multilayer structure parallel to the film is removed. The GISAXS is proved to ba a good tool to investigate the vertical structure in the samples.

If $\psi \neq 0$, the scattering is denoted as the out-of-plane scattering. It is usually used to investigate the lateral structure of the sample. Simialr to “detector cut” described, by making the out-of-plane cut at the critical angle of the material and integrating the intensity over this region, the intensity can be plotted as a function of q_y value. By fitting the obtained curve with a model, which contains the strcutre factor *S(q)* and form factor *P(q)*, the lateral structure of the sample can be resolved [144].

Chapter 3

Samples and experimental methods

3.1 Sample system

The polymers used in the investigation are the homopolymer poly(methoxydiethylenglycol acrylate), denoted as PMDEGA, and a PMDEGA based tri-block copolymer poly(styrene-block-monomethoxydiethylenglycol-acrylate-block-styrene), denoted as P(S-*b*-MDEGA-*b*-S). Both of them are received from our cooperation group in Potsdam (Prof. Dr. Laschewsky). In this section, the details about these two PMDEGA based thermo-responsive polymers are introduced.

3.1.1 Homopolymer PMDEGA

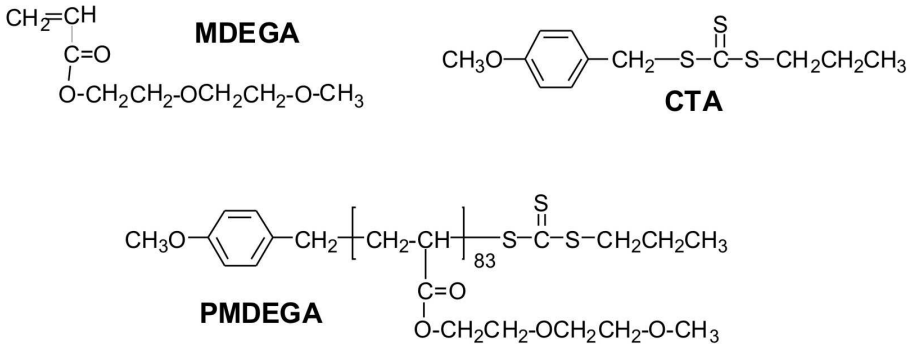

Figure 3.1: *Chemical formulas of the monomer MDEGA, the chain transfer agent CTA and the homopolymer PMDEGA.*

Monomer methoxydiethyleneglycol acrylate (MDEGA) is synthesized from the chain transfer agent (CTA) 4-methoxybenzyl sulfanylthiocarbonylsulfanylpropane according to

the literature [145]. The detail about the polymerization of PMDEGA can be found in literature [52]. The chemical formulas of the monomer MDEGA, the chain transfer agent CTA and the homopolymer PMDEGA are presented in figure 3.1. The number average molecular weight of PMDEGA is determined as 17,000 g/mol by ^{1}H-NMR and the polydispersity is 1.7. As seen in figure 3.1, although there are ester group and ether group in PMDEGA, it is found that only the ether group can act as the H-acceptor and form hydrogen bond in PMDEGA [128]. At low temperature, as the intermolecular hydrogen bonds are favored, the ether group form hydrogen bond with water. When the temperature increases above the transition temperature, the intramolecular hydrogen bonds between the hydrophobic parts of the chains are more favored. Thus, the bound water is detached from the ether groups. By switching between the attchment and detachment of the bound water, the thermo-responsive property of PMDEGA is realized. Moreover, because the side chain in PMDEGA is very large, it hinders the attachment and the detachment of the bound water, which results in a very broad transition region in the PMDEGA based thermo-responsive polymers. The details about the influence of the chemical structure to the transition behavior will be discussed in chapter 4, 5 and 6.

3.1.2 Tri-block copolymer P(S-*b*-MDEGA-*b*-S)

The tri-block copolymer P(S-*b*-MDEGA-*b*-S) is obtained by chain extension of the chain transfer agent CTA7 with PMDEGA in THF at 70 °C up to high conversions [20, 52]. Chemical formulas of P(S-*b*-MDEGA-*b*-S) and CTA7 are presented in figure 3.2. The number average molecular weight of P(S-*b*-MDEGA-*b*-S) is determined as 24,000 g/mol by ^{1}H-NMR and the polydispersity is 1.5.

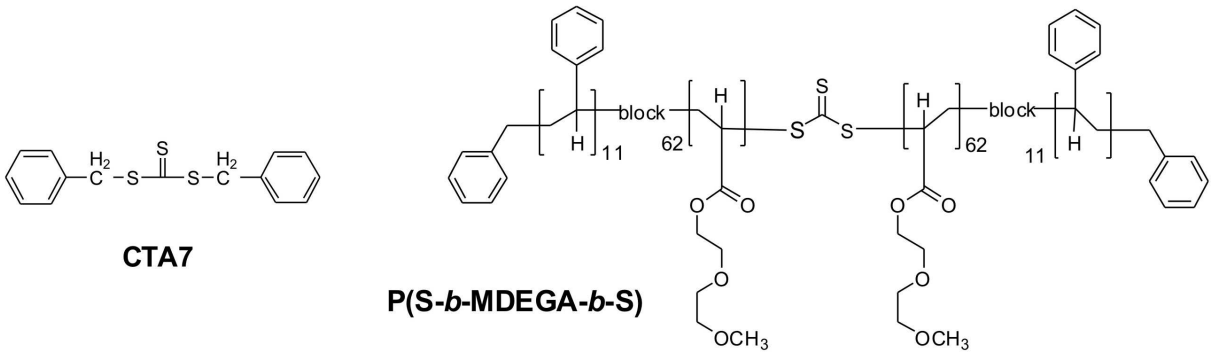

Figure 3.2: *chemical formulas of the chain transfer agent CTA7 and the tri-block copolymer P(S-b-MDEGA-b-S).*

3.2 Sample preparation

3.2.1 Spin coating

Silicon wafer with a defined oxide layer on the surface is used as the solid substrate for the thin hydrogel films. The silicon wafers are p-doped and purchased from Si-Mat with a diameter of 100 mm and a thickness of (525±25) μm. The precut substrates are placed in dichloromethane at 46 °C for 30 minutes, afterwards rinsed several times with Millipore water. Next, the substrates are put into a basic solution which contains 350 mL water, 30 mL H_2O_2 and 30 mL NH_3 at 76 °C for 2 h to remove organic traces. Then, the substrates are stored in Millipore water. Before spin coating, the substrates are throughly rinsed with Millipore water to remove all possible traces of the basic bath [146]. Compressed nitrogen is used to dry the substrates. Because of this cleaning protocol, a hydrophilic oxide layer with a thickness of 5 nm is present on the substrate [46, 128].

Thin PMDEGA and P(S-*b*-MDEGA-*b*-S) films are prepared by spin-coating (2000 rpm, 30 s) from 1,4-dioxane solution at room temperature (relative humidity 40 %) onto the pre-cleaned substrates. A series of solution concentrations are prepared to achieve the films with different thicknesses. The film thickness obtained is related with the selected rotation speed ω, the solution concentration C_0 and the molecular weight of the polymer M, which is described by equation 3.1 [147, 148].

$$d = a\left(\frac{1950\ rpm}{\omega}\right)^{\frac{1}{2}}\left(\frac{C_0}{20\ g/l}\right)\left(\frac{M}{100\ kg/mol}\right)^{\frac{1}{4}}. \tag{3.1}$$

In equation 3.1, the constant a is dependent on the spin coater used and the environment. The film thickness exhibits a linear dependence on the solution concentration. For instance, figure 3.3 shows the linear depencence of the PMDEGA based film thickness to the solution concentration. In the PMDEGA solution (figure 3.3a), the concentration varies from 1 mg/mL to 30 mg/mL, and the thickness obtained is in the range from 2 nm to 162 nm. Whereas in the P(S-*b*-MDEGA-*b*-S) solution (figure 3.3b), the concentration varies from 1 mg/mL to 15 mg/mL, and the thickness obtained is in the range from 3 nm to 82 nm. From the linear fitting, the constant a are calculated to 204 nm (PMDEGA solution) and 174 nm (P(S-*b*-MDEGA-*b*-S) solution).

The relation between the film thickness and the polymer solution concentration can be devided into three regimes [148]. In the first regime, the polymer concentration is very low. As there is not enough polymers in the solution, instead of homogeneous film, only

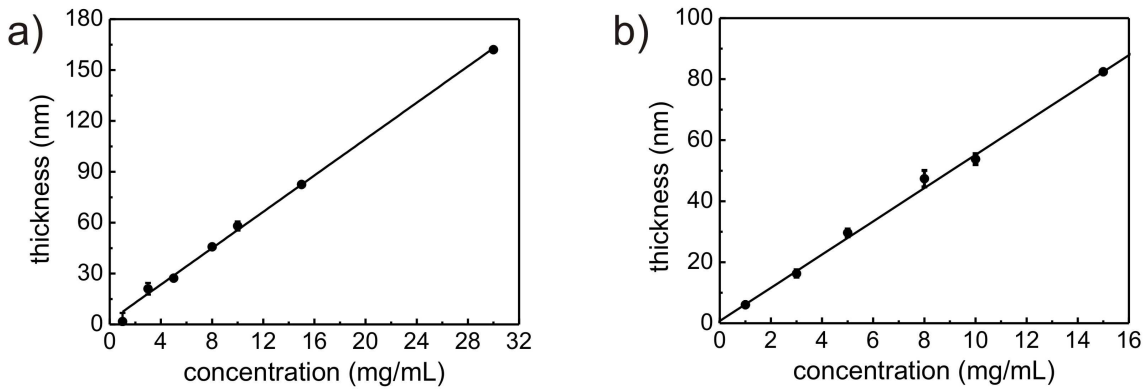

Figure 3.3: *Linear depencence of the film thickness to the solution concenration: (a) PMDEGA solution, (b) P(S-b-MDEGA-b-S) solution.*

the island like structure is obtained by spin coating. When the concentration increases, it comes to the second regime. Because there is enough polymer to entangle with each other in the solution, homogeneous films are obtained. Equation 3.1 can be used in this regime. Further increasing the concentration, the viscosity should be taken into consideration. Thus, equation 3.1 is no longer suitable to calculate the thickness. It still shows a linear dependence on the concentration, but with a increased slope. As seen in figure 3.3, both polymer concentrations are in the second linear regime in this investigation.

3.2.2 Solution casting

Solution casting is used to prepare thick P(S-*b*-MDEGA-*b*-S) films with thickness in μm scale. Kapton foil is used as a flexible substrate. The precut Kapton foil is placed in acetone, and rotated overnight to clean the possible impurities and dust on the foil. Afterwards, the Kapton foil is rinsed with Millipore water to remove possible traces of acetone. Before solution casting, the Kapton foil is dried with compressed nitrogen to remove remaining water from the foil.

P(S-*b*-MDEGA-*b*-S) is an amphiphilic block copolymer, which consists of a hydrophilic PMDEGA block in the center and two hydrophobic PS blocks on the outside of the PMDEGA block. Thus, when P(S-*b*-MDEGA-*b*-S) is dissolved in the solvent, it has the ability to self-assemble into micelles. Moreover, by choosing different selective solvents, micelles with different core-shell structure can be formed. The solvents used to prepare the solutions in this investigation are seperated into two groups. The frist group is the PMDEGA-selective solvents, which contains water, methanol (purity 99%) and ethanol

(purity 99.8%). Wheares the second group is the PS-selective solvents, which contains toluene (purity 99.9%), benzene (purity 99.5%), THF (purity 99.9%), dichloromethane (purity 99.9%) and 1,4-dioxane (purity 99.5%). The defination of the selective solvents is given in section 6.1.1. The concentration of the P(S-*b*-MDEGA-*b*-S) solutions is fixed to 60 mg/mL. All solutions are transparent and do not show any sign of aggregation. The obtained film thickness is 5 μm. Several identical films are prepared to prove reproducibility.

3.3 Measurement method

3.3.1 Optical microscopy

In order to assure the quality of the sample preparation and probe the surface structure in μm scale, the sample surfaces are observed with optical microscopy using a Zeiss Axiotech 25H optical microscope. By switching between four different objects, the magnifications is varied between 1.25x and 50x. A PixeLink S621CU CCD camera is used to record the micrographs.

3.3.2 Atomic force microscopy

A PARK Autoprobe CP atomic force microscope (Thermomicroscopes - Veeco, California, USA) is used to probe the sample surface at high resolution (nanometer scale). The atomic force microscope (AFM) has the advantage that it can measure almost any kinds of surface, such as polymers, ceramics, and biological samples. For this reason, AFM plays an important role to investigate the surface morphology of polymer films. The basic principle of AFM is presented in figure 3.4.

A gold covered, conically shaped silicon tip is mounted on the bottom side of a triangular silicon cantilever with a force constant of 2.1 N/m. The force between the tip and the sample surface depends on the spring constant of the cantilever and distance between the tip and the sample surface, which can be described by Hooke's law with the spring constant k. When the tip approaches to the surface, the cantilever is bend if the spring constant of cantilever is less than the surface. The deflection of the cantilever is detected by the laser beam system, where a laser is reflected from the back of the cantilever and onto a position-sensitive photodiode detector. The measured cantilever deflections are used to generate a map of the surface topography.

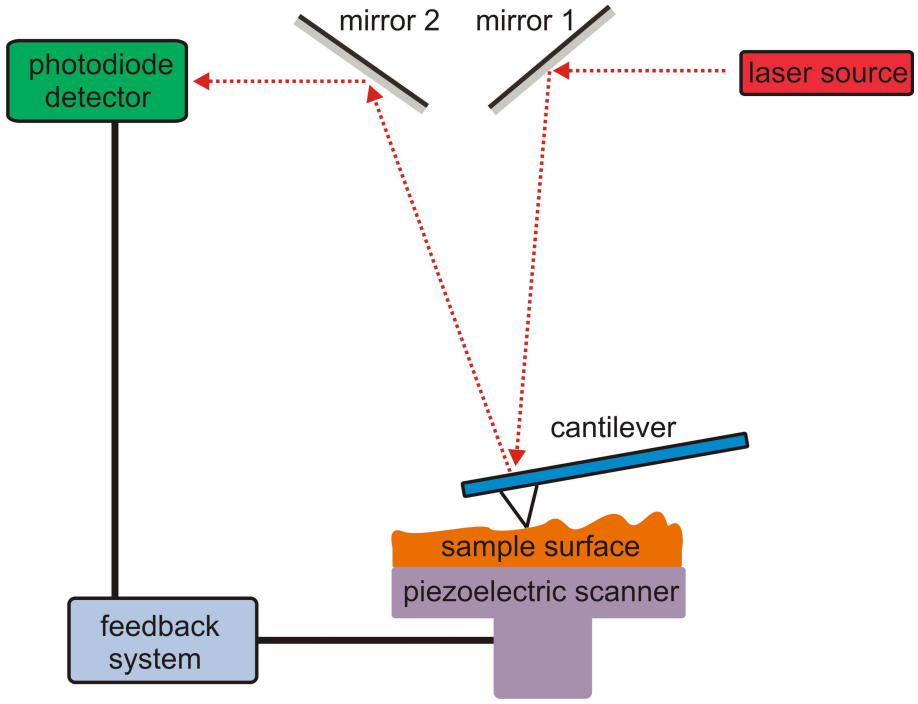

Figure 3.4: *Sketch of the basic principle of AFM.*

For the AFM used in the investigation, the tip is excited by a piezoelectric driver with a frequency of ω (around 60 KHz). The sample is moved horizontally below the tip, which is also controlled by a piezoelectric scanner. The sample-tip distance is less than 100 nm. During the measurement, the changes in amplitude, frequency and phase of the cantilever are detected and a feedback software controls the sample holder to keep the sample-tip distance constant. The software records these detected changes, and calculates the topography and phase images.

According to the sample-tip distance, the scanning modes in the AFM measurement can be divided into: contact mode, tapping mode and non-contact mode. In the investigation, the tapping mode is selected as the operating mode. During the measurement, the amplitude of the cantilever is kept as a constant. The excitation frequency is set above the resonant frequency. The tip still repeatedly touches the sample surface.

In the investigation, all measurements are performed at ambient conditions. At each individual sample position, scans with different ranges from 1×1 μm^2 up to 4×4 μm^2 are performed. The scanned rate varies from 0.25 Hz to 1.0 Hz. Each scanned micrograph consists of 256 lines. Several images are measured for each sample. From the raw data obtained, the background due to the scanner tube movement is fully subtracted to determine the values of the rms roughness over the complete scan area.

3.3.3 White light interferometry

Sample thickness and index of refraction (n) for optical wavelengths are measured with the Filmetrics F20 ThinFilm Measurement System (Filmetrics Inc., San Diego). By adjusting the distance between the sample and the light cable, the spot size of the incident white light beam varies from 500 μm to 1 cm in diameter. The wavelength used for obtaining the characteristic intensity oscillations in the measurement is in the region from 400 nm to 1100 nm.

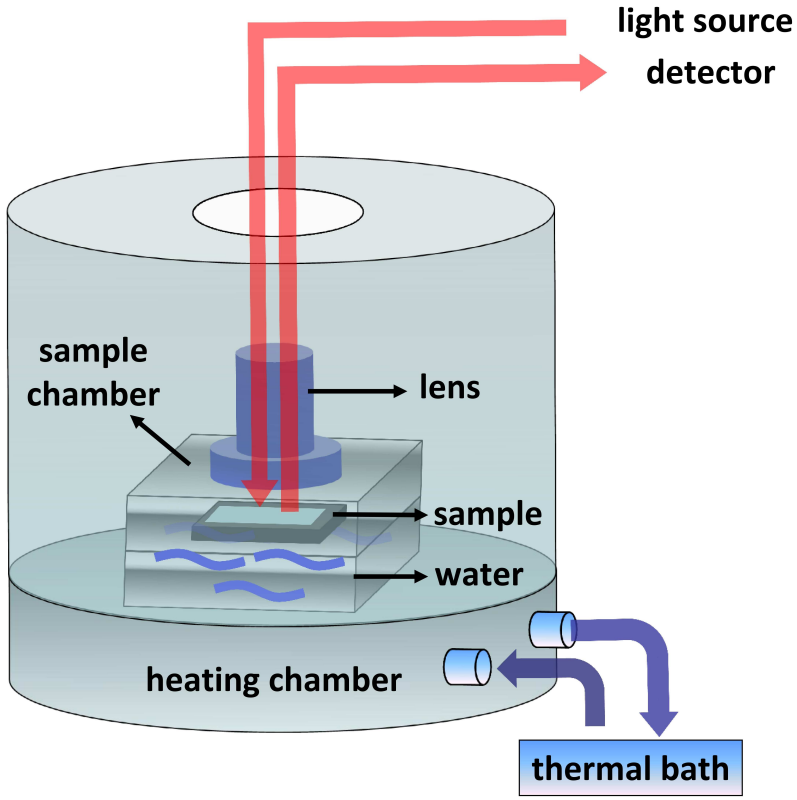

Figure 3.5: *Sketch of the setup for white light interferometry measurements.*

For the transition behavior measurements, an as-prepared film is mounted in water vapor atmosphere in a small aluminum sample chamber. In order to eliminate the condensation of vapor on the glass located on top of the sample chamber, another larger aluminum chamber (the heating chamber) is placed on the outside of the sample chamber. Thus, the whole system is called a double chamber system (see figure 3.5). During the measurement, the variation of the temperature is realized by the thermobar connected to the heating chamber. The white light beam is generated by the light source, and focused through the lens on top of the sample chamber to illuminate the sample with a

very large incident angle, approximately 90°. The reflected beam goes through another optical cable, and is monitored by the detector. As the light made multiple reflections between different parallel surfaces or interfaces, the multiple beams interfere with each other. According to Fresnel equation, this interference results in a net transmission and reflection amplitude depending on the wavelength of the incident beam. Thus, the reflection spectrum obtained shows a series of fringes, where the positions and amplitudes are related to the thickness and optical properties (n). By fiiting the spectrum with a model containing layers of different thicknesses, roughnesses and optical properties, the desired film thickness and optical property are obtained from the fits. Figure 3.6 shows a spectrum (black dots) of the as-prepared PMDEGA film together with fit (red line). As the film is only composed of PMDEGA, single layer model is applied in the fit. The film thickness and refractive index obtained are 38.3 nm and 1.52, respectively

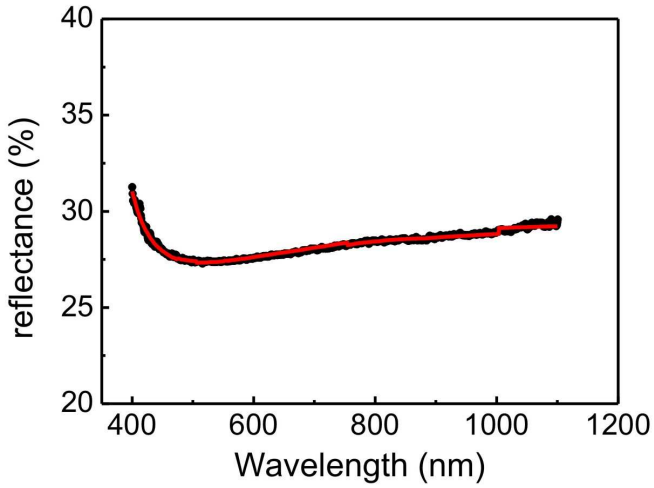

Figure 3.6: *A spectrum of the as-prepared PMDEGA film (black dots) together with fit (red line).*

3.3.4 X-ray reflectivity (XRR)

X-ray reflectivity curves are measured with a Siemens D5000 diffractometer using a reflectivity extension. The measurements are performed in air with a scintillation counter. The samples are fixed on the sample stage by vacuum. A tantalum knife edge is mounted above the sample surface to reduce background and to control the footprint of the X-ray beam on the sample. The measurements are performed at a wavelength of $\lambda = 0.154$ nm (secondary graphite monochromator, Cu Kα). The theory of XRR is discussed in detail in

section 2.3.2. Data are fitted by the program Parratt32 [149] using the Parratt algorithm [135]. To describe the XRR curves of the PMDEGA films, as there is only one component (PMDEGA) in the film, a single layer model is sufficient to fit the curves. In contrast in the P(S-*b*-MDEGA-*b*-S) films, because the film consists of two components with different refractive indices (PS and PMDEGA), a model with multiple layers is necessary to fit the XRR curves. The dispersion (δ) and absorption (β) values are fixed and matched with the values from literature, which are listed in table 3.1 [136]:

Type	δ [10^{-6}]	β [10^{-9}]
Si	7.57	1.75
SiO_2	7.12	9.24
PS	3.62	4.64
PMDEGA	4.18	5.68

Table 3.1: *The dispersion (δ) and absorption (β) values of materials used in this investigation.*

3.3.5 Small-angle X-ray scattering (SAXS)

SAXS experiments are performed in the beam line A2, HASYLAB at DESY in Hamburg, Germany. An X-ray beam with a wavelength $\lambda = 0.15$ nm and a size of 2×3 mm^2 is used. The detector is a MarCCD camera with a resolution of 1024×1024 pixels, which is mounted 2.51 m from the sample. A piece of lead is used as the beamstop to avoid destruction of the detector by the direct beam. The q range used for fitting is 0.015-0.21 Å^{-1}. The q calibration is performed using silver behenate standard.

The as-prepared thick P(S-*b*-MDEGA-*b*-S) film obtained from solution casting, is mounted between two pieces of Kapton foil in a sample holder with five sample positions. The temperature is controlled by a JUMO temperature controller and is measured by a thermocouple directly embedded in one of the sample cells. During the measurement, the as-prepared film is first measured for 600 s at room temperature. Afterwards, 0.3 mL of D_2O is injected into the sample holder, inducing the swelling of the P(S-*b*-MDEGA-*b*-S) film. Then the temperature-dependent measurements are carried out between 30 °C and 50 °C with steps of 2 °C. Each measurement takes 600 s subsequently with a waiting time of 600 s for equilibrium after each change of temperature. Additionally, the blank sample holder filled with D_2O is also measured.

During the data analysis, the 2D scattering pattern of the blank holder with D_2O

is first substracted from the obtained 2D scattering pattern of the film to remove the influence of the scattering from D_2O and holder. Afterwards, a mask is made on the 2D SAXS data to shield the beamstop and the abnormal scattering pattern on the top right corner. This abnormal scattering might result from background scattering at the beamline during the measurement. Finally, the intensity integration is performed on the 2D data with mask to convert the 2D image to a curve, in which the intensity is a function of the q value.

For the analysis of the SAXS curves, the NIST SANS package 7.02 implemented in the software IGOR Pro 6.1 is used [150]. The data are fitted by a model discussed in section 2.3.4. [28, 151].

3.3.6 Small-angle neutron scattering (SANS)

SANS experiments are carried out in the beamline KWS-2 at the FRM II in Garching, Germany. The neutron beam with a wavelength $\lambda = 0.7$ nm ($\Delta\lambda/\lambda = 20$ %) is used. The detector design is based on a modified Anger technology with a ^{6}Li glass as a scintillator [152]. During the meaurement, the sample-detector distances (SDD) is chosen to 2 m and 8 m. Thus, the resulting q covers the range of 0.049-0.45 nm^{-1} and 0.25-1.7 nm^{-1}.

To compare the resulting transition behavior of the thick P(S-*b*-MDEGA-*b*-S) films probed by SAXS and SANS measurements, the identical protocol used in the SAXS measurements is applied in SANS measurements as well. The model and the software used for analysis are also the same as described in section 2.3.4 and section 3.3.5, respectively.

3.3.7 Grazing incidence small-angle X-ray scattering (GISAXS)

GISAXS measurements are carried out in the beam line BW4 of the DORIS III storage ring at DESY in Hamburg, Germany [153]. The selected wavelength is $\lambda = 0.138$ nm. The beam divergence in and out of the plane of reflection is set by two entrance cross-slits. To operate a micro-beam, the X-ray beam is moderately focused to the size of (H×B) 40×80 μm^2 by using an assembly of refractive beryllium lenses [154]. The sample is placed horizontally on a goniometer. A beam stop is used to block the direct beam in front of the detector (MARCCD, 2048×2048 pixels). A second, point-like moveable beam stop is also used to block the specular peak on the detector. The incident angle is set to $\alpha_i = 0.35°$ for the as-prepared PMDEGA film and the P(S-*b*-MDEGA-*b*-S) films with different thermal treatments, whereas $\alpha_i = 0.365°$ for the PMDEGA film after exposed to water vapor. Both incident angles are well above the critical angles of PMDEGA (0.149°)

and silicon (0.20°), therefore instead of total refletion, the X-ray beam penetrates into the film. At the chosen sample-detector distance of 2.22 m (for the as-prepared PMDEGA film and the P(S-*b*-MDEGA-*b*-S) films with different thermal treatments) and 1.99 m (for the PMDEGA film after exposed to water vapor), the Yoneda and the specular peak are well separated on the detector [144, 155, 156, 157]. Thus, both the surface and the internal structure of a film are probed. According to the two dimensional GISAXS pattern, structural information is obtained from vertical and horizontal cuts of the 2d intensity distribution [157]. The vertical cut at $q_y = 0$, called detector cut, contains the information of the structure perpendicular to the surface. The intensity of the q_y-cuts is integrated over a small slice Δq_z in the vertical direction to achieve an improved statistics [157]. The detail for the analysis of GISAXS data is described in section 2.3.5.

3.3.8 Neutron reflectivity

The neutron reflectivity measurements are performed at the D17 reflectometer at ILL Grenoble in the time-of-flight (TOF) mode. The experimental setup of the neutron reflectivity is presented in figure 3.7.

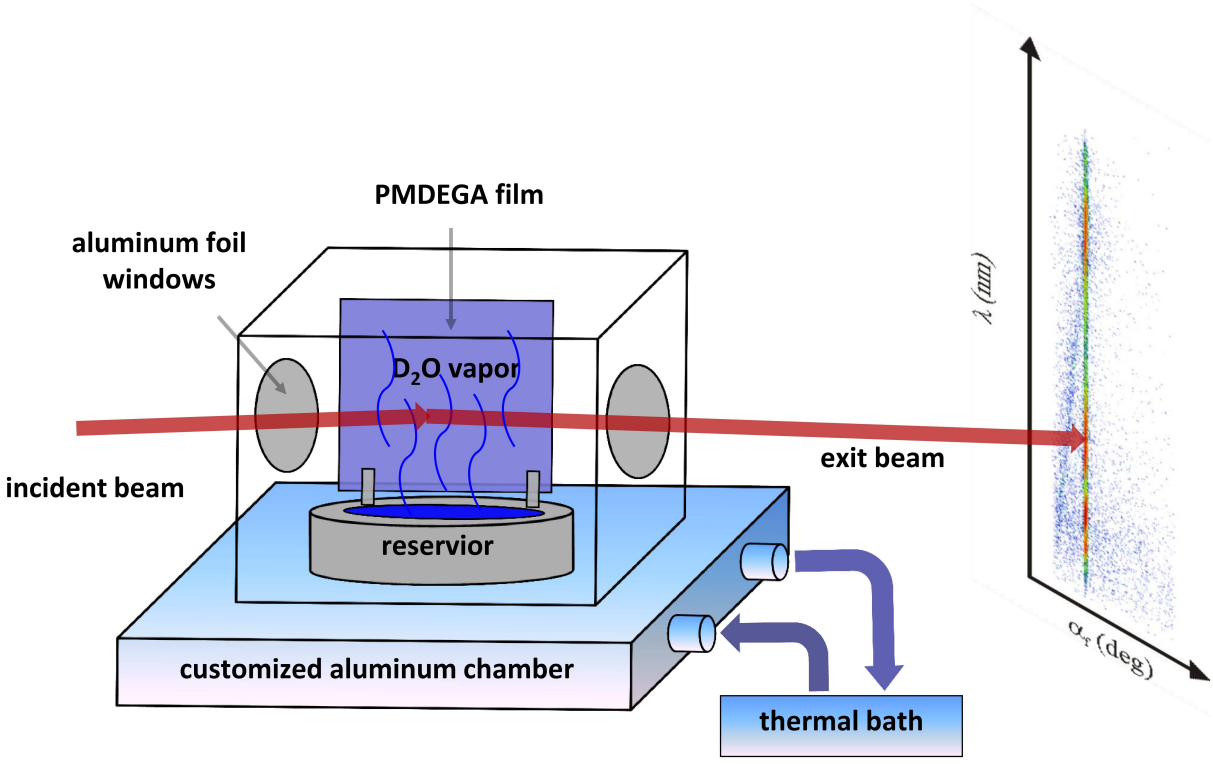

Figure 3.7: *Sketch of the experimental setup for the neutron reflectivity.*

A broad range of wavelengths λ (varies from 2 Å to 24 Å) is used simultaneously for TOF mode and neutrons are registered at the detector as a function of their respective time of flight. The necessary pulsing of the beam is realized by a double chopper system [158]. The largest sample-detector distance of 3.4 m is used in the measurements. The scattered intensity is recorded on a 2D detector. The two dimensional scattering pattern is shown as a function of wavelength [158].

The selected TOF mode, in combination with an experimental instrument resolution, optimized to the thickness of the probed thermo-responsive polymer films, allows the detection of kinetic changes of hydrogel films during the swelling process and during the collapse transition of the swollen film with a high time resolution. Neutron reflectivity scans are performed at one fixed incident angle every 20 s. The as-prepared films are measured with a longer time (7200 s) to obtain a well defined starting condition for the switching kinetics. The probed q_z range varies from 0.01 $Å^{-1}$ to 0.1 $Å^{-1}$, which is selected to cover the critical edges of protonated (Si, PS and PMDEGA) and deuterated (D_2O) substances. All reflectivity curves are fitted by the Motofit software [159]. In the automated batch fit approach of this software, it is possible to analyze all the datasets in series. The scattering length density (SLD) values are fixed from the fit of the initial static sample, and matched with the values from literature, which are listed in table 3.2 [160].

Type	SLD value [$Å^{-2}$]
Si	2.07×10^{-6}
SiO_2	3.47×10^{-6}
PS	1.42×10^{-6}
PMDEGA	1.06×10^{-6}
D_2O	6.36×10^{-6}

Table 3.2: *SLD values of materials used in this investigation.*

During the neutron reflectivity measurement, an as-prepared PMDEGA or P(S-*b*-MDEGA-*b*-S) film is mounted vertically in the customized aluminum chamber (see figure 3.7). Before the neutron reflectivity measurements are carried out, 8 mL D_2O are injected into the water reservoir of the pre-evacuated chamber to install an unsaturated D_2O vapor atmosphere surrounding the film (relative humidity of 79 %). Initially, the temperature is thermostated to 23 °C. Due to the D_2O vapor atmosphere inside the chamber, the film absorbs D_2O and starts to swell. The swelling process reaches its equilibrium state after 300 min. To start the kinetic measurement, a sudden change of temperature is applied

on the chamber. The temperature is increased from 23 °C to 45 °C. Thus, the final temperature is well above the LCST of PMDEGA (39 °C) and P(S-*b*-MDEGA-*b*-S) (36.5 °C) films. This increase of temperature marks the starting point of the switching kinetics (time = 0). Due to the thermal conductivity of the sample chamber, the LCST is passed after 110 s. During the whole time, the sample is monitored by in-situ neutron reflectivity. In addition, to understand the response of the swollen films to different thermal stimuli (above or below the LCST), a second experiment is performed. The temperature is increased from 23 °C to 35 °C. As a consequence, the final temperature is below the LCST of the PMDEGA and P(S-*b*-MDEGA-*b*-S) films. By analyzing the response of the film to the thermal stimulus below or above the LCST, the characteristics of the transition behavior of the PMDEGA based thermo-responsive polymers are obtained.

Time-of-flight mode

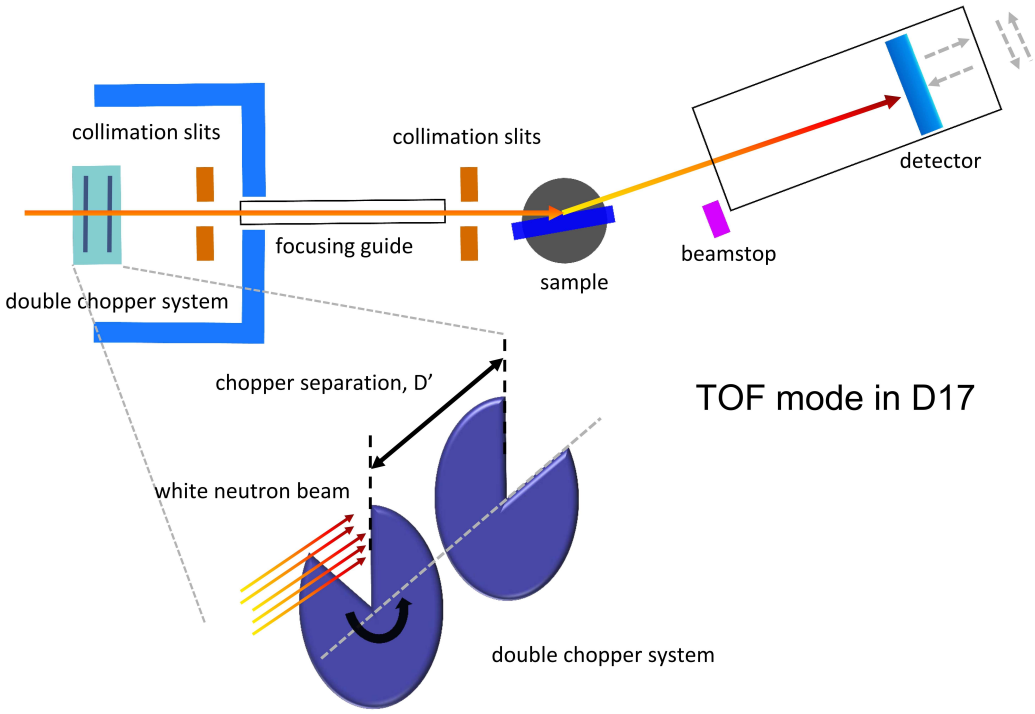

Figure 3.8: *Representative sketch of the TOF mode in neutron scattering measurement.*

In neutron scattering measurements, time-of-flight (TOF) mode is widely used. As the TOF mode can simultaneously measure an entire order of magnitude in a large q range in less than one minute, it is suitable for kinetic measurements [158]. A representative sketch of the TOF mode in neutron scattering measurement is shown in figure 3.8.

The white neutron beam from the reactor firstly passes through a double chopper system to realize the pulsing of the neutron beam. Figure 3.8 presents the detail for the double chopper system in the zero-phase configuration. The two choppers rotate in the same direction with the same speed. When the beam passes the gap on the first chopper and fly over the distance between the two choppers (D'), the gap on the second chopper just rotates to the open position to allow the neutron to pass. At the same time, the gap on the first chopper rotates to closed position. Thus, by the simultaneous open of the second gap and close of the first gap, a neutron pulse containing all wavelength is obtained. The wavelength resolution ($\Delta\lambda/\lambda$) can be described by equation 3.2:

$$\frac{\Delta\lambda}{\lambda} = \frac{\Delta t}{t} = \frac{D'}{D}. \tag{3.2}$$

In equation 3.2, Δt is the pulse width, and D is the distance from the second chopper to the detecotr. It is clear that $\Delta\lambda/\lambda$ is constant for all wavelength, and only depend on the ratio of D' and D. After passing the chooper system, the pulsed beam is focused and illuminate the sample. The scattered beam goes through the detector tube and recorded by the detector as a function of their respective time of flight.

3.3.9 ATR-FTIR

Bound Water in the PMDEGA and P(S-*b*-MDEGA-*b*-S) films is measured by attentuated total reflectance Fourier transform infrared spectroscopy (ATR-FTIR) using a JASCO FTIR-4100 spectrometer. The scaned wavelength covers a range from 650 cm^{-1} to 4000 cm^{-1}. To ensure identical conditions to the neutron reflectivity experiment, the water vapor treatement is performed in the customized aluminum chamber following the same thermal stimulus protocol used in the neutron reflectivity experiments (described in section 3.3.8). In the following, the FTIR and ATR are briefing.

Fourier transform infrared spectroscopy (FTIR) is an analytical method to identify organic substances. FTIR detects the vibration characteristics of chemical functional groups in a sample [161, 162]. Figure 3.9 exhibits the main components of the FTIR device. The IR-source generates an infrared light. Afterwards, the infrared light goes through the splitter and mirrors. When it transmits through the sample, the chemical bonds inside will stretch, contract and bend. Therefore, the absorbed infrared radiation can be correlated to a particular chemical functional group. The absorbed wavelength is independent of the structure of the rest of the molecule. The transimitted infrared light is recorded by a detector. Because the signal from the detecotr is an interferogram, it

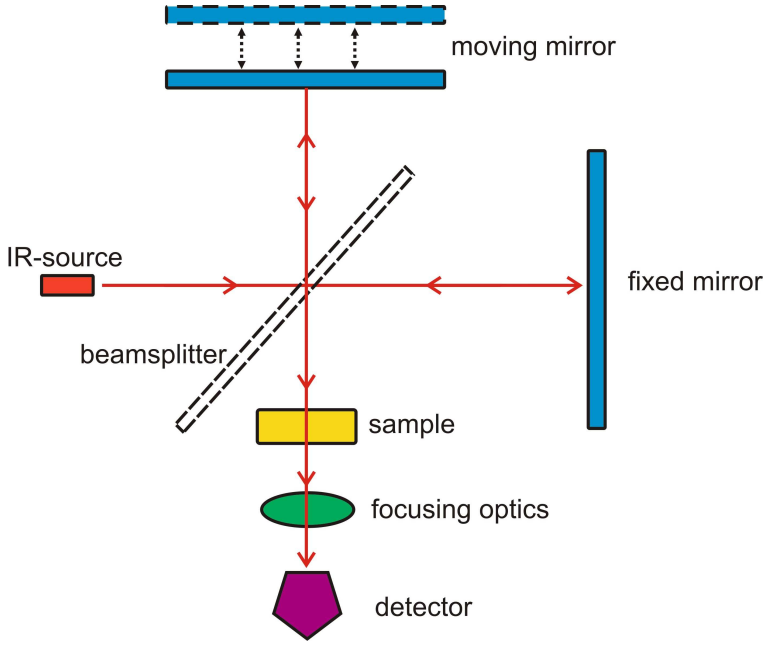

Figure 3.9: *Sketch of the main components of the FTIR device.*

need to be analyzed by Fourier transforms to obtain a single-beam infrared spectrum. In FTIR spectrum, the intensity is usually plotted as a function of wavenumber (cm^{-1}), which is the reciprocal of the wavelength. The intensity is described by the percentage of infrared light transimittance or absorbance at each wavenumber. Thus, by comparing the band wavenumber obtained to the standard infrared bands, a specific functional group in a sample can be identified. For instance, the C-O stretching is around 1100 cm^{-1}. Therefore, when a band at 1100 cm^{-1} is observed in the spectrum, meaning that there are C-O bonds in the sample.

In some cases, because the samples are thick or have a strong absorption of infrared light, the FTIR with transmission mode does not work. For this reason, attentuated total reflectance Fourier transform infrared spectroscopy (ATR-FTIR) is developed. Besides measuring the thick samples or samples with high absorption, due to the fact that the penetration depth of infrared light in ATR-FTIR is only several micro meters, it is also suitable to analyze the surface of the sample [163]. During the ATR-FTIR measurement, the sample is placed on top of the ATR crystal (figure 3.10).

By pressing the sample, it has a good contact with the top surface of the crystal. The infrared light enters into the crystal with a highly refractive index. Thus the light can reflect between the sample and the crystal several times before it leaves the cystal. The penetration depth of the infrared light into the sample depends on the wavelength of the

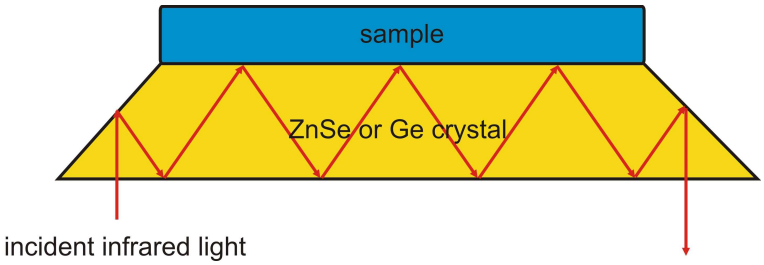

Figure 3.10: *Sketch of the ATR-FTIR geometry.*

incident infrared light λ, and is described by equation 3.3:

$$d_P = \frac{\lambda}{2\pi\sqrt{n_1^2 sin^2(\theta) - n_2^2}}. \tag{3.3}$$

θ is the incident angle, n_1 and n_2 are the refractive indices of the crystal and the sample, respectively. From equation 3.3, it is obvious that the depth of penetration can be controlled by selecting crystals with different refractive index or varing the incident angle of the infrared light.

Chapter 4

Thin PMDEGA films

In this chapter, the main focus is on the structure and thermal responsive behavior of thin PMDEGA films. For this reason, thin PMDEGA films, prepared by spin coating, are first investigated with respect to the surface and internal structure. Then, the as-prepared thin films are exposed to a water vapor atmosphere to study the swelling behavior. Afterwards, the temperature is increased above the LCST to investigate the responsive behavior of the films to a thermal stimulus. Finally, the bound water in the swollen and collapsed films is measured to understand the formation of the hydrogen bonds in the films. The results presented in this chapter have already been published in [46, 128].

4.1 Structural investigation of thin PMDEGA films

In this section, the structure of thin PMDEGA films is investigated. The as-prepared PMDEGA films are first measured by X-ray reflectivity to obtain the film thickness and roughness. According to the images obtained by optical microscopy and atomic force microscopy (AFM), the thin films exhibit a smooth, homogeneous surface both on the large and local scale. However, when the homogeneous thin films are stored in ambient conditions, a dewetting is observed on the surface, which is attributed to the low glass transition temperature (T_g) of PMDEGA. To further study the dewetting behavior, time-dependent surface structures are measured by optical microscopy. Also, AFM is used to measure the films to compare the difference between the as-prepared and aged films. Moreover, since optical microscopy and AFM can only approach the surface structure, grazing incidence small-angle X-ray scattering (GISAXS) is performed on the as-prepared films and films with different thermal stimuli, to investigate the internal structure.

4.1.1 Surface structure of thin PMDEGA films

With the base cleaning applied and via spin coating, smooth and homogeneous PMDEGA films are prepared on Si substrates. Probed by optical microscopy and atomic force microscopy, no heterogeneities are found in the as prepared films with thicknesses above 10 nm. Figure 4.1 shows the surface of the as prepared PMDEGA film with a thickness of 40.2 nm as seen with optical microscopy. The film is homogeneous on a very large surface area. As observed with AFM, the film is homogeneous on a local scale as well (see figure 4.2). There are no visible large defects on the surface. Locally, it has a peak-to-valley surface roughness below 1 nm as determined from the AFM data.

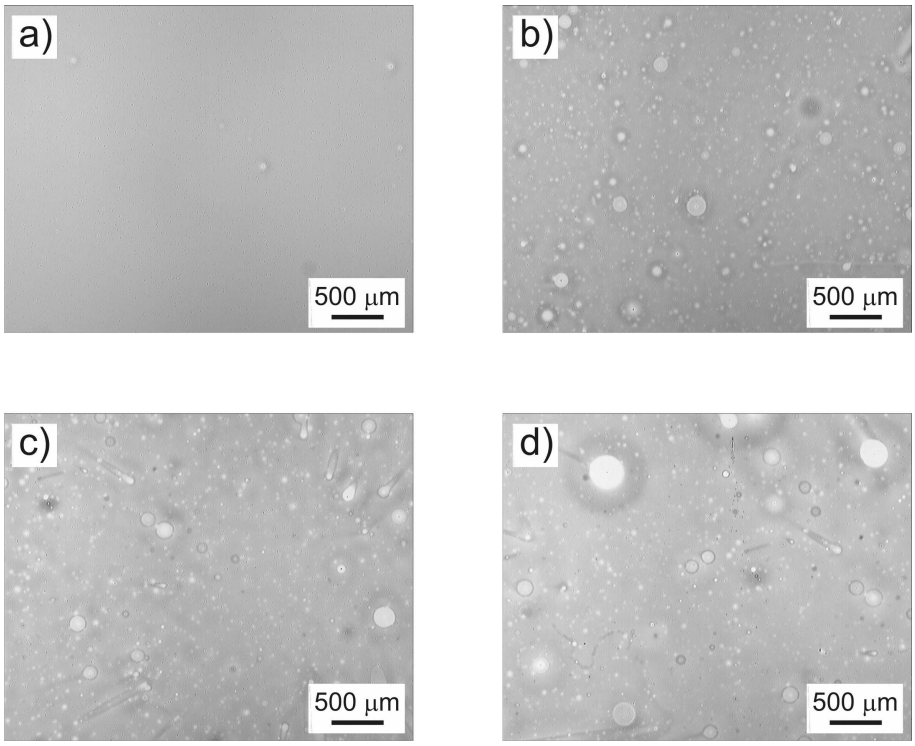

Figure 4.1: *Optical micrographs of PMDEGA film (40.2 nm thickness): (a) as prepared, (b) after 1, (c) 2 and (d) 6 days storage in air under ambient conditions. (The micrographs are measured with a magnification of 2.5 and show an area of 4096×3276.8 μm^2.)*

With X-ray reflectivity (XRR), the film thickness and roughness are obtained. Figure 4.3 shows the measured XRR curves for PMDEGA films of different film thickness together with fits. As the films are prepared from pure PMDEGA, a single layer model is used for the fitting. A film thickness regime from 2 nm to 162 nm is covered in this investigation. In general, within the applied fitting model, the data are well described. The intensity modulation (Kiessig fringes) in the data of the thinnest PMDEGA film (2 nm) is damped,

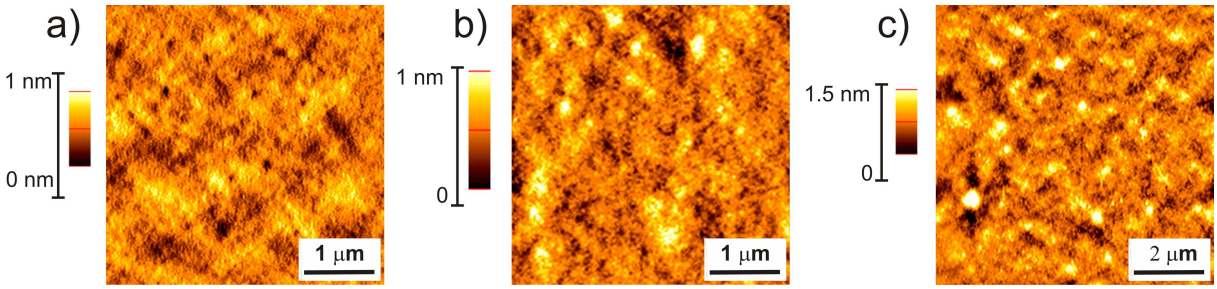

Figure 4.2: *AFM micrographs of thin PMDEGA films (40.2 nm thickness): (a) as-prepared, (b) after swelling in water vapor and (c) after 6 days storage in air under ambient condition (measured on a homogeneous spot). The color code for the heights is individually adapted to emphasize on the surface morphology.*

which is attributed to the imperfections of the PMDEGA layer. Instead of a continuous and homogenous layer of PMDEGA on the Si substrate, the PMDEGA forms islands on it. The PMDEGA islands cause a large surface roughness and result in damped fringes in the XRR curve. When the PMDEGA concentration increases, continuous films are obtained on Si from 1,4-dioxane solutions. Overall, the intensity modulations are well pronounced in the XRR curves due to a small surface roughness (nm regime) of the PMDEGA films.

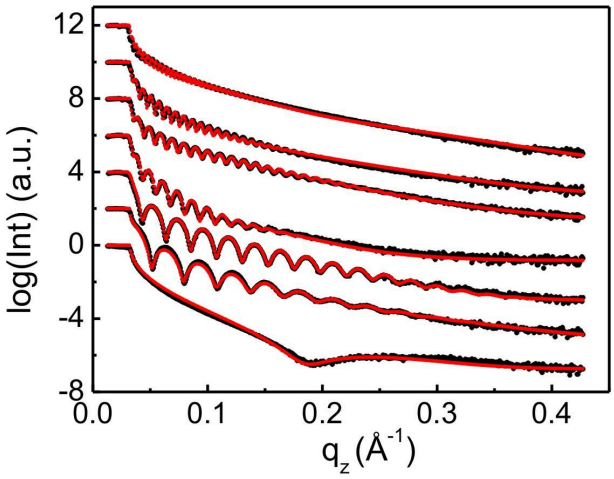

Figure 4.3: *Representative X-ray reflectivity curves (black dots) shown together with model fits (red lines) for the thickness regime covered in this investigation. With increasing film thickness (2, 21, 27, 46, 58, 83, and 162 nm from bottom to top), the curves are shifted vertically for clarity of the presentation.*

In figure 4.4a, the resulting film thicknesses are shown as a function of PMDEGA

concentration in the 1,4-dioxane solutions used for spin coating. The solid line is a linear fit of the data points. It fits the data points well. Figure 4.4c presents the film roughness as a function of PMDEGA concentration. For the lowest concentration, the surface is very flat. The roughness is only 0.5 nm. When the concentration increases, the surface becomes rough. But even on the highest concentration, the roughness is still less than 2 nm. Thus, it is concluded that the overlap concentration is not reached in the addressed concentration regime, and the PMDEGA solutions behave like simple homopolymer solutions in the spin coating process [147, 148].

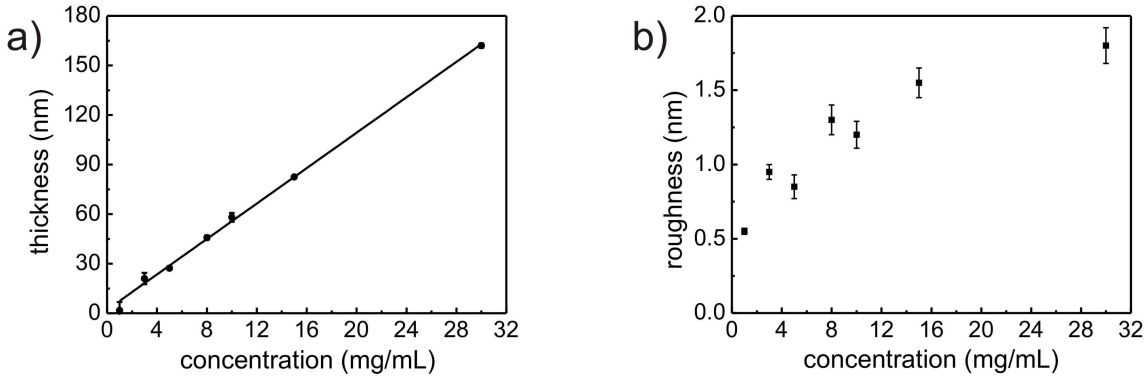

Figure 4.4: *(a) Film thickness and (b) surface roughness plotted as a function of the PMDEGA concentration used for spin-coating. The solid line in (a) is a linear fit.*

All XRR measurements are performed on as-prepared PMDEGA films. During storage in ambient conditions, the films roughen as illustrated with optical micrographs. As an example for this aging, optical images of a film with a thickness of 40.2 nm are shown in figure 4.1 for different storage times. For other PMDEGA film thicknesses, a similar behavior is observed. The as prepared film is optically homogeneous with only very few distortions, which are presented here to illustrate that the polymer surface is in the focal plane of the optical microscopy. An onset of dewetting is visible already after 1 day storage (see figure 4.1). Very clearly, holes of different diameters are seen in the polymer film. The broad distribution of hole diameters indicates a nucleated dewetting process with grains of different nucleation strength being embedded in the PMDEGA film and acting as nucleation sites. Impurities such as dust particles can be excluded due to applied filtering of the solutions used for spin coating. The holes grow with time and a further roughening of the film occurs (see figure 4.1c and figure 4.1d). However, a complete destruction into isolated polymer drops is not found. Thus, the PMDEGA films are not unstable on the base treated Si surfaces, but metastable and are only partially destroyed

in the areas influenced by the non-swollen nucleation sites [164].

A corresponding dewetting behavior was not observed in the PNIPAM based thermo responsive films [43, 44, 45] on identically treated Si surfaces. At first glance, this might be caused by the strong differences in the glass transition temperatures T_g. T_g of PMDEGA is -50 °C, which is well below room temperature [165], whereas T_g of PNIPAM is 142 °C, which is well above room temperature. As a consequence, PMDEGA chains have a sufficiently high mobility on base treated Si, whereas PNIPAM chains do not have this mobility.

4.1.2 Internal structure of thin PMDEGA films

In the previous discussion, the focus is put on the surface morphology of thin PMDEGA films, whereas the internal structure is still not clear. To clarify this question, the long-ranged correlation in thin PMDEGA films is investigated.

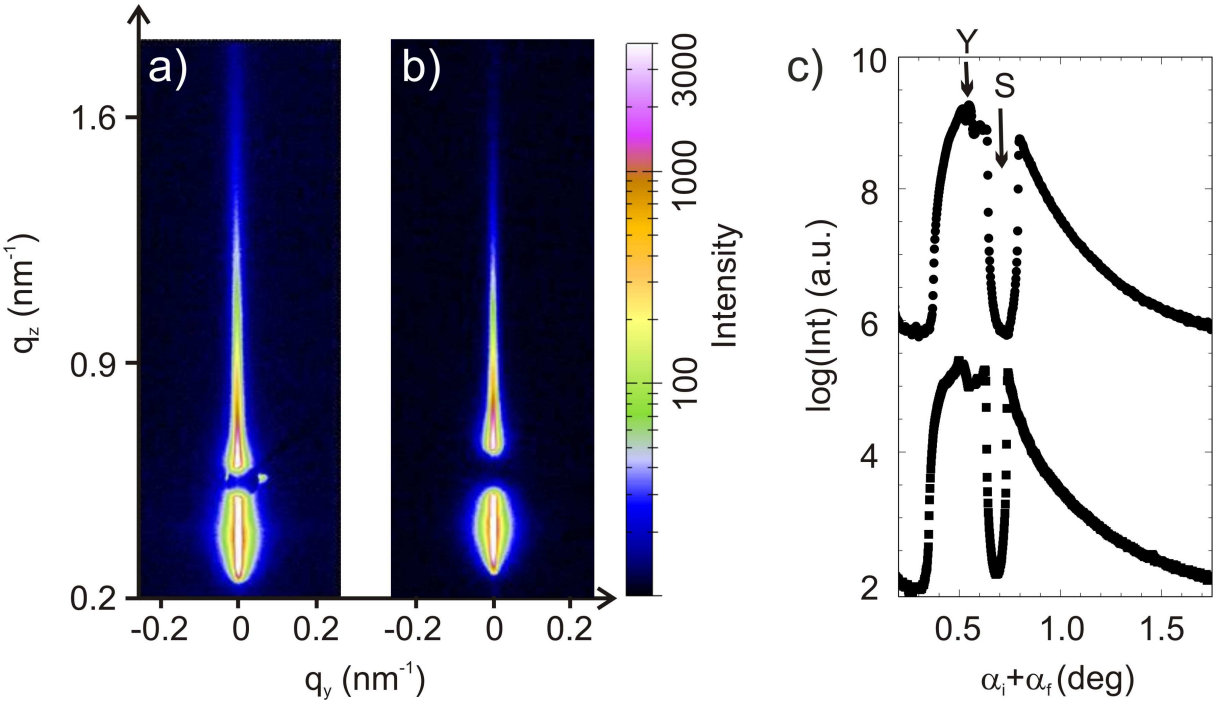

Figure 4.5: *GISAXS data of a thin PMDEGA film with a thickness of 40.2 nm: two dimensional data of (a) the as-prepared film, (b) the film after exposure to water vapor and (c) vertical cuts from these two dimensional data at q_y=0 with Yoneda (Y) and specular (S) peaks indicated (as-prepared film at the bottom and film after exposure to water vapor at the top).*

Using grazing incidence small-angle X-ray scattering (GISAXS), these correlations along the surface normal can be probed [142, 143, 166]. In case the chains are close to immobile in the thin polymer film, a roughness correlation between the solid support and the polymer surface is installed by spin coating. This correlated roughness has been found in many galssy polymers [166]. Being energetically unfavorable for the polymer chain, this correlation is cured if the polymer is sufficiently mobile. In a GISAXS measurement, correlated roughness causes intensity modulations along the vertical direction (q_z axis) due to partial phase coherence of diffusely scattered waves [142].

In figure 4.5, the GISAXS data of a PMDEGA film with a thickness of 40.2 nm are presented together with corresponding vertical cuts. Results from the as-prepared film and film exposed to water vapor atmosphere are compared. Obviously, no intensity modulations is found in the vertical cuts. Only the Yoneda and specular peak are visible, even though the resolution of the setup is highly sufficient to resolve possible modulations. Thus, the as-prepared PMDEGA film has already had sufficient mobility to cure the long ranged correlation installed from spin coating. For this reason, there is no correlated roughness found in thin PMDEGA films. However in PNIPAM films, strong intensity modulations were observed [43], which proves that the PNIPAM films are glassy and frozen-in after spin coating.

4.2 Swelling behavior of thin PMDEGA films

In this section, by applying white light interferometry, the swelling behavior of thin PMDEGA films is measured at different vapor pressures. With increasing the vapor pressure, the swelling capability of the thin film is also enhanced. Due to the high resolution of neutron reflectivity, the swelling process of thin PMDEGA films can be probed in more detail and by this can be divided into two regimes. In the first regime, water will occupy all vacancies and holes in the film, resulting in a constant film thickness while the water content in the film is dramatically increasing. Afterwards, water will start to form hydrogen bonds with PMDEGA chains. Thus the film thickness begins to increase with time.

4.2.1 Swelling capability of thin PMDEGA films

The swelling capability of thin PMDEGA films is investigated by white light interferometry. The PMDEGA films are placed in a sealed chamber which contains a water reservoir

to install a saturated vapor atmosphere. The swelling behavior of PMDEGA films at room temperature is shown in figure 4.6a for an example. The film thickness is 41.9 nm. The relative change in film thickness is monitored as a function of time. By varing the concentration of aqueous sodium chloride solutions, different water vapor pressures are installed in the chamber. During the measurement, the as-prepared PMDEGA films are placed in the chamber for each concentration. Thus, the swelling behavior at different water vapor pressures is investigated.

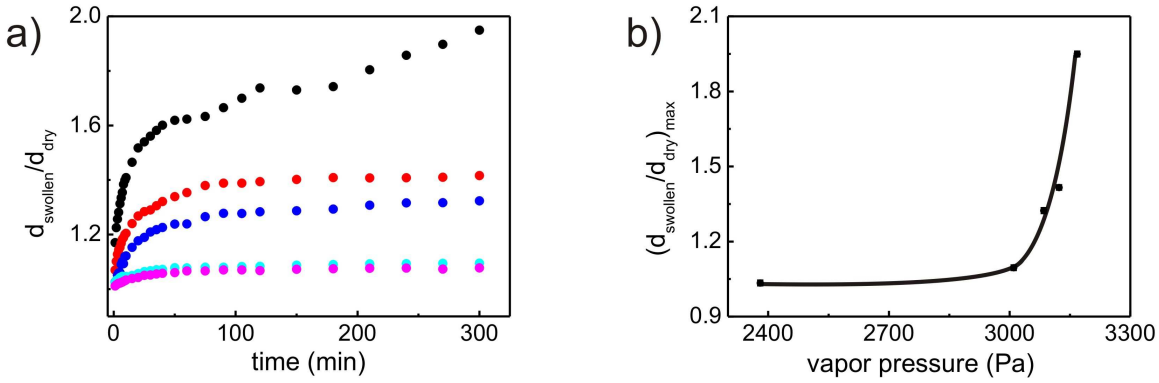

Figure 4.6: *(a) Swelling behavior of PMDEGA films when exposed to sodium chloride solutions with different concentrations. From top to bottom, the concentrations of the sodium chloride solution are 0 (black), 0.045 g/mL (red), 0.09 g/mL (blue), 0.18 g/mL (cyan), 0.36 g/mL (magenta). (b) Ratio of the maximal reached swollen PMDEGA film thickness normalized to the initial dry film thickness as a function of the vapor pressure. The solid line is guide to the eye.*

In figure 4.6a, from the top to the bottom, the concentration of sodium chloride solution increases from 0 to 0.36 g/mL, indicating that the water vapor pressure decreases from 3169 Pa (0 g/mL) to 2380 Pa (0.36 g/mL). At 3169 Pa, the strongest swelling is observed. Equilibrium is reached after 60 min. After this exposure time, films are still homogeneous but slightly roughened as probed with AFM (see figure 4.2). The peak-to-valley surface roughness increases to values above 1 nm. Further increasing the exposure times to longer than 70 min, the swollen film reaches an instable state, and dewetting sets in. In the white light interferometry measurement, the dewetting is observed as a further increase in the film thickness, which is attributed to the film heterogeneities. Because the PMDEGA film has already incorporated water during the initial swelling, the polymer chain mobility is further enhanced compared to the as-prepared films. As a consequence, the dewetting process happening in the dry film under ambient conditions

in days is accelerated to hours in the swollen film.

When the vapor pressure is reduced, the swelling ability of the films also decreases. The tendency of the films to dewet is also less pronounced. Therefore the swelling capability of the investigated PMDEGA films depends on the surrounding vapor pressure. Figure 4.6b summarizes this behavior by plotting the swelling capability (swollen film thickness normalized to the as-prepared film thickness of the respective PMDEGA film) as a function of the vapor pressure. The film thickness of the swollen PMDEGA film depends on the water vapor pressure in a strongly non-linear way. At high vapor pressures (3000 Pa - 3169 Pa), the swelling capability is very sensitive to the vapor pressure. A slight reduction of the pressure induces a dramatically drop of the swelling capability. For this reason, it is defined as pressure sensitive region. Upon further reducing the vapor pressure from 3000 Pa to 2380 Pa, the swelling capability shows less strong dependence on the vapor pressure. Due to the insufficient amount of water molecules present surrounding the PMDEGA film, the film can not reach the full swelling capacity. This region is defined as vapor insensitive region.

Until now only few swelling experiments with thin PNIPAM films were reported in literature, and most of them were related to end-grafted PNIPAM [87, 167, 168]. Comparing the swelling behavior of PMDEGA with PNIPAM end-capped with n-butyltrithiocarbonate (nbc-PNIPAM), there is one prominent difference observed. The swelling capability of thin nbc-PNIPAM film can be up to a factor of 6.5 (the ratio of the maximum swollen film to the as-prepared film) [43], whereas for the PMDEGA the maximal swelling factor is only 1.63 [46]. This difference can be attributed to the different chemical structure of PNIPAM and PMDEGA. To PNIPAM, not only the amide group (H-donor), but also the ether group (H-acceptor) on the side chain can form hydrogen bonds with water. In contrast, there is only the ether group (H-acceptor) on the side chain in PMDEGA. Thus, the bound water in swollen PMDEGA film is much less than in swollen PNIPAM film. Furthermore, it is reported that water cage can be formed around isopropyl group on the end of the side chain in PNIPAM [169]. Thus PNIPAM can absorb more water. The swelling ability of thin PNIPAM film is better than thin PMDEGA film.

4.2.2 Swelling of thin PMDEGA films probed by neutron reflectivity

With white light interferometry, the swelling capability of thin PMDEGA films as a function of the vapor pressure is decided. However, the distribution of the water in the swollen

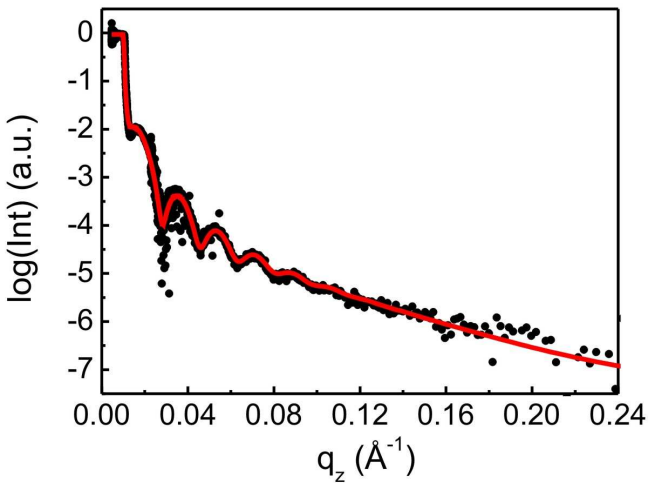

Figure 4.7: *Neutron reflectivity curve (black dots) together with the model fit (red line) for the as-prepared PMDEGA film.*

film during the swelling is not probed with this technique. For this reason, neutron reflectivity is applied to monitor the swelling process of thin PMDEGA films with a thickness of 36 nm. The as-prepared, dry PMDEGA film is measured first. Figure 4.7 shows the corresponding neutron reflectivity curve (black dots) together with the model fit (red line). Because the film is prepared from PMDEGA homopolymer, a simple one layer model is sufficient to fit the data. From the fit, the PMDEGA film thickness of 35.9±0.1 nm, a surface roughness of 0.9±0.2 nm and a SLD value of $(1.06\pm0.02)\times10^{-6}$ Å^{-2}, matching with literature, are determined. Thus, the initial properties of the film subjected to the swelling and the thermal stimulus are consistent with those from white light interferometry.

To set the starting conditions of the kinetic measurement and obtain the moderately swollen hydrogel film, 8 mL D_2O are injected into the reservoir of the customized aluminum chamber. Therefore the as-prepared, dry PMDEGA film is exposed to an unsaturated D_2O vapor atmosphere. In order to limit the film swelling, the relative humidity is controlled at 79%. Simultaneously, the structural changes of the PMDEGA film due to the absorption of D_2O are monitored with in-situ neutron reflectivity. Due to the deuterated water and protonated polymer applied in the measurement, there is an enhanced contrast in neutron reflectivity, which allows to determine the internal distribution of D_2O inside the PMDEGA film as well as the degree of swelling, i.e. the increase in film thickness. Figure 4.8 comprises the neutron reflectivity curves probed during the swelling of the PMDEGA film in D_2O vapor.

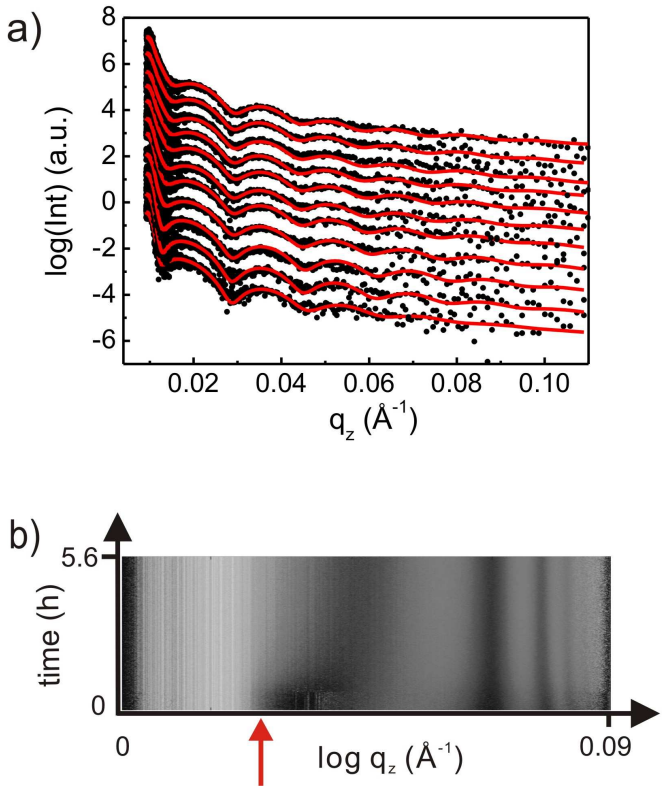

Figure 4.8: *Swelling of the as-prepared, dry PMDEGA film in D_2O vapor atmosphere at 23 °C: (a) Eleven selected neutron reflectivity curves (black dots) together with model fits (red lines). With increasing time the curves are shifted vertically for clarity of the presentation. (b) Two dimensional intensity presentation (mapping) of the specular neutron reflectivity curves versus time as a function of log(q_z). Different scattering intensities are displayed with different grey scale (brighter indicates high and dark low intensity).*

In Figure. 4.8a, eleven selected individual neutron reflectivity curves (black dots) together with model fit (red lines) are shown to illustrate that the intensity oscillations shift towards lower values of the scattering vector component q_z due to the incorporation of D_2O molecules. Again, the data are successfully fitted. In a mapping type of presentation of the neutron reflectivity data (Figure 4.8b), the overall reflected intensity increases, which is attributed to the strong scattering of D_2O absorbed by the PMDEGA film. Moreover, the critical angle of total reflection (marked by the red arrow) shifts towards higher q_z values with time, which is also related to the deuterated material (D_2O) incorporates into the protonated polymer (PMDEGA) film.

All observations show that thin PMDEGA film absorbs D_2O vapor, starts to swell and

thereby gets thicker. By fitting the individual neutron reflectivity curves, more details such as film thickness, roughness and SLD values of the film are determined during swelling. Furthermore, the D_2O volume fraction ($V\%D_2O$) is calculated from equation 4.1:

$$V\%D_2O = \frac{n - n_1}{n_2 - n_1} \times 100\%. \tag{4.1}$$

where n is the SLD obtained from the model fit, n_1 is the SLD of the as-prepared PMDEGA film and n_2 is the SLD of D_2O. Figure. 4.9 presents the resulting relative film thickness d/d_{dry} and the D_2O volume fraction ($V\%D_2O$) as a function of time.

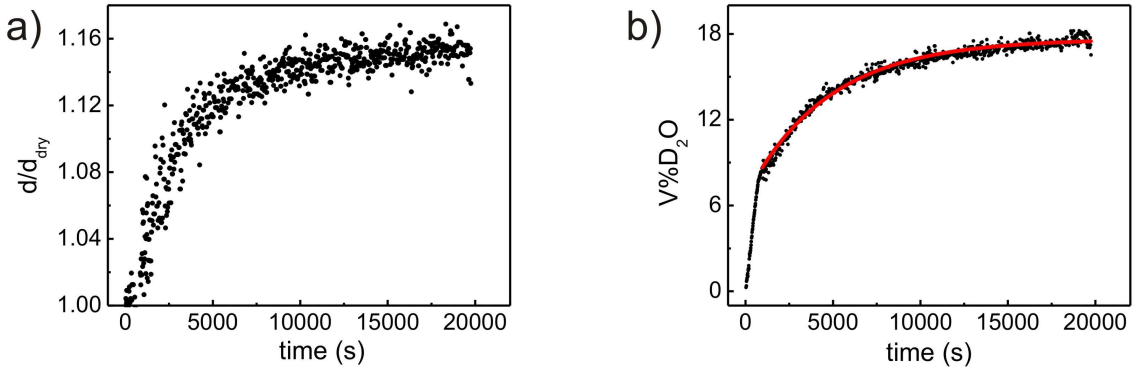

Figure 4.9: *Swelling of PMDEGA film at 23 °C: (a) Relative film thickness and (b) D_2O volume fraction ($V\%D_2O$) as a function of swelling time. The solid line is a fit of a model as explained in the text.*

When the swelling reaches an equilibrium state, the film thickness is only increased 15% in total, and a volume fraction of 18% D_2O is incorporated in the swollen film. Thus, a moderate swelling is successfully installed, accompanied with a limited uptake of water which is the pre-requisite to obtain gel-type films. The swelling process can be analyzed in more detail. As visible in Figure 4.9a, the swelling process can be divided into two regimes. In the first regime, from 0 s (D_2O is injected into the reservoir) to 1500 s, the thin PMDEGA film swells only weakly. The thickness increases from 35.9 nm to 36.6 nm, corresponding to an increase of only 2%. However, the D_2O volume fraction increases much stronger, namely from 0 to 9%. One possible reason for this discrepancy is the free volume present in the PMDEGA film. When the thin film is placed in the D_2O vapor atmosphere, vapor enters into the free volume of the PMDEGA film first. Because D_2O only fills the vacancies and holes, the film thickness does not significantly increase, i.e.

the film does not swell significantly. In the second regime, from 1500 s to 20000 s, due to the affinity of D_2O to the PMDEGA, the PMDEGA chains absorb water and swell. Correspondingly, both the film thickness and the water content increase with time. This second process can be described by a modified diffusion process using a model explaining gel swelling kinetics [170, 171, 172, 173]. In this model, swelling or shrinking follows first-order kinetics, and is not considered as a pure diffusion process, which can be described by equation 4.2:

$$ln\frac{V\%D_2O(\infty) - V\%D_2O(t)}{V\%D_2O(\infty)} = lnB - \frac{t}{\tau} \tag{4.2}$$

where $V\%D_2O(t)$ and $V\%D_2O(\infty)$ are the water uptake at time t and at infinite time (the equilibrium state of swelling), respectively [170, 171, 172]. B is the function related to the shear modulus and the osmotic modulus, and τ is the relaxation time. From the fitting model, $V\%D_2O(\infty) = 17.65\pm0.3$, $\tau = (4.7\pm0.1)\times 10^3$ s and B = 0.66±0.05 are obtained. When comparing to the values found recently for end-capped PNIPAM films [44], the response takes place on a comparable time scale, but is slightly slower.

4.3 Phase transition behavior of thin PMDEGA films

For a thermo-responsive polymer, the phase transition behavior is of most interest. To investigate the transition behavior, the as-prepared PMDEGA film is placed in a vapor atmosphere. After the swelling approaches its equilibrium state, the temperature is increased slowly in steps of 2 °C. Simultaneously, the transition behavior is monitored by white light interferometry. Until now, most studies of the thermo-responsive polymers focused on the transition behavior when the temperature increases slowly. But in some special applications, such as thermal sensors or switches, the temperature will increase dramatically in several seconds. In order to investigate the responsive behavior of thin PMDEGA films to a sudden thermal stimulus, neutron reflectivity measurements are performed.

4.3.1 Transition behavior probed by white light interferometry

For thermo-responsive polymer films, the transition behavior is chracterized by the change of the film thickness. White light interferometry is used to measure the temperature dependence of the film thickness in a water vapor atmosphere. Starting at 31 °C, which

is below the LCST known from bulk investigations, the as-prepared PMDEGA film is exposed to a water vapor atmosphere installed at a fixed salt concentration in the water reservoir of the chamber. The measured changes of the film thickness are shown in figure 4.10a for three different vapor pressures (installed by three sodium chloride solutions with different concentrations). Figure 4.10 compares samples with an equal initial film thickness of 41.9 nm. At a concentration of the sodium chloride solution of 0.023 g/mL (black in figure 4.10a), the PMDEGA film shows the strongest response, with the largest change in film thickness due to the chain collapse. The sodium chloride solutions with higher concentrations (0.045 g/mL and 0.09 g/mL) result in a weaker shrinkage and in a shift of the LCST to slightly higher temperatures. As a consequence, the decrease of the saturated vapor pressure causes the LCST to shift to higher temperature, while the transition becomes broader, which is more clearly seen from the first derivatives shown in figure 4.10b.

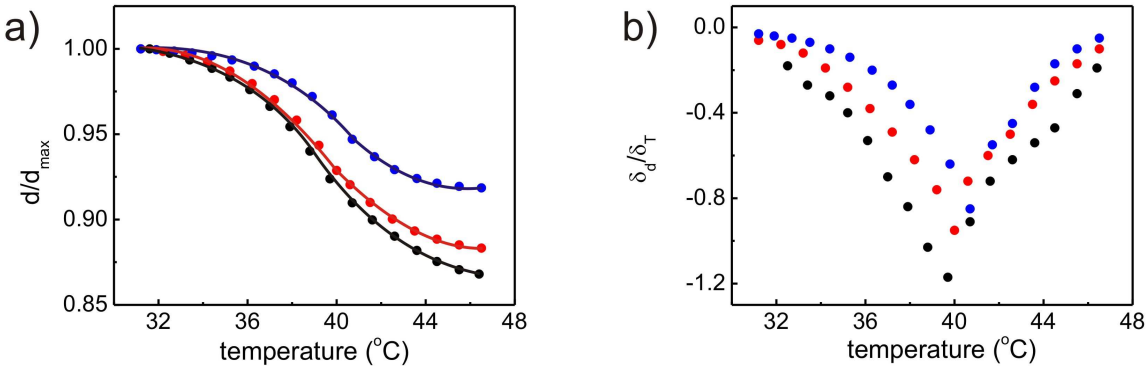

Figure 4.10: *(a) Temperature-dependent changes of the film thickness measured for PMDEGA films when exposed to sodium chloride solution with different concentrations of 0.023 g/mL (black), 0.045 g/mL (red) and 0.09 g/mL (blue). The solid lines are guides to the eye. (b) Corresponding first derivatives of these data.*

In general, all transitions appear broader as compared to the behavior measured for PNIPAM films. This phenomenon is not limited to a selected film thickness as figure 4.11 demonstrates. At a fixed value of the sodium chloride solution concentration (0.045 g/mL), the film thickness dependence of the transition temperature is determined. For film thicknesses between 17.4 and 422.6 nm, a broad transition is also observed. This variation is firstly attributed to the different amount of bound water formed in the polymer chains discussed in section 4.2.1. Additionally, as the side chains of PMDEGA are very large, more time is required to form or break the hydrogen bonds between ether

group and water. Considering these two differences, a much broader transition region in PMDEGA appears reasonable [128].

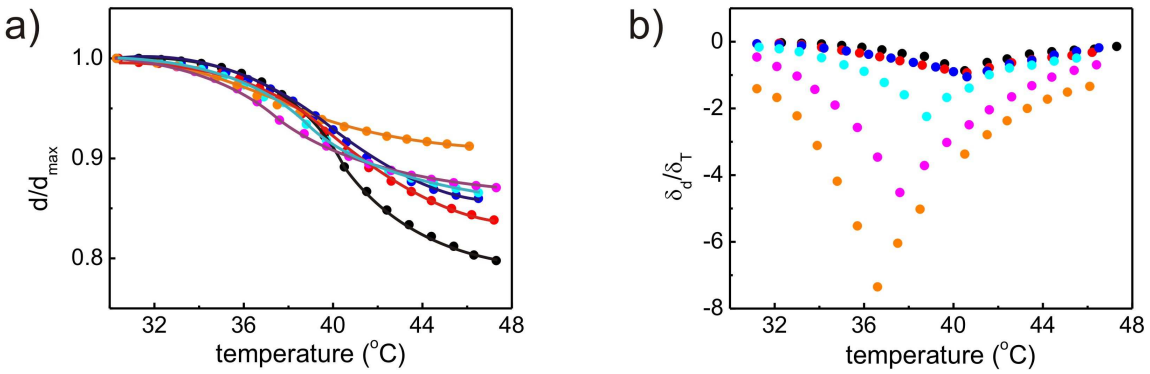

Figure 4.11: *(a) Temperature-dependent changes of the film thickness measured for PMDEGA films exposed to a sodium chloride solution with a concentration of 0.045 g/mL. The film thickness varies from 17.4 (black), 36.5 (red), 41.1 (blue), 80.3 (cyan), 178 (magenta), to 422.6 nm (orange). The solid lines are guides to the eye. (b) Corresponding first derivatives of these data.*

In a previous investigation, thin nbc-PNIPAM film was studied [43]. The thinner the nbc-PNIPAM films were, the stronger was the response to swelling in saturated water vapor atmosphere. Similar to the behavior of PNIPAM based hydrogel films, the strength of the chain collapse also depends on the PMDEGA film thickness. The thin film (thickness 17.4 nm) reduces its thickness by more than 20% when passing the LCST, whereas the thick film (thickness 422.6 nm) shrinks only by 7% (figure 4.11a). Moreover, the LCST decreases slightly with increasing film thickness (figure 4.11b). The thickness-dependent change of the LCST is exhibited in figure 4.12. A plateau is visible in the thin film regime (up to film thicknesses of 40 nm), indicating that an increase of the film thickness does not cause a prominent change of the lcst in this region. Above this critical film thickness, a further increase of the film thickness affects the LCST. A decrease from 40.6 °C (41.1 nm) to 36.6 °C (422.6 nm) is observed.

The thermal response of thin PMDEGA films is very weak when comparing with thin nbc-PNIPAM films. For example, a 10.5 nm thick nbc-PNIPAM film responded by a change of more than 50% in thickness during the shrinkage [43]. As well this weaker response is attributed to the different monomers in these polymer chains and to hydrogen bonds formed in the swollen state [128].

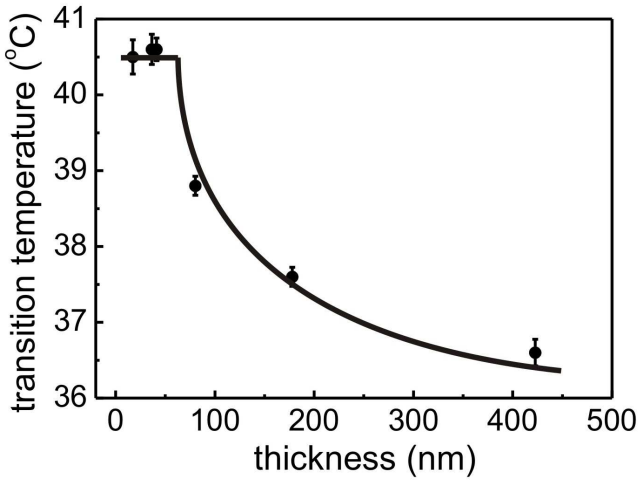

Figure 4.12: *Thickness-dependent change of the LCST measured for thin PMDEGA films (dots). The solid line is a guide to the eye.*

4.3.2 Transition behavior under a sudden thermal stimulus

In the former investigation, the transition behavior of thin PMDEGA films is measured when the temperature increases slowly from room temperature to value above the LCST. In order to find out whether the thermal response of swollen film shows a same or different behavior under a sudden thermal stimulus, neutron reflectivity experiments are performed. After the swelling reaches its equilibrium state, D_2O volume fraction (V%D_2O) of the whole swollen film has increased to 18%. Considering that the film only swells by 15% in thickness, the film is considered to be gel-like. Afterwards, this swollen film is subjected to a sudden change of the temperature (temperature jumps from 23 °C to 45 °C). Figure 4.13a shows eleven selected neutron reflectivity curves (black dots) together with the model fits (red lines). Figure 4.13b displays a two dimensional intensity representation (mapping) of the specular intensities of neutron reflectivity versus swelling time as a function of $\log(q_z)$. During the first 400 s after the change in temperature, the intensity oscillations in the reflectivity curves shifts towards higher values of q_z, wheares the critical angle of total external reflection (marked by the red arrow) shifts towards lower values of q_z. Both observations reveal that D_2O is repelled from the film and the film thickness decreases. Surprisingly, 400 s after the change of temperature, both features shift back. Obviously, the film again absorbs water and gets thicker. In order to obtain more details on the changes introduced by the jump of temperature, all individual reflectivity curves are fitted.

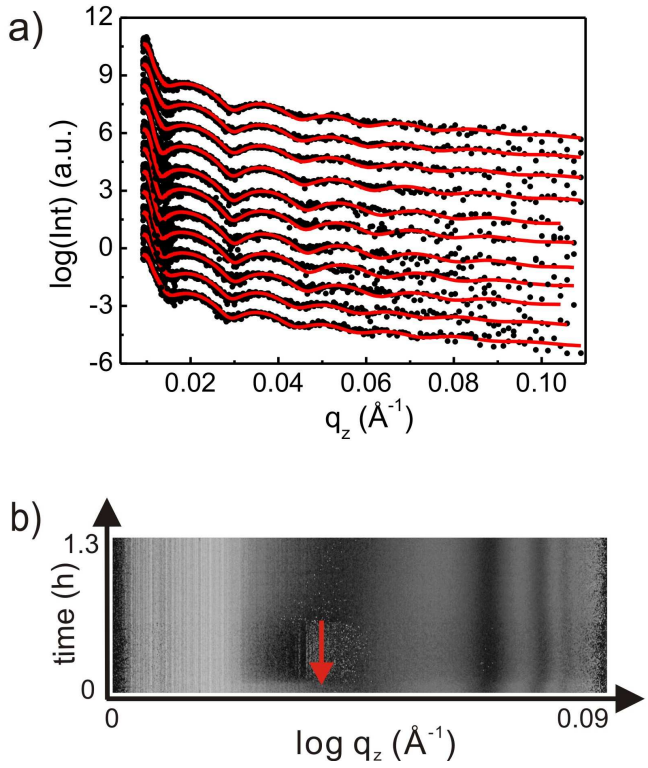

Figure 4.13: *Kinetic changes of the swollen PMDEGA film in D_2O vapor atmosphere during a jump of temperature from 23 °C to 45 °C: (a) Selected neutron reflectivity curves (black dots) together with model fits (red lines). With increasing time the curves are shifted vertically for clarity of the presentation. (b) Two dimensional intensity presentation (mapping) of the neutron reflectivity curves versus time as a function of log(q_z). The red arrow marks the initial position of the critical angle. Different scattering intensities are displayed with different grey scale (bright resembles high and dark low intensity).*

Figure 4.14a and figure 4.14b show the corresponding relative film thickness and the D_2O volume fraction (V%D_2O) as a function of time, respectively.

It is obvious that the initial response of PMDEGA to a jump of temperature from 23 °C to 45 °C, which is above the LCST of thin PMDEGA film (40 °C), is fast. The film reacts by decreasing the water content from 18% to 9%. This water release is accompanied by a shrinkage of the film back to its original thickness. The whole process takes only 400 s.

When the film reaches its initial thickness, however, a D_2O volume fraction of 9% remains in the film. As a consequence, the residual water might occupy vacancies and holes in the porous PMDEGA film which does not add to the film thickness. This water

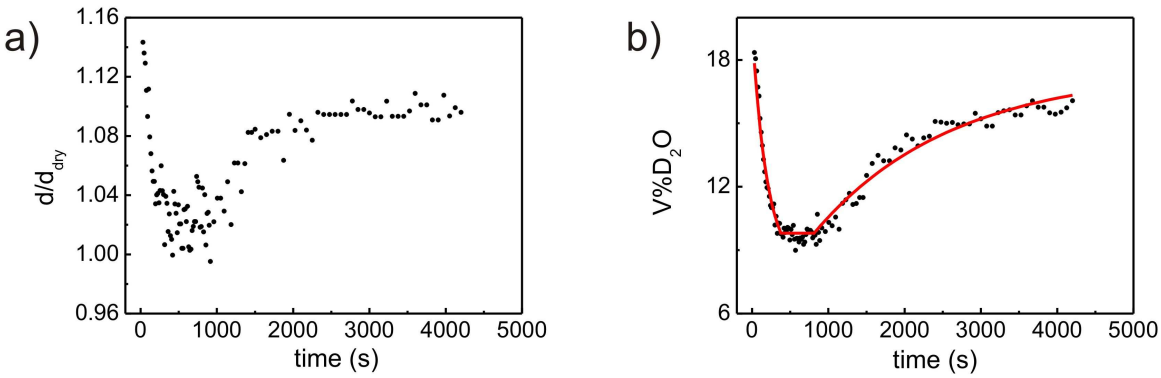

Figure 4.14: *Response of the swollen PMDEGA film to a jump of temperature from 23 °C to 45 °C: (a) Relative film thickness and (b) D_2O volume fraction ($V\%D_2O$) as a function of time. The solid line in (b) is a fit of a model as explained in the text.*

is bounded that strongly to the polymer that it is not repelled from the polymer. After the fast shrinkage process, the film thickness stays constant for 420 s. Surprisingly, after this second stage both the film thickness and $V\%D_2O$ increase again, indicating that the PMDEGA film absorbs water again and thickens. Such a relaxation process was already observed in PNIPAM based thermo-responsive polymer films [43]. A possible reason is kinetically introduced conformational changes of the polymer molecules: after a sudden change of temperature above the LCST, the polymer film responds immediately and collapses. As the film is still located in the D_2O vapor atmosphere after the collapse, the chains could slowly rearrange into a more favorable conformation. Due to this rearrangement, the film is able to bind more water, resulting in an increase of film thickness. Therefore, the hydrogel film reacts with a complex three stage process to the abrupt jump of temperature.

In a second transition behavior measurement under a sudden thermal stimulus, the temperature jumps from 23 °C to 35 °C instead of 45 °C, which is well below the LCST of the thin PMDEGA film with a thickness of 35.9 nm (40.5 °C). The protocol for the initial swelling step remains unchanged. Figure 4.15a and figure 4.15b show the relative film thickness and $V\%D_2O$ as a function of time after the temperature jump to 35 °C.

Because the final temperature (35 °C) is below the LCST of thin PMDEGA film, a collapse of the polymer chains, accompanied with water release and film shrinkage, is not expected. However, the swollen PMDEGA film also responds to the jump of temperature with a shrinkage of the film (figure 4.15a). During the first 500 s, the film shrinks back to its original dry thickness. This shrinkage is accompanied with a decrease of the water

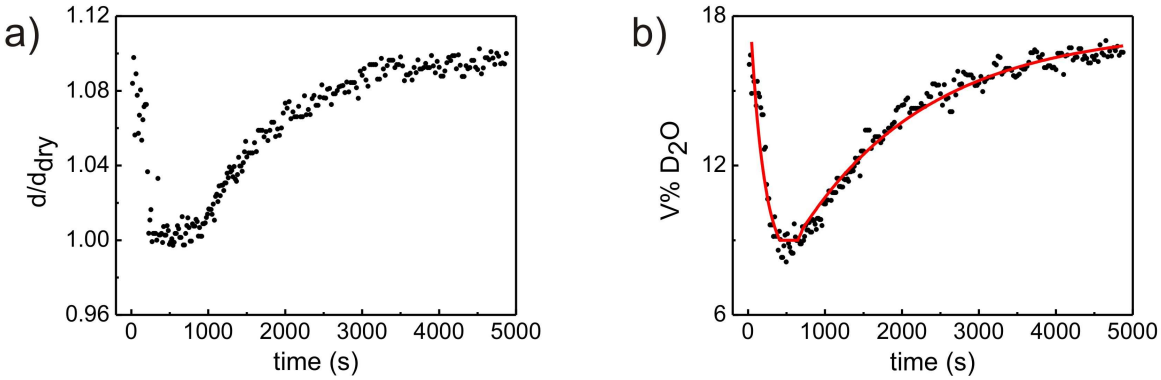

Figure 4.15: *Response of the swollen PMDEGA film to a jump of temperature from 23 °C to 35 °C: (a) Relative film thickness and (b) D_2O volume fraction ($V\%D_2O$) as a function of time. The solid line in (b) is a fit of a model as explained in the text.*

content from 17% to 9%. After a short period with constant film thickness and water content, the PMDEGA film takes up water again and swells back to the value before the jump of temperature. This three stage behavior is similar to the one observed in the case of the temperature jumps from 23 °C to 45 °C. However, the change in thickness as a function of time may appear unexpected. The initial drop in film thickness and water content is attributed to the continuous loss of solvent quality with increasing temperature already below the LCST-type phase transition of PMDEGA. From figure 4.10a, it is clear that even at temperatures as low as 34 °C, the polymer chains already start to collapse and release water. For this reason, even if the final temperature is only set to 35 °C, a partial dehydration of the film occurs. After this shrinkage, polymer chains in the film might slowly rearrange in the D_2O vapor atmosphere. This rearrangement enables the film to reabsorb water, possibly into free volume or micro-voids. As the final temperature is still below the transition temperature, the final state of the film is still a swollen one. For this reason, the final thickness and D_2O volume fraction recover its initial value, as seen in figure 4.15.

4.4 Bound water in PMDEGA films

The neutron reflectivity data presented in section 4.3.2 reveal the amount of water absorbed or repelled from the PMDEGA films, in case the final temperture is below or above the LCST. For a further analysis of the hydrogen bonds formed between PMDEGA and water, attentuated total reflectance-Fourier transform infrared spectroscopy (ATR-FTIR)

measurements are performed.

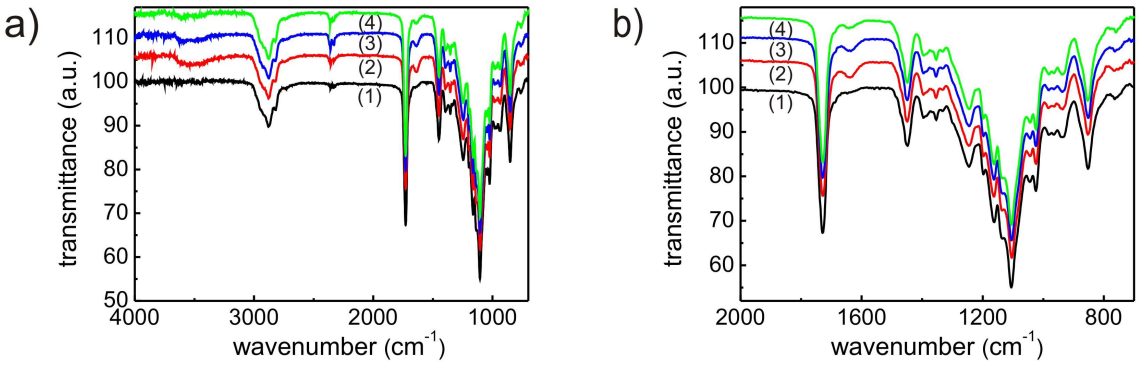

Figure 4.16: *FTIR spectra of PMDEGA films: (a) Whole spectra range form 650 cm^{-1} to 4000 cm^{-1} and (b) zoom into 650 cm^{-1} to 2000 cm^{-1}. From bottom to top the data of (1) as-prepared film, (2) swollen film at 23 °C, (3) swollen film after temperature jumps from 23 °C to 35 °C and (4) swollen film after temperature jumps from 23 °C to 45 °C are shown. The curves are shifted vertically for an improved presentation.*

Figure 4.16a shows the obtained spectra in the wavelength range from 650 cm^{-1} to 4000 cm^{-1}. In the spectra of the as-prepared film (curve 1) two characteristic peaks related to C=O and C-O bonds are observed at 1728 cm^{-1} and 1104 cm^{-1}, respectively. Besides these two peaks, the absorption bands in the range of 2800 - 3000 cm^{-1} are assigned to C-H streching. In the swollen film (curve 2), a band in the range of 3300 - 3600 cm^{-1} is observed, which is attributed to the O-H bond in water, indicating that water is absorbed by the film. Furthermore, a characteristic peak at 1640 cm^{-1} arises. This peak is assigned to hydrogen bonds between C=O and water. The characteristic peak related with the C-O bond does not exhibit any change. Therefore it is concluded that hydrogen bonds can only form between C=O and water. There are no hydrogen bonds found between C-O and water. In order to compare the change of bound water in the swollen films caused by different thermal stimuli, the FTIR spectra are shown over a limited range from 650 cm^{-1} to 2000 cm^{-1} in figure 4.16b. In all spectra the peak at 1640 cm^{-1} is visible, and the intensty varies with temperature. However, the C-O peak still does not present any change. The amount of bound water is extracted from integration of the peak area around 1640 cm^{-1}. For the as-prepared, dry PMDEGA film the value of the peak area is 13. After swelling, the peak area increases to 65, indicating that a significant amount of water is bound to C=O. After the temperature jumps from 23 °C to 35 °C (final temperature below the LCST) the characteristic peak at 1640 cm^{-1}

remains mainly unchanged and the peak area reduces only slightly to a value of 57. In contrast, after the temperature jumps from 23 °C to 45 °C, above the LCST, the value of the peak area significantly drops to 28. However, the peak is still observable, meaning that there is still bound water left in the film. Therefore, due to the final temperature being above the LCST, some hydrogen bonds break and water repels from the film. But not all hydrogen bonds are broken. These results are in agreement with the neutron reflectivity measurements.

4.5 Summary

Thin and homogeneous PMDEGA films on base cleaned Si substrates are successfully prepared by spin coating. By varing the concentration of the 1,4-dioxane solution, the obtained PMDEGA film thickness ranges from 2 nm to 162 nm. The as-prepared thin PMDEGA films are homogeneous and have smooth surface as probed with optical microscopy and atomic force microscopy. Due to the low glass transition temperature of PMDEGA (T_g = -50 °C), the PMDEGA chains show high mobility in ambient conditions. Due to storing film at ambient conditions for one day, an onset of dewetting occurrs. Although rupture of the full film into isolated droplets of PMDEGA is not observed, the films become heterogeneous. Additionally due to the low T_g of PMDEGA, no correlated roughness is observed in the films. The transition behavior is investigated by white light interferometry. When comparing the thermal response of PMDEGA to the one of the well-investigated PNIPAM, three important differences are found. The first one is the absolute value of the LCST is increased from 29.0 °C (nbc-PNIPAM film with a thickness of 40.0 nm) to 40.6 °C (PMDEGA film with a thickness of 41.1 nm). This value is well above (instead of below) body temperature which might offer certain advantages for biomedical applications. The second difference is the width of the transition from a swollen to a collapsed state. PMDEGA exhibits a much broader transition region than PNIPAM. Therefore, switching of thin PMDEGA films will require slightly larger changes in the temperature than PNIPAM. Thirdly, the response of the PMDEGA films is not as strong as in the PNIPAM films, meaning that the changes in film thickness are smaller.

Besides these differences mentioned, the thermal response of PMDEGA also shares some similarities with PNIPAM. The LCST of thin PMDEGA films depends on the film thickness. With increasing film thickness, the transition temperature decreases by 4 °C, from 40.6 °C (41.1 nm) to 36.6 °C (422.6 nm), which is in good agreement with the observations for thin PNIPAM films on identical substrates. However, all these thin films

are non-bulk films and thus the transition behavior is influenced by the interaction with the substrate. In the investigated range of film thickness (up to 422 nm) the bulk hydrogel behavior is not reached.

In order to investigate the thermal responsive behavior under a sudden thermal stimulus, in-situ neutron reflectivity is performed. To obtain thin PMDEGA films with a LCST of 40 °C, the thickness is fixed at 35.9 nm. Thus the LCST-type transition temperature of the PMDEGA films under investigation is close to that of aqueous PMDEGA solutions [46].

By analysis of in-situ neutron reflectivity data, the swelling process of thin PMDEGA films can be divided into two stages. In the first stage, water occupies all holes and vacancies of the PMDEGA film given by the free volume of the film. In the second stage the hydrophilic polymer chains form hydrogen bonds with water and cause the film to swell. By a sudden change of temperature, the swollen PMDEGA films react with a complex response, which is understood as shrinkage, reorganization and reswelling. Above the LCST, the swollen film experiences a shrinkage process, in which the film repels water and its thickness decreases. As the film is still mounted in the vapor atmosphere, a slow rearrangement of the polymer chains can induce a relaxation of the film. During the relaxation process, the film can reabsorb a certain amount of water from the surrounding, and the film structure changes. Besides this complex response, the overall final film thickness and water content of the film is decreased due to the collapse of the polymer chains. For a final temperature chosen below the LCST, the PMDEGA films reacts in a complex manner as well: a shrinkage of the swollen film followed by a relaxation are also observed. However, below the LCST, the final film thickness and water content recover to their initial values which characterized the swollen film before the temperature jump experiment. With GISAXS meaurements, the inner morphology of the as-prepared PMDEGA film and film exposed to water vapor atmosphere do not give rise to differences. Very likely the high chain mobility of the PMDEGA molecules due to the low glass transition temperature of PMDEGA (T_g = -50 °C) equilibrates possible differences. Thin PMDEGA films might be a good candidate for applications such as thin film sensors, as the chain conformation and film morphology are not influenced by the temperature treatment and the working conditions of the thin film sensors will not depend on the temperature history.

Chapter 5

Thin P(S-*b*-MDEGA-*b*-S) films

By the modification of both ends of the hydrophilic PMDEGA block with hydrophobic PS blocks, an amphiphilic tri-block copolymer P(S-*b*-MDEGA-*b*-S) is obtained, which has the ability to self-assemble into micellar structures in solution. In this chapter, the focus is on the structure and the transition behavior of thin P(S-*b*-MDEGA-*b*-S) films. Thus, similar to thin PMDEGA films, the surface and internal strcutre of thin films are investigated. In addition, the swelling capability of the as-prepared P(S-*b*-MDEGA-*b*-S) films is meausred at different water vapor pressures. Then the transition behavior of thin P(S-*b*-MDEGA-*b*-S) films with a thickness of 39.0 nm is investigated for two different thermal stimuli. In the first series, the temperature slowly increases from 30 °C (below the LCST of bulk P(S-*b*-MDEGA-*b*-S)) to 50 °C (above the LCST of bulk P(S-*b*-MDEGA-*b*-S)) in steps of 1 °C. Simultaneously, the temperature-dependence of the film thickness is monitored by white light interferometry. According to the first derivative of the film thickness as a function of temperature, the LCST is determined as 36.5 °C. In the second series, the temperature suddenly jumps from 23 °C to 35 °C or 45 °C. The thermal responses of thin films are monitored by neutron reflectivity. Additionally, the influence of the hydrophobic PS blocks to the transition behavior is investigated. Finally, bound water in the swollen and the collapsed films is measured by ATR-FTIR to understand the formation of hydrogen bonds in the films.

5.1 Structural investigation of thin P(S-*b*-MDEGA-*b*-S) films

In this section, the structure of thin P(S-*b*-MDEGA-*b*-S) films is studied. Similar to the investigation of thin PMDEGA films, the structral investigation consists of two parts. In the first part, the surface structure of the as-prepared films is imaged by optical microscopy. The films obtained are homogeneous and have a smooth surface. However, due to the low glass transition temperature of PMDEGA, dewetting is also observed in thin P(S-*b*-MDEGA-*b*-S) films when stored at ambient conditions, which is similar to thin PMDEGA films. To further study the dewetting behavior, the time-dependent evolution of the surface structure is measured with optical microscopy. Moreover, AFM is also used to obtain the surface images of the dewetted films on a local scale. In the second part, as optical microscopy and AFM can only approach the surface structure, X-ray reflectivity (XRR) and neutron reflectivity (NR) measurements are performed to obtain film thickness and density profile. Furthermore, grazing incidence small-angle X-ray scattering (GISAXS) measurements are performed on the as-prepared film and the swollen films with different thermal stimuli to probe the change of internal morphology.

5.1.1 Surface structure of thin P(S-*b*-MDEGA-*b*-S) films

By base cleaning and spin coating, thin and homogenous P(S-*b*-MDEGA-*b*-S) films on silicon substrates are successfully prepared. Figure 5.1 shows the optical micrographs of a film stored in ambient conditions for different storage times. In figure 5.1a, no heterogeneity is visible for the as-prepared film. However, after storage in ambient conditions for only one day, an onset of dewetting is found (figure 5.1b). Plenty of tiny holes and rings are observed on the surface. Further prolongation of the storage time to 4 days or even 30 days does not result in a pronounced change of these surface structure (figure 5.1c and 5.1d).

To obtain a view of the aged film on a local scale, AFM measurements are performed on the film stored in ambient conditions for 30 days (figure 5.2). Firstly, although the film is heterogeneous on large scale, a complete destruction into isolated polymer drops is not found. As seen from the AFM images, the polymer surface has still flat parts. The rms-roughness obtained is less than 4 nm. Secondly, due to the aging, plenty of tiny holes (diameter of 80 nm) are visible on the surface. This surface structure is attributed to the high mobility of the PMDEGA chains in the film. As the T_g of PMDEGA is

very low (-50 °C), instead of having a frozen chain conformation, the PMDEGA chains have a high mobility. It causes the chains to rearrange themselves after the preparation. This rearrangement results in the observed aging of the film. Additionally, PMDEGA is water soluble. When the film is stored in ambient conditions, it will absorb water vapor from air. The absorbed water will even increase locally the chain mobility and cause the observed spots [46]. However, due to the hydrophobic modification of the PMDEGA block by PS blocks, physical crosslinks are present inside the film. Thus, the movement of the PMDEGA chains is hindered by these crosslinks. For this reason, the dewetting of thin P(S-*b*-MDEGA-*b*-S) films is not as severe as in the case of thin PMDEGA films [46].

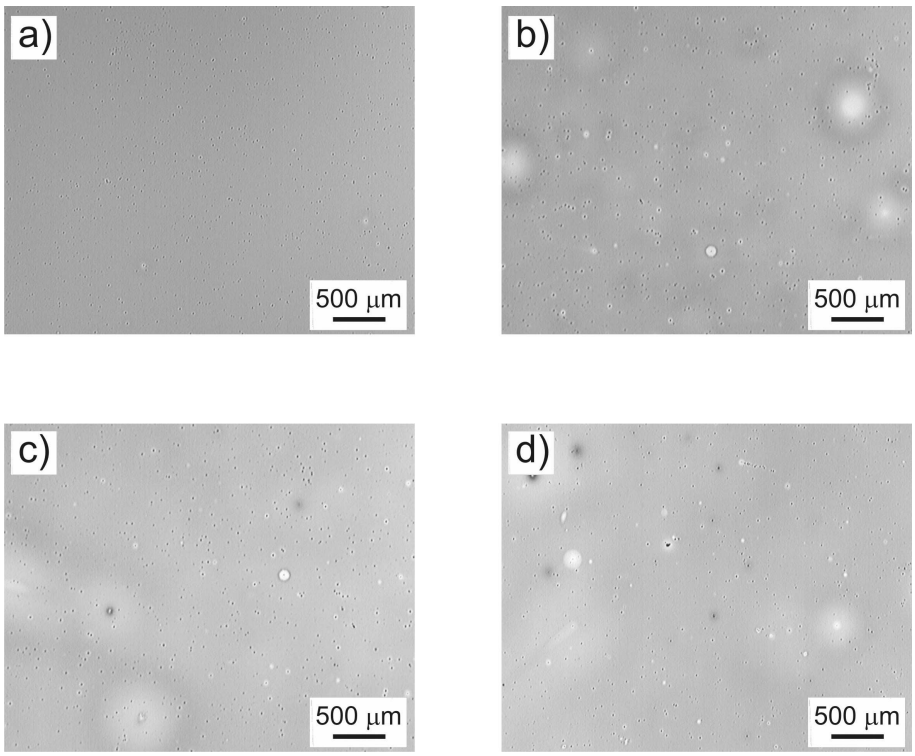

Figure 5.1: *Optical micrographs of thin P(S-b-MDEGA-b-S) film (thickness of 39.0 nm): (a) as-prepared, after storage in ambient conditions for (b) 1 day, (c) 4 days, (d) 30 days. The micrographs are measured with a magnification of 2.5 and show an area of 2560 × 1920 μm^2.*

With optical microscopy and AFM, only the surface morphology of the thin P(S-*b*-MDEGA-*b*-S) films is obtained. However, the internal structure of these films is still unclear. To gain more information about film thickness and density profile, a series of thin P(S-*b*-MDEGA-*b*-S) films with different thicknesses are prepared and measured with X-ray reflectivity (XRR) in a significantly large area.

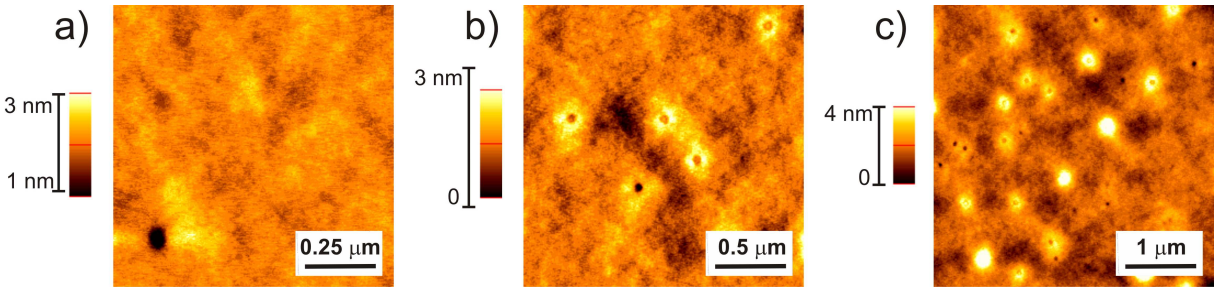

Figure 5.2: *AFM images of thin P(S-b-MDEGA-b-S) film (thickness of 39.0 nm) stored in ambient conditions for 30 days. The scan size varies from (a) 1×1 μm^2, (b) 2×2 μm^2, to (c) 4×4 μm^2. The color code is adjusted independently to emphasize on the surface morphology.*

Figure 5.3a shows the XRR curves of thin P(S-*b*-MDEGA-*b*-S) films (black dots) together with the fit (red lines).

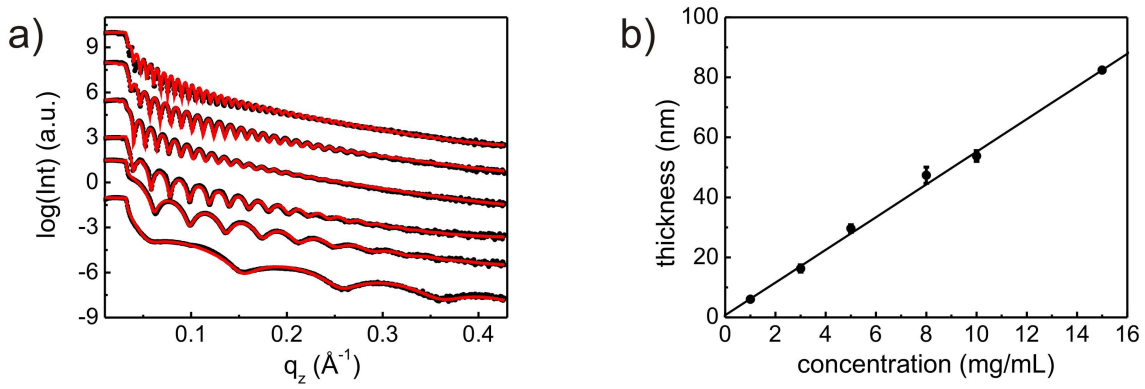

Figure 5.3: *(a) X-ray reflectivity curves (black dots) are shown together with model fit (red lines) for thin P(S-b-MDEGA-b-S) films. With increase of film thickness (6, 16, 30, 47, 54, and 82 nm from bottom to top), the number of fringes increases. The curves are shifted vertically for clarity of the presentation. (b) Film thickness is plotted as a function of the P(S-b-MDEGA-b-S) solution concentration used for spin coating. The solid line is a linear fit.*

From these six reflectivity curves, it is obvious that even for the thinnest film (the bottom one), the intensity oscillations (Kiessig fringes) are well pronounced. It indicates that even for the lowest concentration used in spin coating (1 mg/mL), a homogenous film is obtained on the substrate. Further increasing the concentration (from bottom to top), the number of fringes in the curves is increasing, indicating that the films become thicker.

Generally, the data are well described by the applied fitting model, which is composed of two layers: the bottom layer is a thin PMDEGA layer, and the top layer is a mixture of PMDEGA and PS. From the fits, the film thickness obtained varies from 6 nm to 82 nm.

Figure 5.3b shows film thickness as a function of the solution concentration. The soild line is a linear fit. Thus it is obvious that the film thickness shows a linear dependency on the solution concentration. As a consequence, in the regime of the solution concentration investigated, the overlap concentration is not reached and only a linear behavior is observed. This behavior of the P(S-*b*-MDEGA-*b*-S) solution in the spin coating process is similar to a simple homo polymer solution [46]. From the determined linear dependency, the desired film thickness can be easily accessed by selecting the appropriate concentration of the solution used in spin coating.

5.1.2 Internal structure of thin P(S-*b*-MDEGA-*b*-S) films

According to the results of the XRR measurements, thin P(S-*b*-MDEGA-*b*-S) films consists of two layers. The bottom layer, which is in direct contact with the substrate, is a pure PMDEGA layer, while the top layer is a mixture of PMDEGA and PS. Due to the low contrast between PMDEGA and PS in XRR measurements, the distribution of PMDEGA and PS in the top layer is still unknown. Therefore, neutron reflectivity measurements are performed on a selected as-prepared P(S-*b*-MDEGA-*b*-S) film to further investigate the internal structure. Figure 5.4 shows this neutron reflectivity curve (black dots) together with the model fit (red line).

The density profile of the film is achieved from the fit. A four-layer profile has to be used: the bottom layer, with a direct contact to the substrate, has an SLD of 1.06×10^{-6} Å^{-2} and a thickness of 4.1 nm. According to table 3.2, this SLD value indicates that this layer is composed of pure PMDEGA. Due to base cleaning, the substrate is expected to be hydrophilic. Because PMDEGA is hydrophilic as well, it is reasonable that the bottom layer is pure PMDEGA. Additionally, this result is also in agreement with the XRR measurements. On top of this PMDEGA layer, the other three layers show a sandwich like structure. In the center, there is a thick layer with an SLD of 1.06×10^{-6} Å^{-2} and a thickness of 25.1 nm. This SLD value indicates that the center layer is composed of PMDEGA as well. Both the other two layers (one is located between the thin and thick PMDEGA layers, and another is direct contact with air) have an SLD of 1.42×10^{-6} Å^{-2} and a thickness of 5.1 nm. According to the SLD value, these two thin layers are considered to be PS layers. Combining these four layers together, the total

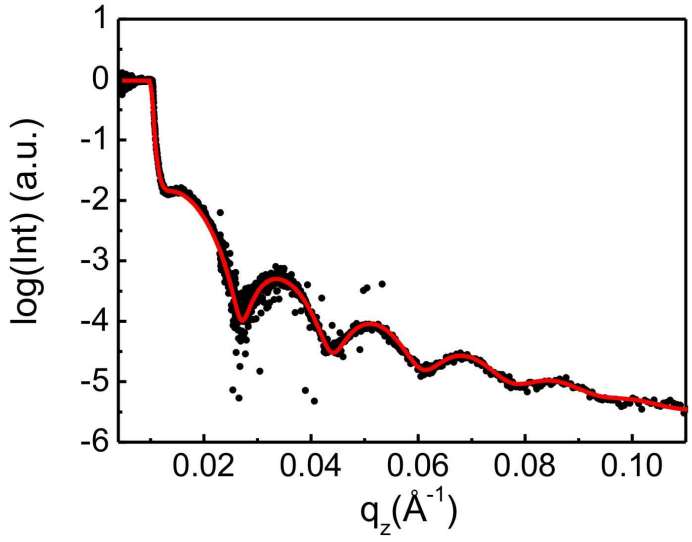

Figure 5.4: *Neutron reflectivity curve (black dots) together with model fit (red line) for the as-prepared P(S-b-MDEGA-b-S) film. The fitting model is described in the text.*

thickness of the as-prepared P(S-*b*-MDEGA-*b*-S) film is determined as 39.4 nm.

Besides XRR and neutron reflectivity, grazing incidence small-angle X-ray scattering (GISAXS) is also a powerful method to investigate the internal structure parallel to the surface (lateral structure) and the long ranged correlation in thin P(S-*b*-MDEGA-*b*-S) films. If polymer chains do not have mobility, a roughness correlation between the solid substrate and the polymer surface in the film can occur due to spin coating [174]. In GISAXS measurements, correlated roughness will cause intensity modulations along the vertical direction (q_z axis).

In the previous investigation of thin PMDEGA films [46], no matter the films are as-prepared or with different thermal stimuli, no correlated roughness was observed. This behavior is caused by the low glass transition temperature of PMDEGA (T_g = -50 °C). In order to confirm the multilayer structure observed in neutron reflectivity, as-prepared P(S-*b*-MDEGA-*b*-S) film and films with different thermal stimuli are measured with GISAXS. Figure 5.5 shows the corresponding two dimensional data. Similar to thin PMDEGA films, no correlated roughness observed in the GISAXS data. This is also caused by the low T_g of PMDEGA, which induces the rearrangement of the PMDEGA layers in the films after preparation, and finally eliminates any long-ranged correlations with the substrate or in the film.

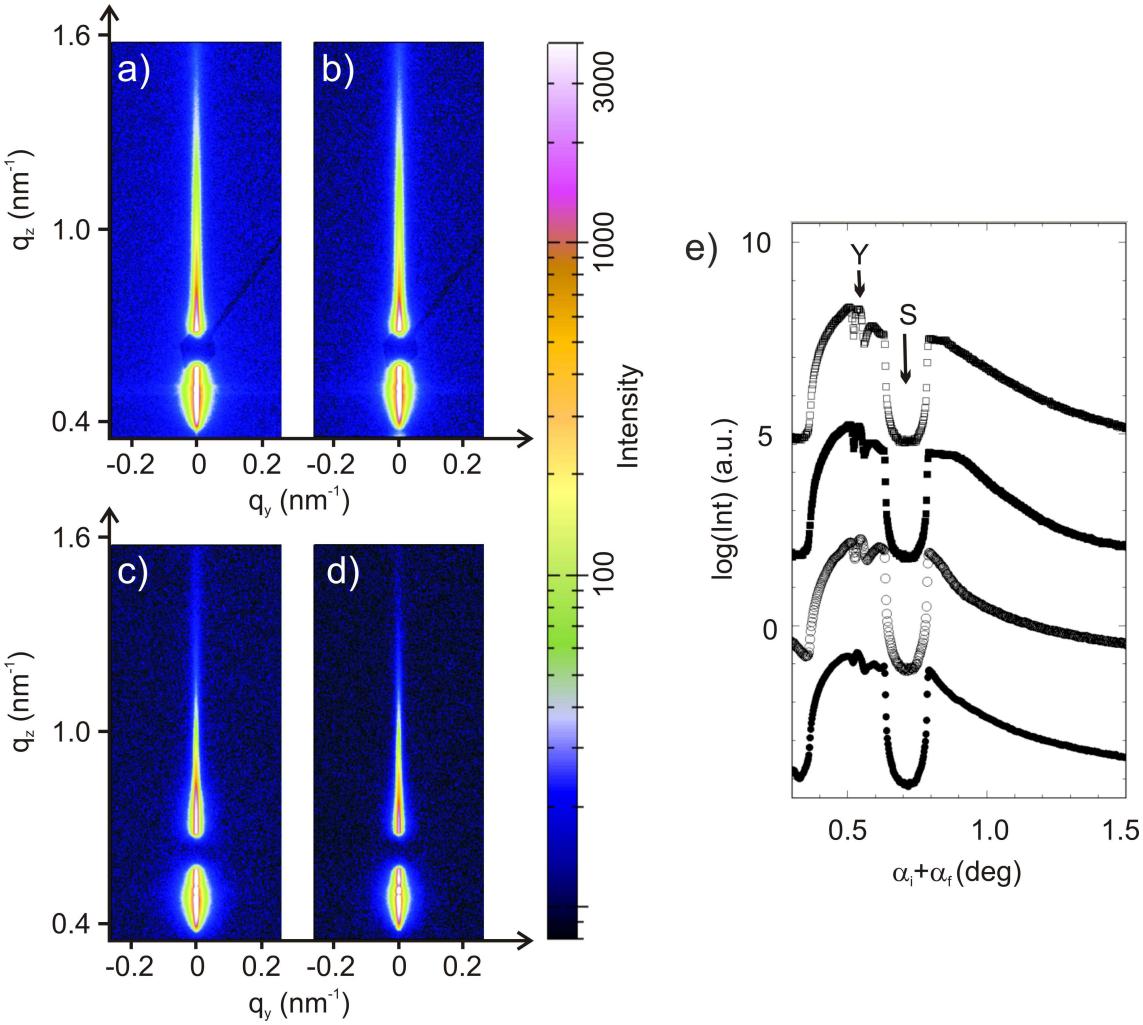

Figure 5.5: *Two dimensional GISAXS data of thin P(S-b-MDEGA-b-S) films with a thickness of 39.4 nm: (a) as-prepared, (b) after exposure to D_2O vapor, (c) first exposure to D_2O vapor, then temperature jumps from 23 °C to 35 °C (below the LCST), (d) first exposure to D_2O vapor, then temperature jumps from 23 °C to 45 °C (above the LCST), (e) vertical cuts from these two dimentional data, as-prepared (solid circle), after exposure to D_2O vapor (open circle), first exposure to D_2O vapor, then temperature jumps above (solid square) and below (open square) the LCST, at q_y=0 with Yoneda and specular peak indicated with Y and S, respectively.*

5.2 Swelling behavior of thin P(S-*b*-MDEGA-*b*-S) films

The swelling behavior of thin PMDEGA films is discussed in section 4.2.1. Due to the hydrophobic modification of both ends of the PMDEGA block by PS blocks, physical crosslinks are formed in thin P(S-*b*-MDEGA-*b*-S) films, which are assumed to influence the swelling behavior of thin films. By white light interferometry, the swelling behavior of thin P(S-*b*-MDEGA-*b*-S) films is measured under different water vapor pressures. Similar to thin PMDEGA films, the swelling capability of thin P(S-*b*-MDEGA-*b*-S) films also depends on the vapor pressure. By the high resolution of neutron reflectivity, it is found that both thin PMDEGA and P(S-*b*-MDEGA-*b*-S) films share the same swelling process, which can be divided into two regimes. In the first regime, water vapor immediately occupies all the free volume in the film. The absorbed water accelerates the mobility of the PMDEGA chains, inducing the film thickness to shrink slightly while water content in the film dramatically increases. Afterwards, the swelling comes to the second regime. Water starts to form hydrogen bonds with the PMDEGA chains, and the film swells with time. However, due to the physical crosslinks in the film, the swelling capability of P(S-*b*-MDEGA-*b*-S) films is less than thin PMDEGA films.

5.2.1 Swelling capability probed by white light interferometry

In the previous investigation, it is observed that the swelling capability of thin PMDEGA films depends on the vapor pressure (humidity) [46]. By replacing water with sodium chloride solution, the saturated vapor pressure is reduced and the swelling capability of thin PMDEGA films is also decreased [46]. Moreover, the swelling capability can be generally divided into two regimes. In the first regime, where the vapor pressure is above 3000 Pa (3000 Pa - 3169 Pa), the swelling capability is sensitive to the water vapors pressure. A slight reduction of the pressure induces a remarkable drop of the swelling capability, therefore it is denoted as sensitive regime. However, when the vapor pressure is below 3000 Pa (2380 Pa - 3000 Pa), the swelling capability stays constant and is independent of the vapor pressure. Thus, this regime is denoted as non-sensitive regime. To address the swelling behavior, thin P(S-*b*-MDEGA-*b*-S) films with a thickness of 39.0 nm are measured at different vapor pressures (figure 5.6a). The variation of vapor pressure is realized by applying sodium chloride solutions with different concentrations. In figure 5.6a, the concentration increases from 0 g/mL (pure water) to 0.36 g/mL (saturated

sodium chloride solution) from top to bottom. When the concentration of the sodium chloride solution increases, less and less water molecules are present in the air surrounding the polymer film. Because there are insufficient number of water molecules in contact with the thin P(S-*b*-MDEGA-*b*-S) films, the swelling capability is hindered. In figure 5.6b, the swelling capability (swollen film thickness normalized to the as-prepared film thickness of the respective P(S-*b*-MDEGA-*b*-S) film) is plotted as a function of the vapor pressure. The solid line in figure 5.6b shows the similar dependence of swelling capability as compared with thin PMDEGA films [46]. The full pressure region can be divided into a pressure sensitive region and a non-sensitive region as well. Besides this similarity, one pronounced difference should be noted. In case of thin PMDEGA films, due to the lack of physical crosslinks, the swollen film will be unstable and start to dewet after exposure to pure water for 90 min. However, the instability of thin P(S-*b*-MDEGA-*b*-S) films is not observed even after exposure to pure water for 200 min. Thus, it is concluded that the physical crosslinks in thin P(S-*b*-MDEGA-*b*-S) film only slightly influence its swelling behavior, while may prevent the dewetting to take place in swollen films.

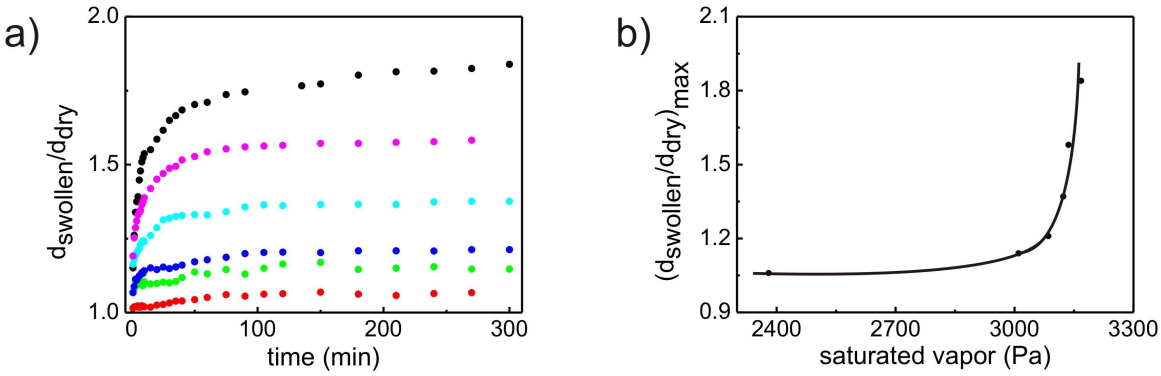

Figure 5.6: *(a) Swelling behavior of thin P(S-b-MDEGA-b-S) films (thickness of 39.0 nm) when exposed to sodium chloride solution with different concentrations. From top to bottom, the concentration of sodium chloride solution are 0 (black), 0.022 g/mL (magenta), 0.045 g/mL (cyan), 0.09 g/mL (blue), 0.18 g/mL (green), 0.36 g/mL (red). (b) Ratio of the swollen P(S-b-MDEGA-b-S) film thickness to the as-prepared film thickness as a function of the vapor pressure. The solid line is guide to the eye.*

5.2.2 Swelling behavior probed by neutron reflectivity

The swelling capability of thin P(S-*b*-MDEGA-*b*-S) films exhibits a nonlinear dependency on the vapor pressure in white light interferometry measurements. But the details about the swelling process still remain unclear. By in-situ neutron reflectivity measurements, the swelling process of thin PMDEGA films can be resolved and divided into two regimes [128]. Therefore, in order to study the swelling process of thin P(S-*b*-MDEGA-*b*-S) films, the in-situ neutron reflectivity measurements are performed again.

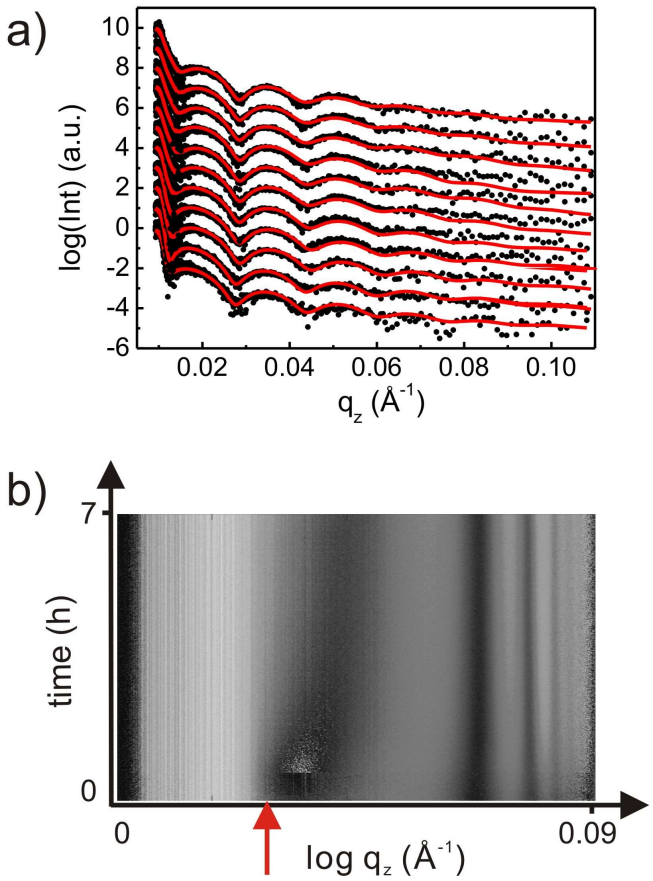

Figure 5.7: *Swelling of the as-prepared P(S-b-MDEGA-b-S) film in D_2O vapor atmosphere at 23 °C: (a) Selected neutron reflectivity curves (black dots) together with model fit (red lines). With increasing time the curves are shifted vertically for clarity of the presentation. (b) Two dimensional intensity presentation (mapping) of the specular neutron reflectivity curves versus time as a function of log(q_z). Different scattering intensities are displayed with different grey scale (brighter resembles high and dark low intensity). The red arrow marks the initial position of the critical angle.*

The as-prepared film is first mounted in the customized neutron cell described in section 3.3.8. Afterwards, the cell is evacuated to remove air and water vapor in it. Then 8 mL D_2O are injected into the reservoir and the film is exposed to unsaturated D_2O vapor atmosphere (relative humidity 79%). Simultaneously, the swelling of the film is monitored by in-situ neutron reflectivity. Figure 5.7a shows eleven selected neutron reflectivity curves (black dots) together with model fit (red lines) from the beginning (on the bottom) to the end (on the top) of the swelling process. In figure 5.7a, the intensity oscillations show no pronounced shift to the scattering vector component q_z, indicating that the film thickness has no prominent change during the swelling process. Therefore, it is concluded that thin P(S-*b*-MDEGA-*b*-S) films do not swell in unsaturated D_2O vapor atmosphere. However, in a mapping type of presentation of the neutron reflectivity data (figure 5.7b), the critical angle (marked with red arrow) prominently shifts towards higher q_z value and the overall reflected intensity increases with time. These observations show that although the film does not swell, it still absorbs D_2O molecules. Due to the strong scattering of D_2O, the critical angle shifts and the overall scattering intensity becomes stronger. By fitting of individual neutron reflectivity curves with the model described in section 5.1.2, more details such as film thickness and SLD value are obtained. Additionally, D_2O volume fraction ($V\%D_2O$) can be calculated from SLD value by equation 4.1.

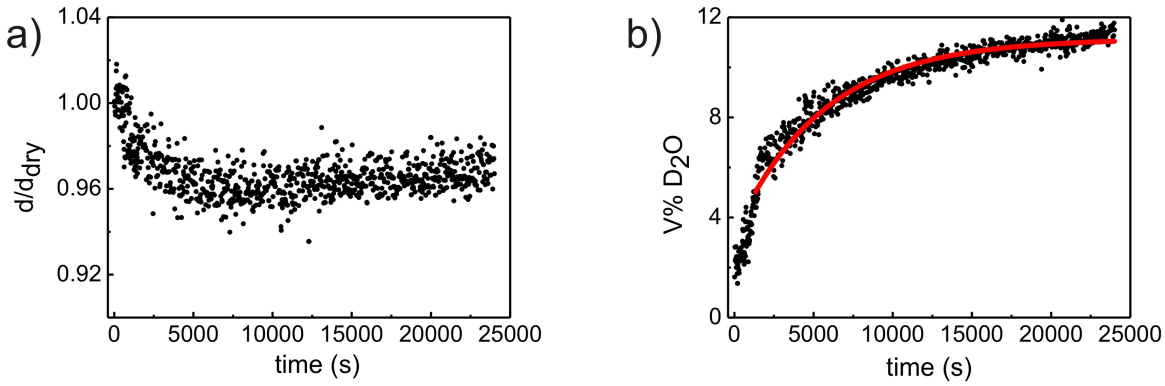

Figure 5.8: *Swelling of the as-prepared P(S-b-MDEGA-b-S) film at 23 °C: (a) Relative film thickness, (b) D_2O volume fraction ($V\%D_2O$) as a function of time. The solid line is a fit of a model as explained in the text.*

Figure 5.8a and 5.8b present the relative film thickness d/d_{dry} and D_2O volume fraction ($V\%D_2O$) as a function of time, respectively. As seen in figure 5.8a and 5.8b, although the swelling process of thin P(S-*b*-MDEGA-*b*-S) films still can be devided into two regimes, it shows a different behavior. In the first regime, from 0 s (D_2O is injected into the reservoir)

to 2000 s, instead of thickening, the film shrinks from 39.4 nm to 37.8 nm. Simultaneously D_2O amount in the film dramatically increases from 0 to 6%. This behavior is dissimilar to thin PMDEGA films investigated previously [46]. The no swelling and shrinkage of thin P(S-*b*-MDEGA-*b*-S) films will be explained respectively. No swelling of the films is attributed to the following reasons: firstly, simialr to thin PMDEGA films, thin P(S-*b*-MDEGA-*b*-S) film also has a porous structure. When the film is mounted in D_2O vapor atmosphere, the D_2O molecules immediatly enter the free volume in the porous film. Therefore, the film thickness stay unchanged but water content increases. Secondly, the vapor pressure in the cell is unsaturated (relative humidity 79%). Thus there is no sufficient D_2O molecules surrounding the film and the swelling capability is hindered. Thirdly, the hydrophobic modification introduces physical crosslinks inside the film, which also prevents the swelling of the film. Combining all these three factors together, there is no swelling observed in the measurement. While the shrinkage of the film is related to the rearrangement of the PMDEGA chains in the film. By spin coating, the as-prepared film is in a metastable state. The PMDEGA chains can slowly rearrange themselves to an energetically favorable state. When the film is mounted in the water vapor atmosphere, the absorbed water will even accelerate the mobility of the PMDEGA chains. Therefore the PMDEGA chains can easily rearrange themselves into more favored conformation, causing film thickness to decrease. Regarding all these four factors, instead of thickening in D_2O vapor atmosphere, the swollen film is even 4% thinner in the first 2000 S. In the second regime, from 2000 s to 24000 s, as PMDEGA is soluble in D_2O, the PMDEGA chains form hydrogen bonds with D_2O. Both the film thickness and water content increase with time. Although the final swollen film absorbs 11% D_2O, the film thickness is still 3% thinner than the as-prepared film (figure 5.8a).

To confirm that thin P(S-*b*-MDEGA-*b*-S) films can abosorb D_2O while slightly shrink in D_2O vapor atmosphere, neutron reflectivity is repeated on another as-prepared P(S-*b*-MDEGA-*b*-S) film. The protocol for the measurement is same.

Figure 5.9a and 5.9b show the relative film thickness and D_2O volume fraction ($V\%D_2O$) as a function of time, respectively. When the swelling reaches the equilibrium state, the film is still 3% thinner than the as-prepared film and D_2O volume fraction increases 12%. Both results are similar to the former film measured. Regarding the film thickness keeps unchanged, the amount of D_2O absorbed is remarkable. For this reason, thin P(S-*b*-MDEGA-*b*-S) film is a promising candidate for the applications such as water storage.

From the previous invesitgation of thin PMDEGA films [128], the second regime of swelling can be described by a diffusion process with a model explaining gel swelling

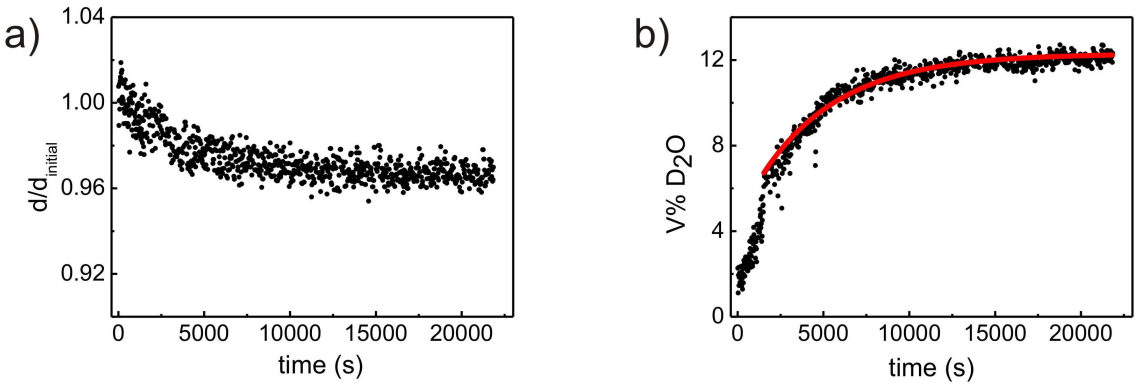

Figure 5.9: *Swelling of another as-prepared P(S-b-MDEGA-b-S) film at 23 °C: (a) Relative film thickness, (b) D_2O volume fraction ($V\%D_2O$) shown as a function of time.*

kinetics [170, 171, 172, 173]. This model can also be applied on thin P(S-*b*-MDEGA-*b*-S) films, the resulting parameters are present in table 5.1.

sample	$V\%D_2O(\infty)$	$\tau/10^4 s$	B
the first swollen P(S-*b*-MDEGA-*b*-S) film (figure 5.8)	12.3	0.46	0.46
the second swollen P(S-*b*-MDEGA-*b*-S) film (figure 5.9)	11.2	0.56	0.41

Table 5.1: *Values of $V\%D_2O(\infty)$, τ and B of the swollen P(S-b-MDEGA-b-S) films.*

5.3 Phase transition behavior of thin P(S-*b*-MDEGA-*b*-S) films

The hydrophobic PS blocks on both ends of PMDEGA block, not only influence the stability and swelling capability of thin P(S-*b*-MDEGA-*b*-S) films, but also affect the transition behavior. To investigate the influence of hydrophobic modification to the transition behavior, white light interferometry measurement is performed on thin P(S-*b*-MDEGA-*b*-S) film with a thickness of 39.0 nm. In the measurements, temperature increases from 30 °C (below the LCST of bulk P(S-*b*-MDEGA-*b*-S)) to 50 °C (above the LCST of bulk P(S-*b*-MDEGA-*b*-S)) in steps of 1 °C. Simultaneously the temperature-dependence of the film thickness is monitored by white light interferometry. Then the transition behavior obtained is compared to thin PMDEGA film with a similar thickness to study the influence of the hydrophobic PS blocks. Moreover, the thermal response of swollen P(S-*b*-MDEGA-

b-S) film to sudden thermal stimuli (temperature jumps from 23 °C to 35 °C or 45 °C) is measured with in-situ neutron reflectivity.

5.3.1 Transition behavior probed by white light interferometry

From the previous investigation, it is reported that the hydrophobic modification of the PNIPAM chains with hydrophobic groups, e.g. PS chains, shifts the LCST to lower temperature [44]. As PMDEGA is a novel thermo-responsive polymer, there is few investigation on the influence of the hydrophobic modification to the transition behavior of PMDEGA. To clarify this question, white light interferometry is used to measure the transition behavior of thin P(S-*b*-MDEGA-*b*-S) film. Figure 5.10a shows a temperature-dependence of the film thickness measured for a thin P(S-*b*-MDEGA-*b*-S) film when exposed to water vapor. The initial film thickness is 39.0 nm.

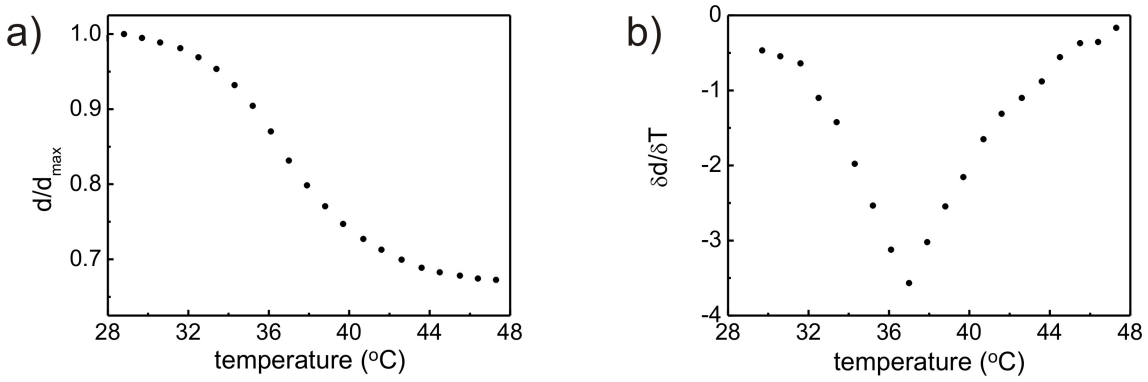

Figure 5.10: *(a) Temperature-dependent change of the film thickness measured for thin P(S-b-MDEGA-b-S) film when exposed to water vapor. (b) Corresponding first derivative of the data. The initial film thickness is 39.0 nm.*

When the temperature approaches to the LCST, the hydrogen bonds formed in the swollen film start to brake. Therefore the film repels water and shrinks. In contrast to PNIPAM based films, which exhibit a sharp transition region [43], thin P(S-*b*-MDEGA-*b*-S) films show a very broad transition region, which is similar to thin PMDEGA films recently reported [46]. This variation is attributed to the different chemical structures discussed in section 4.3.1. To determine the LCST, the first derivative of thickness over temperature is plotted as a function of temperature in figure 5.10b. As seen in the curve, the LCST of thin P(S-*b*-MDEGA-*b*-S) film with a thickness of 39.0 nm is determined as 36.5 °C. Because the LCST of thin PMDEGA film with a thickness of 41.1 nm is 40.6 °C,

it is confirmed that due to the hydrophobic PS blocks on the both ends of PMDEGA block, the LCST shifts to lower temperature, which is similar to the PNIPAM based thermo-responsive polymer films reported [43].

5.3.2 Transition behavior under a sudden thermal stimulus

In section 5.3.1, the transition behavior is measured when the temperature increases slowly above the LCST (in steps of 1 °C). But in certain applications, e.g. fire alarm sensors, the temperature abruptly jumps to a higher value. Therefore, the response of thin P(S-*b*-MDEGA-*b*-S) films to a sudden thermal stimulus is also important.

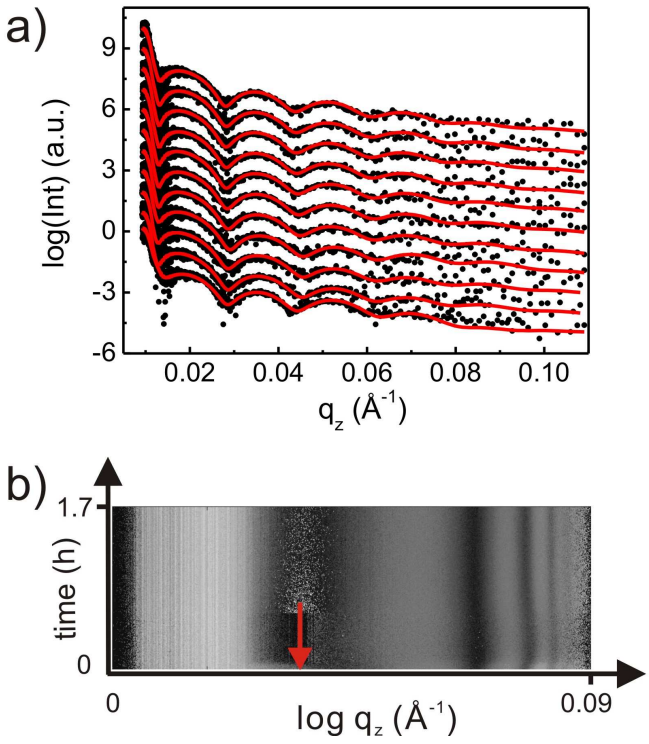

Figure 5.11: *Kinetic changes of the swollen P(S-b-MDEGA-b-S) film in D_2O vapor atmosphere when the temperature jumps from 23 °C to 45 °C: (a) Eleven selected neutron reflectivity curves (black dots) shown together with model fit (red lines). With increasing time the curves are shifted vertically for clarity of the presentation. (b) Two dimensional intensity presentation (mapping) of the neutron reflectivity curves versus time as a function of $log(q_z)$. The red arrow marks the initial position of the critical angle. Different scattering intensities are displayed with different grey scale (Bright resembles high and dark low intensity).*

After the swelling reaches an equilibrium state, the temperature suddenly jumps from 23 °C to 45 °C. Eleven selected neutron reflectivity curves (black dots) are shown together with model fit (red lines) in figure 5.11a. The curves are shifted vertically for clarity of the presentation. The initial state is at the bottom, while the final state is at the top. After the jump of temperature, the intensity oscillations immediately shift towards higher q_z value when comparing the first and the second curve at the bottom of figure 5.11a. Then the oscillations slowly and slightly shift back to lower q_z. The curve in the final state does not show a prominent change to the one in the initial state. Therefore it is concluded that when temperature jumps above the LCST, the swollen P(S-*b*-MDEGA-*b*-S) film immediately responses with a shrinkage. Then the collapsed film slowly recovers back to its initial thickness. Simultaneously the critical angle of total external reflection (marked with red arrow) shifts towards lower q_z, then slowly shifts back to higher q_z (figure 5.11b). The shift of the critical angle indicates that D_2O is first repelled from the film, then reabsorbed again. This relaxation behavior is observed in thin PMDEGA film as well [128]. In order to obtain more details, individual curves are fitted by the model introduced in section 5.1.2.

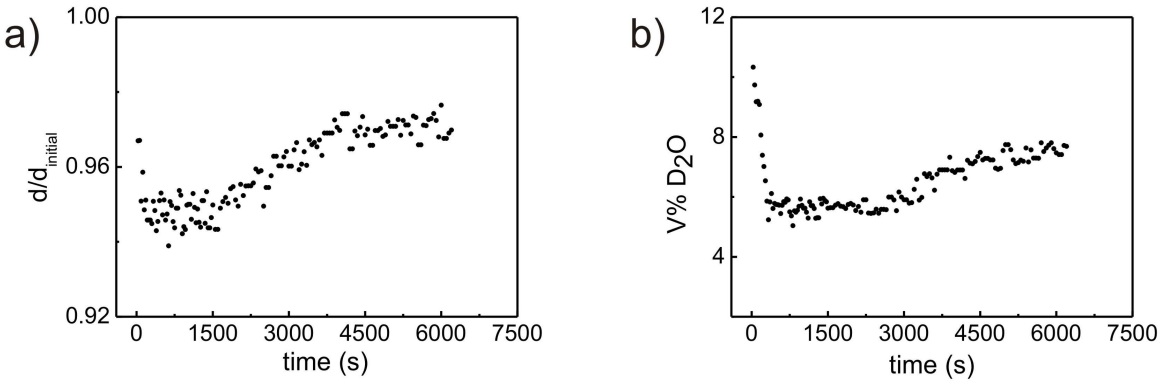

Figure 5.12: *Response of the swollen P(S-b-MDEGA-b-S) film to a jump of temperature from 23 °C to 45 °C: (a) Relative film thickness and (b) D_2O volume fraction ($V\%D_2O$) shown as a function of time.*

Figure 5.12a and 5.12b show the relative film thickness d/d_{dry} and D_2O volume fraction ($V\%D_2O$) as a function of time, respectively. From figure 5.12, it is obvious that the response of swollen film can be divided into three regimes when the temperature jumps from 23 °C to 45 °C, which is above the LCST of thin P(S-*b*-MDEGA-*b*-S) film with a thickness of 39.0 nm (36.5 °C). In the first regime (0 s - 160 s), the relative film thickness shrinks 2%, and the water content abruptly drops from 11% to 6%. This regime is denoted

as shrinkage regime. When film thickness reaches its minimum value, there is still 6% D_2O left in the film (see figure 5.12b). This residual water is exactly same as the amount of water occupying the free volume in the porous film during the first step of swelling (figure 5.8b). Because similar behavior is also observed in the collapsed PMDEGA films [128], it is concluded that this part of D_2O is bound so strongly to the PMDEGA based polymer that it can not be repelled from the polymer. In the second regime (160 s - 2500 s), both film thickness and water content keep unchanged. The chains slowly reorganize themselves in the D_2O atmosphere. For this reason, it is denoted as reorganization regime. Afterwards, it comes into the third regime (reswelling regime): both film thickness and water content ($V\%D_2O$) slowly increase, indicating that the film starts to reabsorb water and become thicker. This relaxation process has been observed in thin PNIPAM and PMDEGA based films as well [44, 128]. This interesting relaxation can be comprehended as following: when the temperature suddenly jumps above the LCST, the swollen film immediately responses and starts to collapse. But this collapse occurs in such a short time that the polymer chains do not have time to reorganize themselves to obtain a more energenically favored comformation. Therefore, the collapsed chains can spontaneously reorganize themselves. As the film is still mounted in vapor atmosphere, the film can reabsorb water during this relaxation process. Thus both film thickness and water content increases. But there is one noticeable difference between the relaxation of thin PMDEGA and P(S-*b*-MDEGA-*b*-S) films. The relaxation of the collapsed PMDEGA films still can be described by the model from Li [170]. But to the collapsed P(S-*b*-MDEGA-*b*-S) film, as the physical crosslinks might be in a more entangled conformation, the relaxation process is more complicated, and can not be simply described by the model from Li.

From the discussion above, it is clear that when the temperature suddenly jumps above the LCST, both the swollen PMDEGA and P(S-*b*-MDEGA-*b*-S) films first shrink, then reorganize themselves in vapor atmosphere, finally slowly relax. In addition, the response of the swollen PMDEGA film to a sudden jump of temperature below the LCST also contains the three steps mentioned above. The only difference is due to the final temperature is below the LCST, the collpased PMDEGA film fully recovers back to its initial swollen state. But until now, it is still unclear that whether the response of swollen P(S-*b*-MDEGA-*b*-S) film to a thermal stimulus below the LCST also contains three steps. In order to verify this question, another swollen P(S-*b*-MDEGA-*b*-S) film is measured with neutron reflectivity again. In this measurement, the temperature jumps from 23 °C to 35 °C instead of 45 °C, which is well below the LCST of thin P(S-*b*-MDEGA-*b*-S) film. Figure 5.13a and 5.13b show relative film thickness d/d_{dry} and D_2O volume fraction

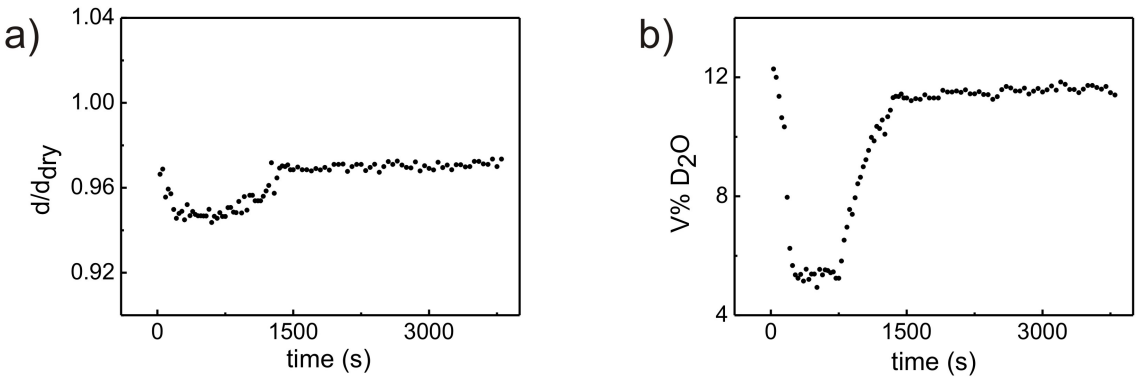

Figure 5.13: *Response of the swollen P(S-b-MDEGA-b-S) film to a jump of temperature from 23 °C to 35 °C: (a) Relative film thickness and (b) D_2O volume fraction ($V\%D_2O$) shown as a function of time.*

($V\%D_2O$) as a function of time, respectively. As seen in Figure 5.13a, when the temperature increases to 35 °C, the film immediately shrinks 4%. It is accompanied with a reduction of water content from 12% to 6%. The unexpected shrinkage of film thickness and drop of water content are attributed to the characteristic broad transition region of thin P(S-*b*-MDEGA-*b*-S) film. From figure 5.10a, it is obvious that even at low temperature (32 °C), the swollen film has already started to collapse and release water. For this reason, even the temperature only reaches 35 °C, the collapse of the swollen film still can take place. After the shrinkage, the film also slowly reorganize itself in D_2O vapor atmosphere. But one pronounced difference is that the time needed for the reorganization (700 s) is much shorter than the former case when the temperature jumps above the LCST (2000 s). This phenomenon might be attributed to the degree of collapse. When the final temperature is above the LCST, the chains are in the fully collapsed state, thus it takes longer time to rearrange them. But when the final temperature is below the LCST, the chains do not compeletely collapse. Therefore, shorter time is required for the reorganization. Afterwards, as the film is still placed in D_2O vapor atmosphere, the film can absorb water again. Because the final temperature is still below the LCST, film can recover from the collapsed state to the swollen state. Both film thickness and water content reach their initial values. This three-step collapse is similar to the swollen PMDGEA films probed previously [128]. As a consequence, it is confirmed that to the PMDEGA based films, no matter the final temperature of a sudden thermal stimulus is below or above the LCST, the swollen films first collapse, then reorganize themselves, finally relax. The only difference is the films are still in the collapsed state when the final temperature

is above the LCST, but recover to the swollen state when the final temperature is below the LCST.

5.4 Bound water in P(S-*b*-MDEGA-*b*-S) films

According to the previous investigation of thin PMDEGA films, it is found that although there are both C=O and C-O existed in PMDEGA chains, hydrogen bonds can only form between water and C=O [128]. As P(S-*b*-MDEGA-*b*-S) is hydrophobically modified the PMDEGA block with PS blocks, it is unknown that whether the PS blocks will influence the formation of hydrogen bonds. To address this question, ATR-FTIR measurement is performed on thin P(S-*b*-MDEGA-*b*-S) films as well.

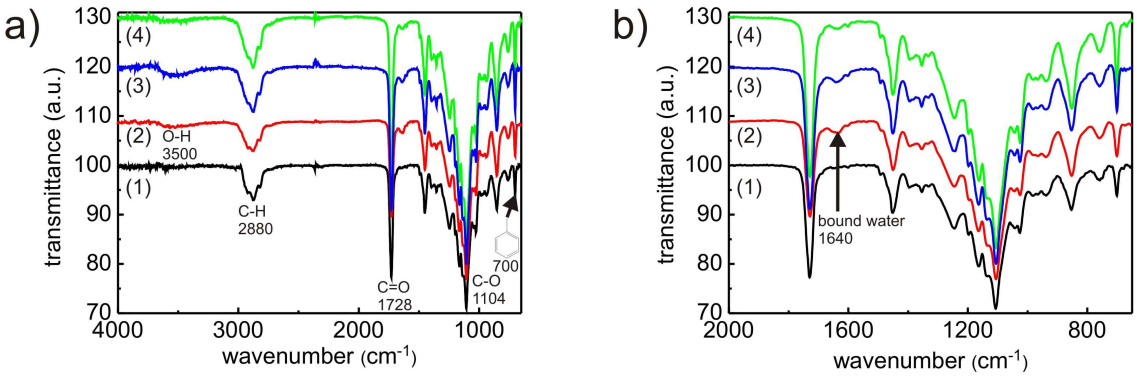

Figure 5.14: *FTIR spectra of thin P(S-b-MDEGA-b-S) films: (a) whole spectral range form 650 cm^{-1} to 4000 cm^{-1} and (b) zoom into 650 cm^{-1} to 2000 cm^{-1}. From bottom to top the data of: (1) the as-prepared film, (2) the swollen film at 23 °C, (3) the film first exposure to D_2O vapor, then the temperature jumps from 23 °C to 35 °C and (4) the film first exposure to D_2O vapor, then the temperature jumps from 23 °C to 45 °C. The curves are shifted vertically for an improved presentation.*

Figure 5.14a presents the obtained spectra in the wavelength range from 650 cm^{-1} to 4000 cm^{-1}. Curve 1 shows the whole spectra of the as-prepared film, which is similar to the as-prepared PMDEGA film probed previously [128]. Two characteristic peaks related to C=O and C-O bonds are observed at 1728 cm^{-1} and 1104 cm^{-1}, respectively. Besides these peaks, the absorption bands in the range of 2800 - 3000 cm^{-1} are assigned to C-H stretching. However, one prominent difference between P(S-*b*-MDEGA-*b*-S) and PMDEGA is an additional peak visible at 700 cm^{-1}. This peak is attributed to the

benzene ring from polystyrene [175]. After swelling in water vapor atmosphere for 2 hours, the swollen film (curve 2) emerges a band in the range of 3300 - 3600 cm^{-1}, which is related to the O-H bond in water. Therefore, it is proved that water is absorbed by the film. Furthermore, a characteristic peak at 1640 cm^{-1} arises. This peak can be assigned to hydrogen bonds between C=O and water. While the characteristic peak related to the C-O bond does not show any change after swelling. Thus it is confirmed that to P(S-*b*-MDEGA-*b*-S), hydrogen bonds are also only formed between C=O and water. To compare the change of bound water in the swollen film caused by different thermal stimuli, the spectra of limited range from 650 cm^{-1} to 2000 cm^{-1} are plotted in figure 5.14b. Besides the as-prepared film (curve 1), the characteristic peak at 1640 cm^{-1} is observable in the other three curves and the peak area varies with temperature. However, the peak related to C-O bond stays unchanged in these four curves. By integration of the peak area around 1640 cm^{-1}, the amount of bound water in each film can be obtained. For the as-prepared P(S-*b*-MDEGA-*b*-S) film (curve 1), the value of the peak area is 6.57. After swelling in water vapor atmosphere (curve 2), the peak area dramatically increases to 57.35, indicating that a significant amount of water is bound to C=O. After the temperature jumps from 23 °C to 35 °C (curve 3), the characteristic peak at 1640 cm^{-1} stay unchanged and the peak area only slightly reduces to 53.26. However, when the temperature jumps from 23 °C to 45 °C (curve 4), although this peak is still visible, the peak area significantly drops to 30.01. Thus, it indicates that due to the final temperature is above the LCST, some hydrogen bonds are broken, and water is repelled from the swollen film. But there is still bound water left in the film. These results are in agreement with the data obtained from neutron reflectivity measurements.

5.5 Summary

Thin and homogeneous P(S-*b*-MDEGA-*b*-S) films on silicon substrates are prepared by spin coating from 1,4-dioxane solution. With optical microscopy, the as-prepared film exhibits a smooth surface. Due to the low glass transition temperature of PMDEGA (T_g = -50 °C), the high mobility of the PMDEGA chains causes the dewetting of the films. As probed with optical microscopy and AFM, the onset of dewetting occurs only storing at ambient conditions for one day. However, as the hydrophobic PS blocks can form physical crosslinks inside the films, which hinder the further aging of the film, the dewetting observed is not as severe as in the case of thin PMDEGA films. In addition, the high mobility of PMDEGA chains also enhances the disorder of the parallel structure

in the as-prepared film, which results in no correlated roughness observed by GISAXS measurements. Exposure to vapor or with different thermal stimuli will even accelerate the mobility of the PMDEGA chains, inducing more disorder in the film.

The LCST of thin P(S-*b*-MDEGA-*b*-S) film with a thickness of 39.0 nm is determined as 36.5 °C by white light interferometry. As probed by neutron reflectivity, the swelling process of thin P(S-*b*-MDEGA-*b*-S) films can be devided into two steps. In the first step, water occupies the free volume in the porous film. Because water accelerates the mobility of the PMDEGA chains, the rearrangement of the PMDEGA chains causes the film to shrink 4% instead of swelling. Afterwards the swelling comes into the second step. The hydrophilic PMDEGA chains absorb water, and induce the film to swell. When the swelling reaches an equilibrium state, the film is still 3% thinner than the as-prepared film, whereas the water content increases 11%.

When the temperature jumps from 23 °C to 45 °C (above the LCST), the swollen P(S-*b*-MDEGA-*b*-S) film immediately collapses. It repels water and shrinks. The collapsed chains can slowly reorganize themselves to a more energetically favored conformation. Because the film is still mounted in vapor atmosphere, it can slowly reabsorb surrounding D_2O and swell. But overall, due to the collapse of PMDEGA chains, the final film thickness and water content are still less than the initial values of the swollen film.

Unexpectedly, when the temperature jumps from 23 °C to 35 °C (below the LCST), the response of the swollen film still possesses three steps (shrinkage, reorganization and reswelling). However, because the final temperature is below the LCST, the film thickness and water content slowly recover to their initial values characterizing the swollen film before the jump of temperature. In addition, as the collpased film is not in the fully collapsed state, the reorganization time is much shorter when comparing to the former case (final temperature is above the LCST and the film is fully collapsed).

With ATR-FTIR measurement, it is found that hydrogen bonds are only formed between C=O and water. By integrating the characteristic peak of bound water, it is observed that the bound water dramatically decreases when the final temperature is above the LCST. However, the characteristic peak does not vanish even in the collpased film, indicating that there is still residual bound water, which is in agreement with the data obtained from neutron reflectivity measurements.

As a consequence, due to the relaxation behavior observed in the PMDEGA based thermo-responsive polymer films under sudden thermal stimuli, they may not be a good candidate for applications such as thermo-sensitive switches. However, thin P(S-*b*-MDEGA-*b*-S) films can absorb 12% water, while the film thickness stays constant. Therefore, it is

a promising candidate for applications such as water storage.

Chapter 6

Thick P(S-*b*-MDEGA-*b*-S) films

In the previous chapters, the main focus is on thin PMDEGA based hydrogel films (nm scale) prepared by spin coating. With XRR and neutron reflectivity, it is confirmed that thin P(S-*b*-MDEGA-*b*-S) films show a multilayer structure. However, from the chemical structure of P(S-*b*-MDEGA-*b*-S) (see figure 3.2), it is clear that this amphiphilic tri-block copolymer has the ability to self-assemble thermo-responsive micelles in solution, which possess a core-shell structure. Nevertheless in thin P(S-*b*-MDEGA-*b*-S) films, the micellar structure is not observed, which may be reorganized by the substrate interaction after spin coating. In order to successfully transfer the micelles from the solution to the film, solution casting is used to prepare the films. Moreover, by choosing different selective solvents, P(S-*b*-MDEGA-*b*-S) is expected to form micelles with different structure. Therefore, this chapter contains four sections: in the first section, the PMDEGA- and PS-selective solvents are introduced. Then the internal structure and the transition behavior of thick P(S-*b*-MDEGA-*b*-S) films prepared from the PMDEGA-selective solvents are investigated by SAXS. In the second section, the P(S-*b*-MDEGA-*b*-S) films prepared from the PS-selective solvents are meausred by SAXS as well. Afterwards the internal structure and the transition behavior are compared to the films prepared from the PMDEGA-selective solvents. In the third section, the films prepared from ethanol (PMDEGA-selective) and THF (PS-selective) are measured by SANS to gain further insight into the internal structure and the transition behavior of thick P(S-*b*-MDEGA-*b*-S) films.

6.1 Films prepared from the PMDEGA-selective solvents probed by SAXS

As mentioned above, due to the chemical structure of P(S-*b*-MDEGA-*b*-S), micelles with various structures are expected to form by choosing different selective solvents. The Hildebrand solubility parameter is used to describe the influence of the solvents on the resulting structure in thick P(S-*b*-MDEGA-*b*-S) films.

material	Hildebrand parameter	PMDEGA-selective solvents	Hildebrand parameter	PS-selective solvents	Hildebrand parameter
PS	9.13	water	23.5	toluene	8.9
PMDEGA	19.2	methanol	14.5	1,4-dioxane	9.0
		ethanol	12.9	THF	9.1
				benzene	9.1
				dichloromethane	9.9

Table 6.1: *Hildebrand parameters of PS, PMDEGA and eight solvents used for preparing the P(S-b-MDEGA-b-S) films in the SAXS measurements.*

Table 6.1 lists the Hildebrand solubility parameters of PS, PMDEGA and the solvents used in SAXS measurements [176, 177]. The Hildebrand solubility parameter of PMDEGA is calculated by the formula from Hoftyzer and Van Krevelen [178]. From table 6.1, it is obvious that the solvents from the PMDEGA-selective group (water, methanol and ethanol) prefer to dissolve PMDEGA, as the difference of the Hildebrand solubility parameters of PMDEGA (H_{PMDEGA}) and the PMDEGA-selective group ($H_{PMDEGA-selective}$) is much smaller than the difference of H_{PS} and $H_{PMDEGA-selective}$. In contrast, the solvents from the PS-selective group (toluene, 1,4-dioxane, THF, benzene and dichlomethane) prefer to dissolve PS. As a consequence, P(S-*b*-MDEGA-*b*-S) is expected to form micelles with different core-shell structures in these two groups of solvents. In the PMDEGA-selective solvents, the PS blocks will form the core of the micelle, while the PMDEGA blocks will be the shell. Whereas in the PS-selective solvents, the core-shell structure will be reversed. By solution casting, these micelles with core-shell structure are assumed to transfer from the solutions to the thick films [179].

6.1.1 Internal structure of dry films prepared from the PMDEGA-selective solvents

To prove the assumption that the micellar structure is transferred from the solutions to the films, three dry films prepared from the PMDEGA-selective solvents are firstly investigated with SAXS. Due to the thick films (5 μm) used in the measurements, a strong signal is obtained.

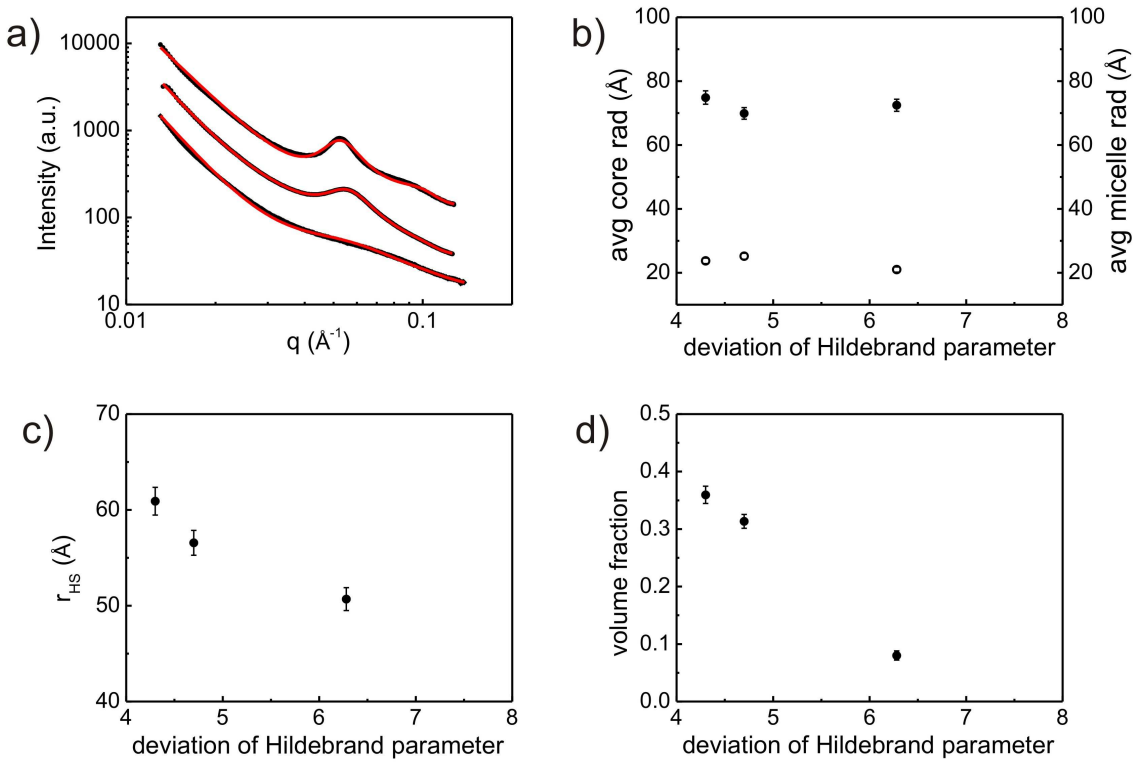

Figure 6.1: *(a) SAXS scattering curves of the dry P(S-b-MDEGA-b-S) films from the PMDEGA-selective solvents (black dots) shown together with fits (red lines) (from top to bottom: water, methanol and ethanol). (b) The micelle radius (solid circle) and the core radius (open circle) obtained from the fits (equation 2.39). (c) The hard-sphere radius and (d) the volume fraction of the micelles as a function of the deviation of the Hildebrand solubility parameter between PMDEGA and the PMDEGA-selective solvents in these three films.*

Figure 6.1a shows the SAXS scattering curves of the films prepared from the PMDEGA-selective solvents. Firstly, a very strong forward scattering in the low q region is observed in the three films, indicating that large domains are formed by the micelles in the dry

films. Secondly, a pronounced correlation peak is visible in the q region of 0.05 - 0.06 $Å^{-1}$. This correlation peak results from the structure factor (equation 2.36). It presents the correlation between the neighboring micelles. By the equation $d = 2\pi/q$, the intermicellar distance can be calculated, which is around 120 Å. When the Hildebrand solubility parameter reduces from 23.5 (water) to 12.92 (ethanol), the amplitude of the correlation peak decreases as well. Because the Hildebrand solubility parameter of water is the closest to PMDEGA in the PMDEGA-selective solvents, a well-defined micellar structure is formed in water, which is later transferred from the aqueous solution into the thick film by solution casting. When the solvent is changed from water to methanol, although the difference of the Hildebrand solubility parameter between PMDEGA and the solvent does not show a prominent change (PMDEGA-water is 4.3, while PMDEGA-methanol is 4.7), due to the shrinkage of the amplitude, it is clear that the degree of order in the micellar structure has already been significantly influenced by the exchange of solvents. As seen from the SAXS curves, the micellar structure formed in methanol is not as well established as in water. When the solvent is further switched to ethanol, the correlation peak is only faintly visible, indicating that the micellar structure is even less pronounced in ethanol. Thirdly, the position of the correlation peaks in the three films slightly shifts towards higher q values when the Hildebrand solubility parameter decreases. As mentioned above, the correlation peak is attributed to the structure factor. This shift shows that the intermicellar distance shrinks. Fourthly, a shoulder is always presented in the q region from 0.08 $Å^{-1}$ to 0.09 $Å^{-1}$. This shoulder is independent of the solvent used and attributed to the form factor of the micelle. From the q value, the average micellar radius is estimated to be around 70 - 80 Å.

In order to obtained more details about the micellar structure, the individual scattering curves are fitted by the model described in section 2.3.4 (equation 2.39). The fitting results are presented in figure 6.1b - 6.1d as a function of the deviation of Hildebrand solubility parameter between PMDEGA and the PMDEGA-selective solvents. From figure 6.1b, it is clear that both the core radius and the shell thickness in the three films show similar values, which are 22 Å and 50 Å, respectively. The hard-sphere radius (half of the intermicellar distance) decreases from 61 Å (water) to 51 Å (ethanol) (see figure 6.1c). Moreover, a decreasing tendency is observed in the volume fraction of the micelles as well (see figure 6.1d). The value drops from 0.36 (water) to 0.08 (ethanol). Because the volume fraction is related to the occupied volume in the hard-sphere, a higher volume fraction indicates a more dense packing of the micelles in the film. Thus, it is concluded that the micelles are most densely packed in the thick film prepared from water.

6.1.2 Transition behavior of films prepared from PMDEGA-selective solvents

After characterizing the dry films prepared from the PMDEGA-selective solvents, the transition behavior of these films is investigated. In order to obtain the swollen films, liquid D_2O is injected into the cell. When the swelling reaches an equilibrium, the temperature is increased from 30 °C to 50 °C in steps of 2 °C. The swollen films experience an overall increase of temperature crossing the transition temperature. Simultaneously, the whole transition process is monitored by SAXS.

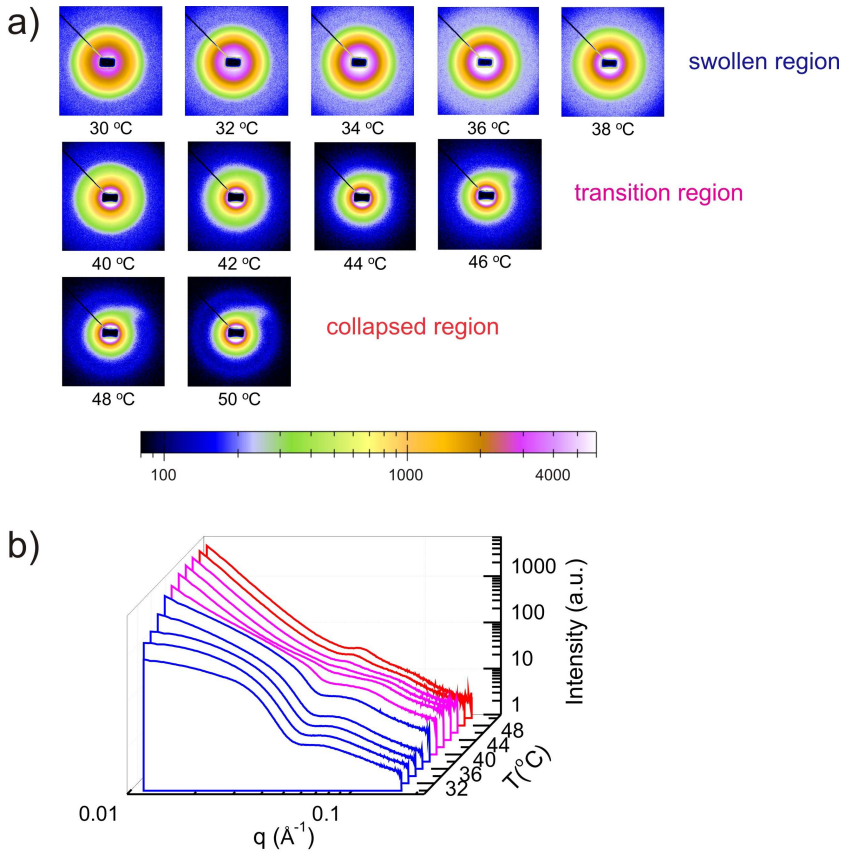

Figure 6.2: *(a) 2D SAXS pattern of the film prepared from water and immersed in liquid D_2O from 30 °C to 50 °C. (b) Integrated SAXS data at representative temperatures. The three separated regions (swollen, transition and collapsed) are colored differently (blue, pink and red, respectively) for clarity of the presentation.*

The 2D SAXS pattern of the film prepared from water at representative temperatures are shwon in figure 6.2a as an example. The color code used in these images is identical. From figure 6.2a, it is obvious that the transition process of the swollen P(S-*b*-MDEGA-

b-S) film can be devided into 3 regions. In the first region, when the temperature is below 40 °C, the scattering pattern does not show a pronounced change. As the micelles absorb D_2O and swell, this region is denoted as "swollen region". When the temperature is heated up to 40 °C, the scattering pattern immediately changes and differs from the former ones, which is used to define the starting point of the second region. Further increasing the temperature from 40 °C to 46 °C, the intensity of the scattering pattern continues to decrease. When the temperature is above 46 °C, the scattering patterns again stay unchanged. Therefore, the second region is defined from 40 °C to 46 °C, and denoted as "transition region". While the third region with the temperature above 46 °C, is denoted as "collapsed region".

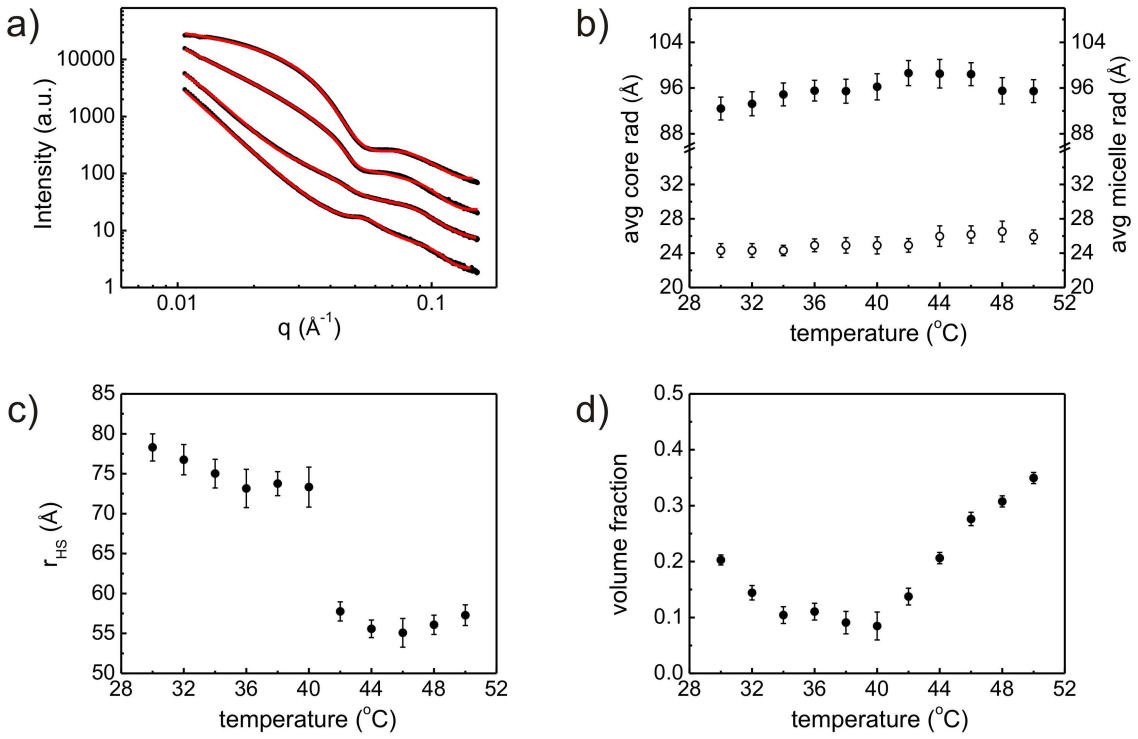

Figure 6.3: *(a) Four representative SAXS scattering curves of thick film prepared from water and immersed in liquid D_2O (black dots) shown together with fits (red lines) at 32 °C, 38 °C, 42 °C and 48 °C from top to bottom. (b) Temperature-dependence of the core radius (open circle) and the micelle radius (solid circle). (c) Temperature-dependence of the hard-sphere radius of the micelles. (d) Temperature-dependence of the volume fraction of the micelles.*

From the scattering patterns (figure 6.2a), it is confirmed that the P(S-*b*-MDEGA-

b-S) film shows a transition behavior from the swollen state to the collapsed state, but the detail is still unclear. Thus, four representative SAXS curves of the film prepared from water at 32 °C, 38 °C, 42 °C and 48 °C in liquid D_2O are shwon in figure 6.3a. Comparing the scattering curves of the swollen film at 32 °C to the dry film (figure 6.1a), the strong forward scattering observed in the low q region in the dry film is replaced by a flat intensity plateau in the swollen film. This indicates that the large domains in the film no longer exist. As PMDEGA chains absorb D_2O and swell, the micelles with swollen PMDEGA shells rearrange themselves and the domain boundaries vanish.

When the temperature increases above the transition temperature (40 - 42 °C), a strong forward scattering reappears in the low q region (figure 6.3a), showing that the collapsed micelles in the film form large domains again. Simultaneously, the correlation peak in the curves shifts from 0.042 $Å^{-1}$ to 0.055 $Å^{-1}$. Thus the intermicellar distance shrinks from 75 Å to 57 Å, meaning that the collapsed micelles tend to move close to each other. Moreover, as seen in figure 6.2b, instead of an abrupt change of the scattering curve when the temperature crosses the transition temperature, a gradual change of the scattering curve is observed to the P(S-*b*-MDEGA-*b*-S) film prepared from water. This finding is in agreement with the former investigation about thin PMDEGA films [46]. Therefore, it is concluded that PMDEGA based thermo-responsive polymers exhibit a broad transition region.

To obtain more details about the transition behavior of the swollen micelles, the scattering curves are fitted by the model described by equation 2.39. Figure 6.3b shows temperature-dependence of the core radius and the micelle radius. Because the core consists of PS blocks, it is reasonable that the core radius stays constant and is independent of the temperature. Surprisingly, the micelle radius also exhibits no shrinkage, even when the temperature is well above the transition temperature. This behavior is similar to P(S-*b*-MDEGA-*b*-S) solutions investigated previously [20], and totally different from the transition behavior of the PNIPAM based block copolymer [126], in which the swollen shell dramatically shrinks when the temperature is above the transition temperature. In contrast to the constant shell, the hard-sphere radius (r_{HS}) dramatically shrinks when the temperature is above the transition temperature (see figure 6.3c). The value of r_{HS} decreases from 74 Å (below the transition temperature) to 58 Å (above the transition temperature). It is noted that r_{HS} below the transition temperature is even smaller than the micelle radius, which may have two reasons. The first reason is the bridge connections of the neighboring micelles. Due to the overlap of the micelles, the diameter of the micelles obtained from the fits is slightly larger than the real distance between the micelles. The

second reason is that the hard-sphere structure factor is not a good model assumption any longer, as the micelles formed in the film may not have a well defined spherical shape, and even show size polydispersity. Additionally, as mentioned previously, the collapsed micelles have a tendency to densely pack in the film. The volume fraction stays constant before the temperature approaches the transition temperature. After crossing the transition temperature, the volume fraction gradually increases from 0.09 to 0.35 (see figure 6.3d).

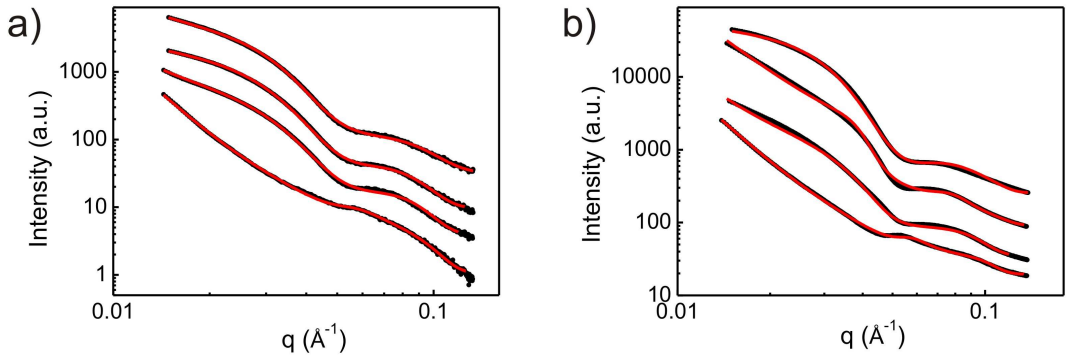

Figure 6.4: *Four representative SAXS scattering curves of the films prepared from (a) ethanol and (b) methanol (black dots) shown together with fits (red lines) at 32 °C, 38 °C, 42 °C and 48 °C from top to bottom, respectively.*

Until now, the transition behavior of the film prepared from water is understood. To compare it with the films prepared from the other PMDEGA-selective solvents, four representative scattering curves of the films prepared from ethanol and methanol at 32 °C, 38 °C, 42 °C and 48 °C are plotted in figure 6.4a and 6.4b, respectively. Similar to the curves of the film prepared from water, the forward scattering strongly increases and the correlation peak shifts towards higher q values when the temperature passes the transition temperature. Both indicate that the collapsed micelles approach close to each other and start to form large domains.

To summarize the transition behavior regarding the films prepared from the PMDEGA-selective solvents, figure 6.5 presents the parameters obtained from the fits to the SAXS data. Firstly, it is obvious that the swollen PMDEGA shells exhibit no pronounced shrinkage in all films (see figure 6.5a). Secondly, from figure 6.5b, it is clear that the hard-sphere radii immediately drop when the temperature passes the transition temperature, which is in the region between 40 °C and 42 °C. Thus, the starting point of the aggregation is used to define the transition temperature of thick P(S-*b*-MDEGA-*b*-S) films prepared from the

PMDEGA-selective solvents, which is around 40 - 42 °C. Thirdly, the volume fraction gradually increases when the temperature approaches the transition temperature. This increase also proves that the aggregation process takes place in the collapsed micelles. Moreover, the hard-sphere radii and the volume fractions in the final state almost reach the same values in all three films. Within the fitting uncertainties, it is concluded that the transition behavior of thick P(S-*b*-MDEGA-*b*-S) films prepared from the PMDEGA-selective solvents is independent of the solvents used to prepare the films.

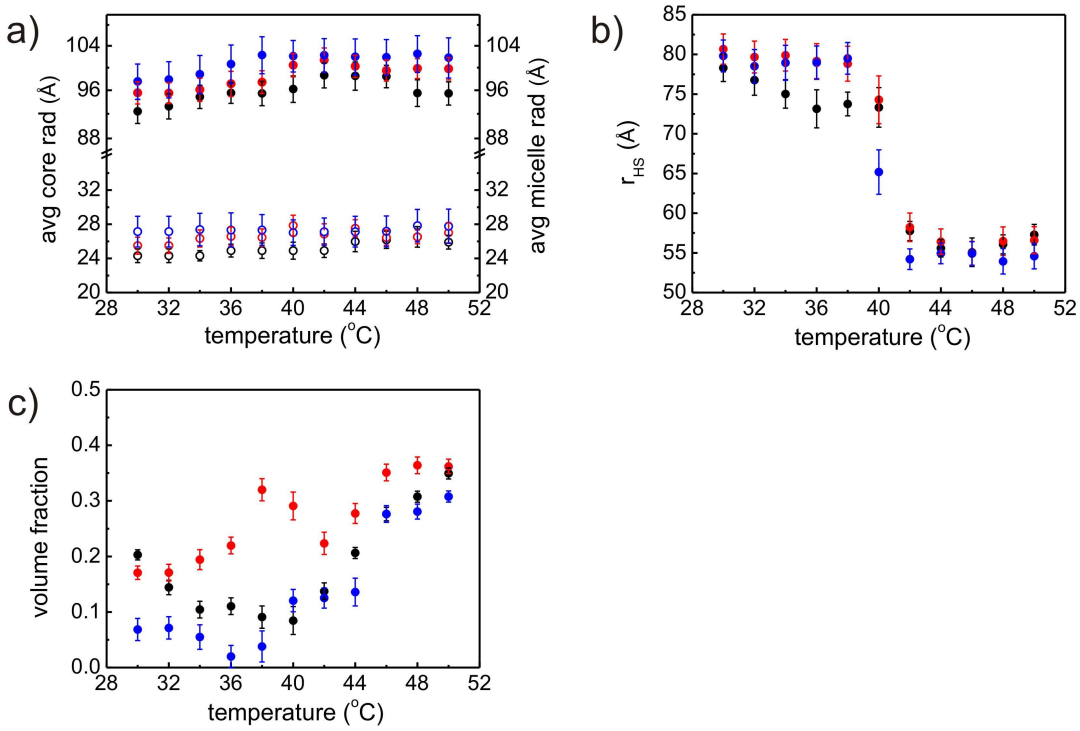

Figure 6.5: *(a) Temperature-dependence of the core radii (open circle) and the micelle radii (solid circle) of the films prepared from water (black), methanol (red) and ethanol (blue). (b) Temperature-dependence of the hard-sphere radii of the micelles. (c) Temperature-dependence of the volume fractions of the micelles.*

In the end of this section, figure 6.6 is used to describe the swelling and transition process of thick P(S-*b*-MDEGA-*b*-S) films prepared from the PMDEGA-selective solvents. From the SAXS data of the as-prepared films, it is confirmed that the micellar structure is formed in solutions and successfully transferred into the thick films by solution casting. During the evaporation of the solvents, the shells of the micelles stay intact, and do not merge in the films. By the injection of D_2O into the films, the micelles can absorb D_2O and swell. When the temperature increases above the transition temperature, the

collpased micelles tend to approach close to each other and form large domains, wheares the swollen PMDEGA shells do not show a pronounced shrinkage.

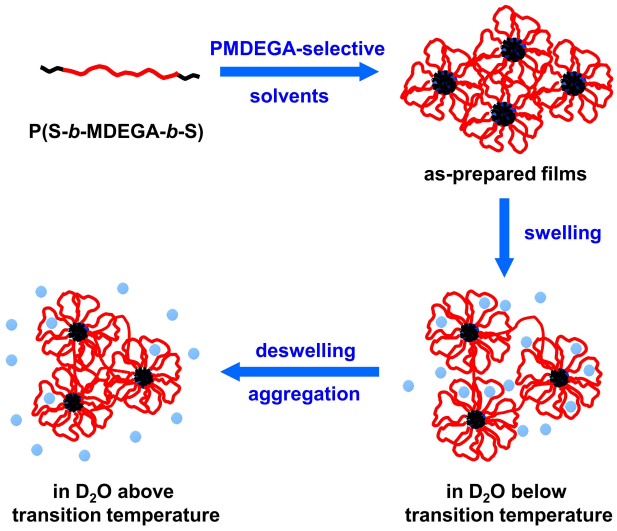

Figure 6.6: *The swelling and transition process of thick P(S-b-MDEGA-b-S) films prepared from the PMDEGA-selective solvents.*

6.2 Films prepared from the PS-selective solvents probed by SAXS

According to the discussion in section 6.1.1, the micelles in the thick films prepared from the PMDEGA-selective solvents exhibit a well-established core-shell structure as expected. When the temperature passes the transition temperature, the formation of large domains from the collapsed micelles is observed. However it is still unclear whether the films prepared from the PS-selective solvents show the same micellar structure and transition behavior. To clarify this question, the individual SAXS scattering curves of the films prepared from the PS-selective solvents are also fitted.

6.2.1 Internal structure of films prepared from the PS-selective solvents

Firstly, the internal structures of the films prepared from the PS-selective solvents are investigated. The scattering curves are plotted together with fits in figure 6.7a. As the

PS blocks have a preference to contact with the PS-selective solvents, a reversed core-shell micellar structure is assumed to form in the solvents. Thus, the micellar structure is set PMDGEA to be the core and PS to be the shell in the fit.

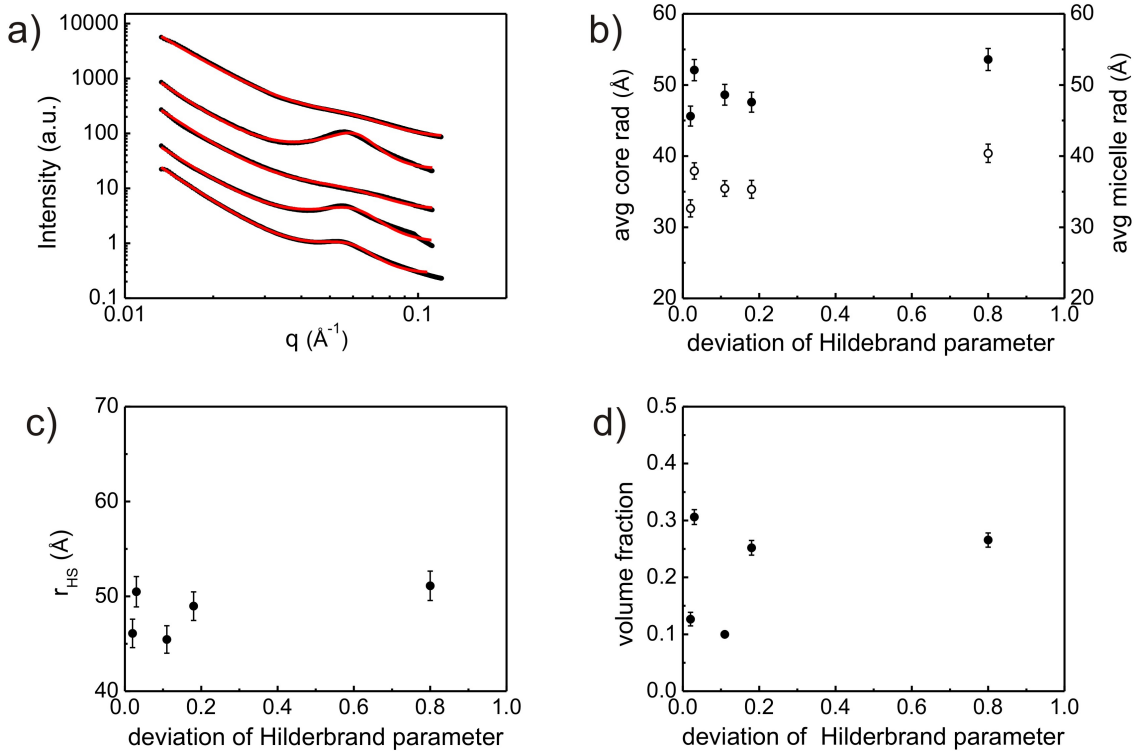

Figure 6.7: *(a) SAXS scattering curves of the dry P(S-b-MDEGA-b-S) films prepared from the PS-selective solvents (black dots) shown together with fits (red lines) (from top to bottom: benzene, THF, 1,4-dioxane, toluene, dichloromethane). (b) The micelle radius (solid circle) and the core radius (open circle) obtained from the fits (equation 2.39). (c) The hard-sphere radius and (d) the volume fraction of the micelles as a function of the deviation from Hildebrand solubility parameter of PS and the PS-selective solvents.*

Comparing the scattering curves of the films prepared from the PS-selective solvents (figure 6.7a) to the ones of the PMDEGA-selective solvents (figure 6.1b), two similarities are found. The first one is the strong forward scattering observed at low q region, exhibiting that micelles form large domains in the dry films as well. The second one is a pronounced correlation peak, which is also visible in the films prepared from THF, toluene and dichloromethane. However, this peak is hardly seen in the films prepared from benzene and 1,4-dioxane. Because the deviation of the Hildebrand solubility parameter of benzene (9.1) and PS (9.13) is smallest, a well defined micellar structure should

form according to the hypothesis, which should show a prominent correlation peak in the scattering curves. However, instead of a prominent peak at 0.06 $Å^{-1}$, only a shoulder is observable for the film prepared from benzene. Thus, it is concluded that the formation of micelles with core-shell structure is very complex. It is not suffient to explain it with a simple approach based on the Hildebrand solubility parameter. Unlike the films prepared from the PMDEGA-selective solvents, the peak positions in these scattering curves are all around 0.06 $Å^{-1}$, showing that the intermicellar distances are all similar (≈100 Å).

From the fits, the core radius (PMDEGA) and the shell thickness (PS) are around 36 Å and 13 Å (figure 6.7b), while the hard-spheres radii are between 45 and 50 Å (figure 6.7c). Comparing to the values obtained from the PMDEGA-selective solvents, it is noted the PMDEGA block occupies different volumes in the films prepared from different selective solvents. For instance, in the PMDEGA-selectice solvents, PMDEGA forms the shell, and the occupied volume is equal to 1,518,085 $Å^3$. Wheares in the PS-selectice solvents, PMDEGA forms the core, and the occupied volume dramatically reduces to 195,333 $Å^3$. For the PS block, the analogous situation is found as well. When PS forms the core, the occupied volume is 44,579 $Å^3$. However, the occupied volume increases to 297,224 $Å^3$ when PS is the shell. This variation of the occupied volume may be attributed to the different packing degree of PMDEGA or PS chains in the micelles. For example, when P(S-*b*-MDEGA-*b*-S) is dissolved in the PMDEGA-selective solvents, PMDEGA chains are supposed to be the shell of the micelle and stay in the swollen state. Thus, these micelles with swollen PMDEGA chains are transferred into the films by solution casting. Although the solvent evaporates during the sample preparation, a shell with loosely packed PMDEGA is left in the film. On the contrary, no matter whether in the solution or in the film, the PS cores always stay the densely packed state in the PMDEGA-selective solvents. This loose or dense packing explains why the same block shows a different volume in the shell and the core.

6.2.2 Transition behavior of films prepared from the PS-selective solvents

According to the discussion in section 6.1.2, exchanging the PMDEGA-selective solvents used to prepare the films will not influnce the transition behavior. To further investigate the influnce of the solvents, thick films prepared from the PS-selective solvents are measured as well. Four representative scattering curves of the film prepared from benzene and immersed in D_2O at different temperatures are displayed in figure 6.8a as an example.

These four representative scattering curves do not show pronounced differences compared to the ones of the film prepared from water (see figure 6.3). The increase of forward scattering at low q region and the shift of the correlation peak towards higher q values are observed when the temperature passes the transition temperature. Both behaviors are consistent with the former ones, indicating that no matter which kind of selective solvents is used to prepare the films, the swollen micelles always first collapse before they aggregate to form large domains.

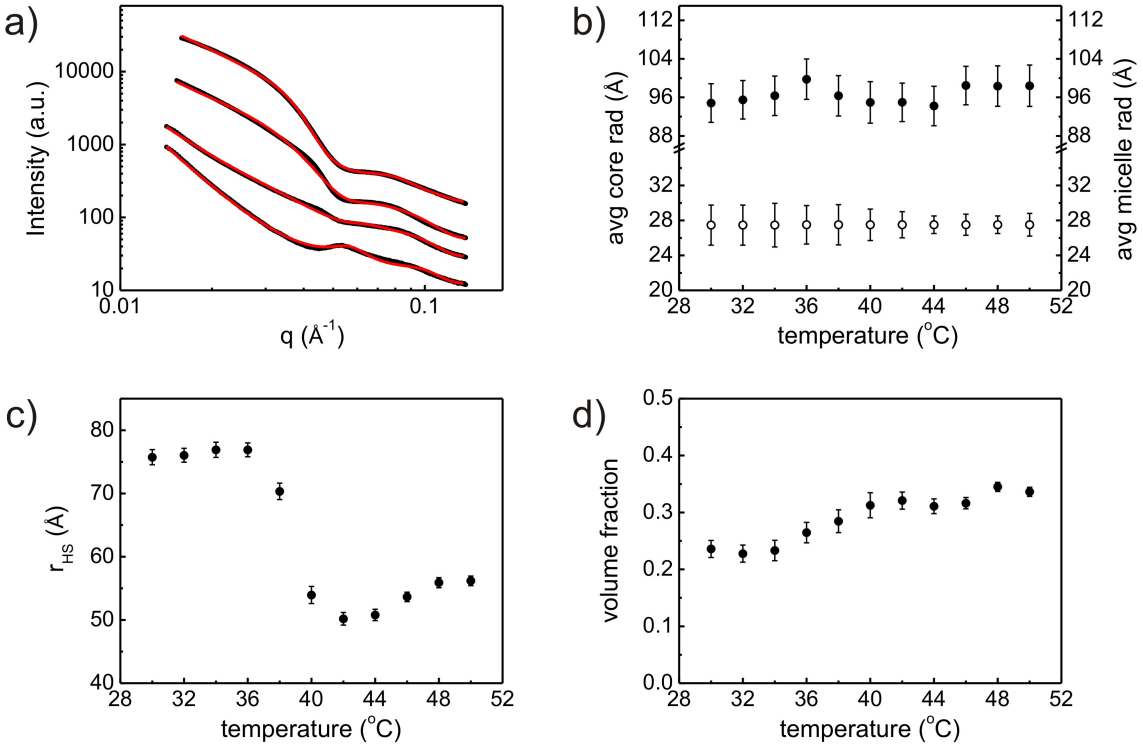

Figure 6.8: *(a) Four representative SAXS scattering curves of thick film prepared from benzene and immersed in liquid D_2O (black dots) shown together with fits (red lines) at 32 °C, 38 °C, 42 °C and 48 °C from top to bottom. (b) Temperature-dependence of the core radius (open circle) and the micelle radius (solid circle) when the temperature increases from 30 °C to 50 °C. (c) Temperature-dependence of the hard-sphere radius of the micelles. (d) Temperature-dependence of the volume fraction of the micelles.*

To obtain the transition behavior in detail, the model described by equation 2.39 is used again to fit the SAXS data. Due to the selective effect of D_2O, in the swollen micelles, PS and PMDEGA are assumed to form the core and the shell, respectively. As seen in figure 6.8a, this model fits the scattering curves very well. Therefore, it is concluded that

although the micellar structure in the dry film prepared from benzene contains PMDEGA as the core and PS as the shell, the core and the shell are reversed due to the exposure to D_2O for 10 min.

Although the swollen films prepared from different selective solvents show the same core-shell micellar structure, three noticeable differences are found.

The first visible difference is the core radius in the swollen micelles prepared from the PS-selective (benzene) or the PMDEGA-selective (water) solvents. The core radius of the swollen micelle in the film prepared from water is 24 Å, whereas the core radius increases to 27 Å in the film prepared from benzene. The reversal of the core and shell during immersion in D_2O may result in the variation of the core radius. In the film prepared from water, injection of D_2O does not change the core-shell structure, and only induces the PMDEGA shell to swell. However, the reversal takes place in the film prepared from benzene, which causes the new core (PS) to be in a state of less dense packing. Thus, the core radius is slightly larger in the swollen film prepared from benzene. In contrast to the core radius, the swollen PMDEGA shells show similar values (70 Å) in both films prepared from water and benzene.

The second pronounced difference is the width of the transition region. As discussed in section 6.1.2, the film prepared from water has already presented a broad transition region (40 - 42 °C). But the transition region of the film prepared from benzene is even broader (36 - 42 °C). Instead of abrupt collapse, the swollen micelles gradually switch to the collapsed state. One possible reason will be discussed below.

The third prominent difference is the value of the volume fraction. The volume fraction of the swollen micelles in the film prepared from benzene is 0.23, much higher than the value obtained from the film prepared from water (0.14). It may also relate to the reversal of the core and the shell. Because the PMDEGA chains need to transfer from the core to the shell during the reversal, this transfer induces additional entanglement of the swollen PMDEGA chains between neighboring micelles.

The transition behavior of the films prepared from different selective solvents not only show three differences, but also share three similarities. Firstly, no pronounced shrinkage of the swollen micelles is observed as well when the temperature crosses the transition temperature. Both the core radius and the micelle radius stay constant during the transition process. Secondly, the hard-sphere radius also remarkably drops from 76 Å in the swollen state to 56 Å in the collapsed state (see figure 6.8c). Both values are similar to the film prepared from water. Thirdly, the volume fraction also shows the same increasing tendency. Although the initial values are different as discussed above, the final

values reached in both films are around 0.35. Thus, it is concluded that when the films are in the collapsed state, there is no structural difference between the films prepared from the PMDEGA- and PS-selective solvents.

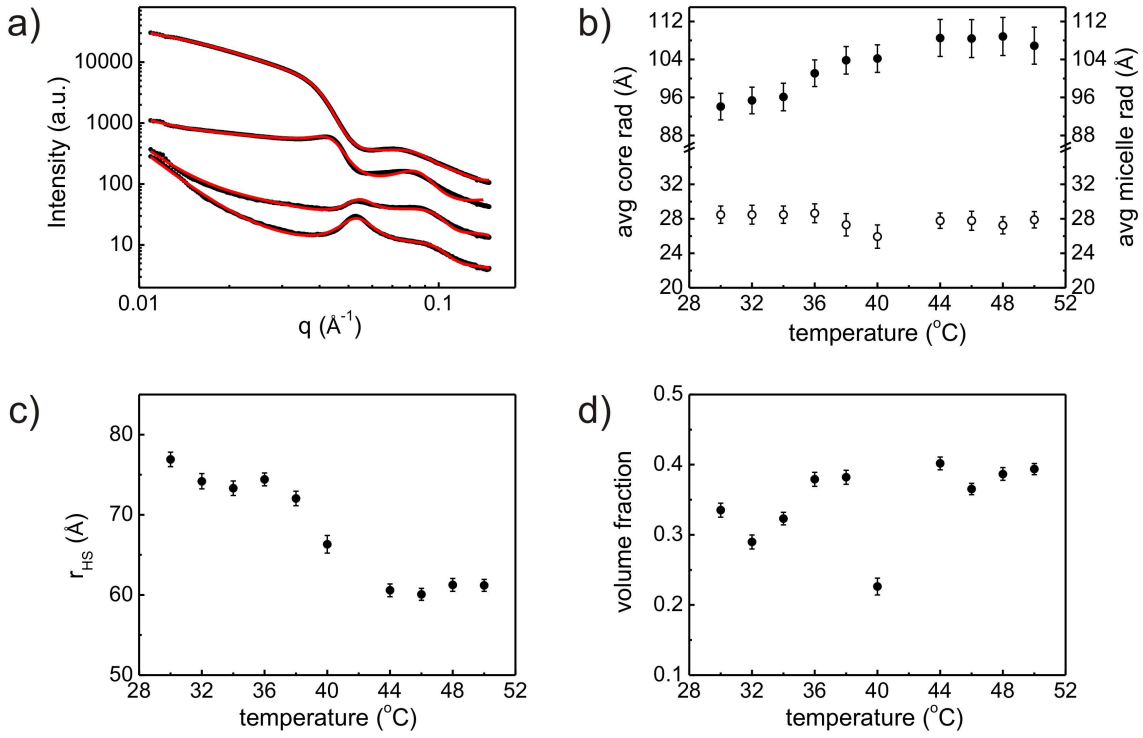

Figure 6.9: *(a) Four representative SAXS scattering curves of thick film prepared from THF and immersed in liquid D_2O (black dots) shown together with fits (red lines) at 32 °C, 38 °C, 42 °C and 48 °C from top to bottom. (b) Temperature-dependence of the core radius (open circle) and the micelle radius (solid circle) when the temperature increases from 30 °C to 50 °C. (c) Temperature-dependence of the hard-sphere radius of the micelles. (d) Temperature-dependence of the volume fraction of the micelles.*

From the resulting data of the films prepared from the PMDEGA- (water) and PS- (benzene) selective solvents, the influence of the selective solvents on the structure and the transition behavior of the films is obtained. Although the final collapsed state of the micelles is the same, the initial state of the swollen micelles as well as the transition behavior depend on the solvents used to prepare the films. However, because the correlation peak is hardly observable in the film prepared from benzene, there is supposedly no well formed micellar structure in the film. Though it is found that the transition behaviors of the films prepared from the PMDEGA-selective solvents are independent on whether

the micelles are well defined or not in the dry films. To clarify if this also holds for the PS-selective solvents, the film prepared from THF is measured with SAXS. The reason to select THF is that the film prepared from THF exhibits the most pronounced correlation peak (see figure 6.7), indicating that there is a very well established micellar structure in the film.

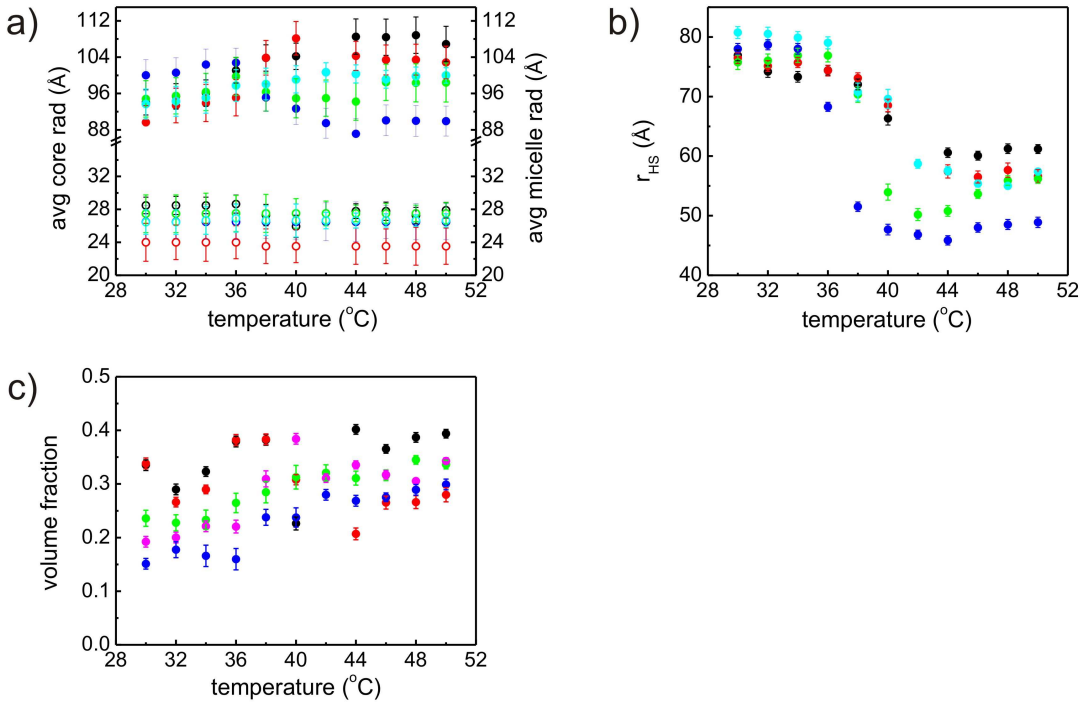

Figure 6.10: *(a) Temperature-dependence of the core radius (open circle) and the micelle radius (solid circle) of the swollen films prepared from THF (black), toluene (red), benzene (green), dichloromethane (purple) and 1,4-dioxane (blue). (b) Temperature-dependence of hard-sphere radius of the micelles in the five films prepared from the PS-selective solvents. (c) Temperature-dependence of volume fraction of the micelles in the five films prepared from the PS-selective solvents.*

Figure 6.9a shows the four representative SAXS scattering curves at 32 °C, 38 °C, 42 °C and 48 °C (from top to bottom). While figure 6.9b - 6.9d present the parameters obtained from the fits. The fit parameter at 42 °C is not presented in figure 6.9b - 6.9d, because the fit to the SAXS curve at this temperature does not show good agreement. In figure 6.9a, the first difference found is a more pronounced correlation peak observed in the range of 0.04 - 0.06 $Å^{-1}$. Though this correlation peak is also visible in the curves from benzene, its amplitude is very small. The higher amplitude of the peak indicates better

packing of the collapsed micelles in the film prepared from THF, which causes the volume fraction of the micelles to be higher (figure 6.9d). The second difference is the further swelling of the micelles when the temperature is well above the transition temperature. For instance, the micelle radius continues to increase from 96 Å (30 °C) to 106 Å (50 °C), wheares the core radius stays constant (28 Å), showing that the growth of the shell is driven by the PMDEGA shell.

Besides these two differences, there are also some similarities found between the films prepared from benzene and THF. Firstly, when the temperature is below the transition temperature, the scattering curve is similar, meaning there is no pronounced difference between these two films in the initially swollen state. Both of them show a reversed core-shell micellar structure after the injection of D_2O. Secondly, the evolution of the forward scattering with increasing temperature is visible, indicating that the collpased micelles form large domains above the transition temperature. Additionally, the shift of the correlation peak towards higher q values is observed as well, showing that the intermicellar distance shrinks and the micelles approach each other. Although the shrinkage of the swollen micelles is not found when the temperature is above the transition temperature, the intermicellar distance gradually decreases from 75 Å to 60 Å. Thirdly, the transition region of the film prepared from THF is also very broad (36 - 44 °C), which is similar to the film prepared from benzene. As a consequence, it is concluded that the reversal of the core and the shell after immersed in D_2O causes additional entanglements of the PMDEGA chains in the swollen films. Due to these entanglements, the attachment and detachment of water to the ether groups are hindered [46, 169], which further influence the transition behavior of the micelles from the swollen state to the collapsed state.

Figure 6.10 plots the resulting parameters obtained for the films prepared from the PS-selective solvents. To provide a better understanding of the internal structure and the transition behavior, figure 6.11 is used to summarize this section. Due to the selective effect of D_2O, the core-shell micellar structure is reversed when the dry films are immersed in D_2O, which causes additional entanglement of the PMDEGA chains in the shell. When the temperature is increased, no pronounced shrinkage of the swollen micelles is observed. Both the core and the shell stay constant when the temperature is well above the transition temperature, which is similar to the films prepared from the PMDEGA-selective solvents. However, due to the additional entanglement mentioned above, the films prepared from the PS-selective solvents exhibit a significantly broader transition region. Although the initial value of the volume fraction of the micelles is higher, it still gradually increases with temperature, and the final state of the hard-sphere radius and volume fraction are

similar to the ones obtained for the films prepared from the PMDEGA-selective solvents.

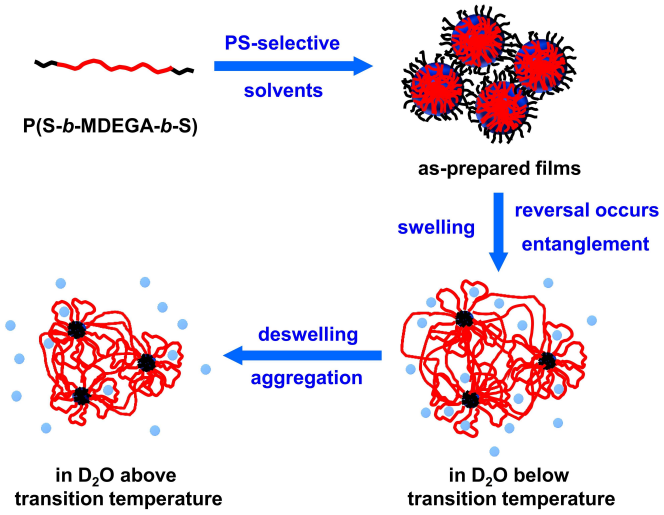

Figure 6.11: *The swelling and transition process of thick P(S-b-MDEGA-b-S) films prepared from the PS-selective solvents.*

6.3 Transition behavior of swollen films probed by SANS

From the SAXS measurements discussed in section 6.1 and section 6.2, it is concluded that the transition behaviors of thick P(S-*b*-MDEGA-*b*-S) films are influenced by the different selective solvents used. In order to gain further insight, thick P(S-*b*-MDEGA-*b*-S) films prepared from ethanol (PMDEGA-selective solvent) and THF (PS-selective solvent) are investigated as well by SANS with the same protocol.

6.3.1 Transition behavior of swollen films prepared from ethanol

Figure 6.12a presents the four individual scattering curves of the film prepared from ethanol at 32 °C, 38 °C, 42 °C and 48 °C from top to bottom. The evolution of the scattering curves is similar to the results obtained from SAXS measurement. At low temperature (32 °C), the micelles absorb D_2O, and stay in the swollen state. As a flat plateau is observed in the low q region, there is also no large domains in the swollen film. Besides this plateau, a shoulder in the q range of 0.07 - 0.12 $Å^{-1}$ is visible. This shoulder

is attributed to the form factor of the micelles. The micelle radius can be approached by the equation $d = 2\pi/q$, which yields a value around 80 Å. When the temperature increases to 38 °C, the forward scattering rises in the low q region, indicating that the collapsed micelles start to form large domains. Further increasing the temperature to 42 °C and 48 °C, a more pronounced forward scattering is observed, revealing that the domains grow larger and larger. Simultaneously, the correlation peak shifts towards higher q values, showing that the collapsed micelles tend to approach each other. However, the position of the shoulder in the high q region stays unchanged even when the temperature is well above the transition temperature, indicating that, though the aggregation of the micelles takes place, the micelle radius does not undergo a pronounced shrinkage.

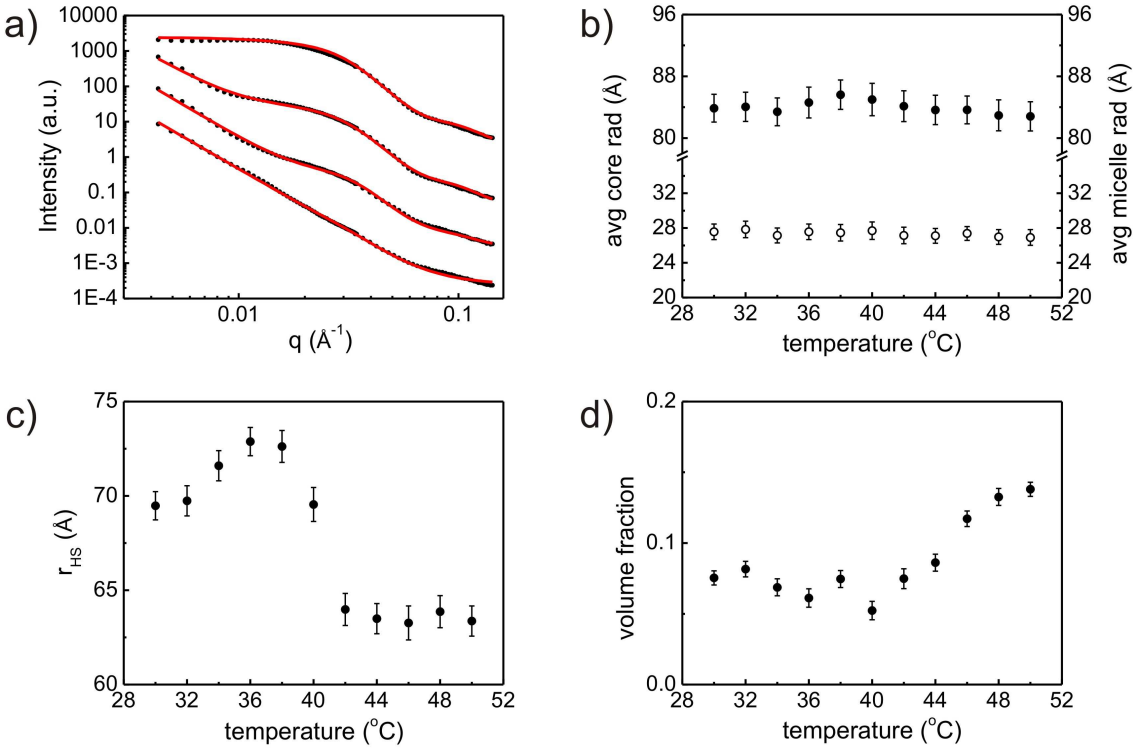

Figure 6.12: *(a) Four representative SANS scattering curves of thick P(S-b-MDEGA-b-S) film prepared from ethanol (black dots) shown together with fits (red lines) at 32 °C, 38 °C, 42 °C and 48 °C from top to bottom. (b) Temperature-dependence of the core radius (open circle) and the micelle radius (solid circle) when the temperature increases from 30 °C to 50 °C. (c) Temperature-dependence of the hard-sphere radius of the micelles. (d) Temperature-dependence of the volume fraction of the micelles.*

To obtain the transition behavior in more detail, the individual scattering curves are

fitted by the same model for SAXS measurements [28, 151]. From figure 6.12b, both the core radius and the micelle radius stay constant when the temperature is increased. No shrinkage of the swollen shell has been observed in the results from SANS measurements. Thus, it is confirmed that the micelles formed by P(S-*b*-MDEGA-*b*-S) do not exhibit a volume shrinkage when the temperature is above the transition temperature. Besides this similarity, the core radii obtained from both measurements have similar values as well, which are 27 Å. However, the micelle radii obtained show a slight difference. It is 96 Å in SAXS measurement, whereas only 84 Å in SANS measurement. This variation of the micelle radii might be related to the different sample cells used for the measurements. According to figure 6.12c, the hard-sphere radius (r_{HS}) also exhibits a prominent shrinkage from 72 Å to 64 Å when the temperature passes the transition temperature. This shrinkage indicates that the collpased micelles tend to approach each other. The transition temperature is corresponding around 40 - 42 °C. It is the same value as obtained from SAXS measurement. Moreover, the volume fraction of the micelles stays around 0.07 before the temperature approaches the transition temperature (figure 6.12d). Afterwards, it slowly increases with temperature from 0.07 to 0.14, showing that the collpased micelles are packed more densly. As a consequence, the results from SANS measurement confirm the transition behavior of the film prepared from the PMDEGA-selective solvents observed in SAXS measurements.

6.3.2 Transition behavior of swollen films prepared from THF

According to the discussion above, the transition behavior of thick P(S-*b*-MDEGA-*b*-S) film prepared from ethanol (PMDEGA-selective solvents) shows no difference in SAXS and SANS measurements. To confirm that the transition behavior of the film prepared from the PS-selective solvents is also not dependent on the measurement, SANS measurements are repeated on thick P(S-*b*-MDEGA-*b*-S) film prepared from THF. Figure 6.13a presents the four individual scattering curves at 32 °C, 38 °C, 42 °C and 48 °C from top to bottom.

Some similarities are found, when comparing the scattering curves of the films prepared from THF and ethanol. Firstly, the evolutions of the forward scattering with the temperature in the low q region are seen in both films. Secondly, a shoulder is visible in the q region of 0.06 - 0.11 $Å^{-1}$ (see figure 6.13a), showing that the micelle radius (form factor) is around 88 Å. Thirdly, both the core radius and the micelle radius stay unchanged (see figure 6.13b). There is no observable shrinkage of the swollen micelles. Fourthly, when the temperature increases above the transition temperature (40 - 42 °C), the hard-sphere

radius (r_{HS}) also dramatically drops from 71 Å to 63 Å (see figure 6.13c). The decrease of r_{HS} means that the collpased micelles tend to approach each other. Fifthly, the volume fraction of the micelles gradually increases from 0.05 (40 °C) to 0.15 (50 °C), showing that the collapsed micelles densely pack and form large domains. These five findings are exactly the same as the results from SAXS measurement. Thus, the SANS measurements confirm the observations of the SAXS measurements.

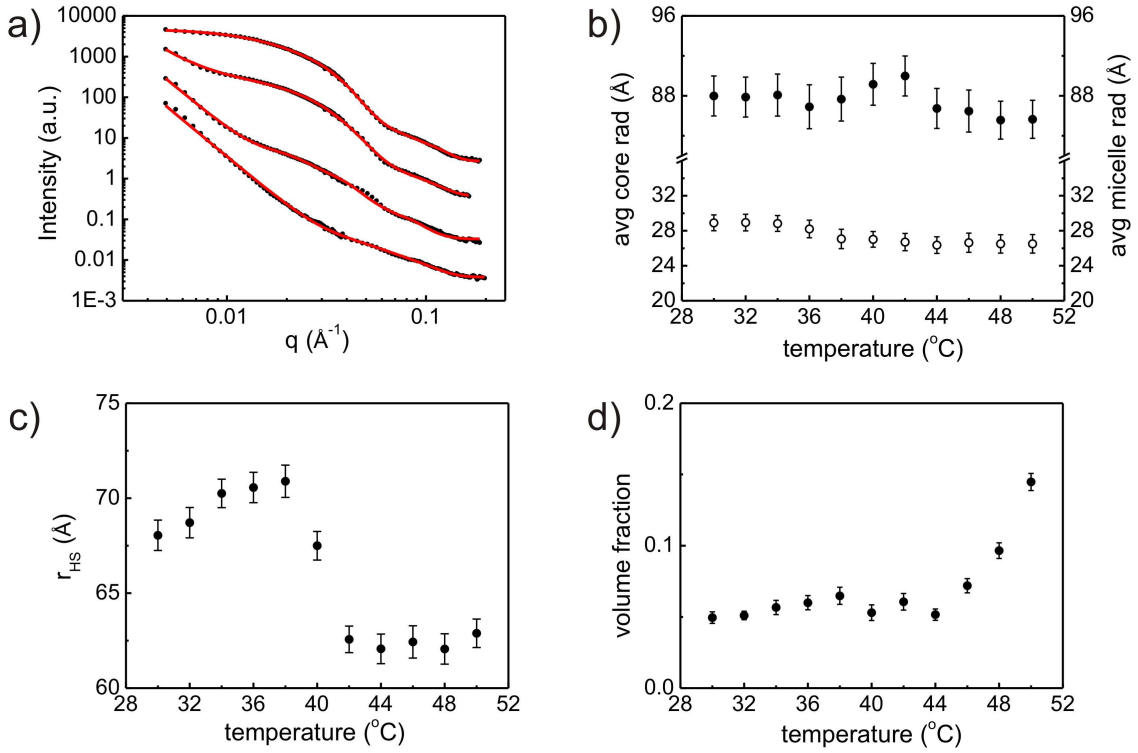

Figure 6.13: *(a) Four representative SANS scattering curves of thick P(S-b-MDEGA-b-S) film prepared from THF (black dots) shown together with fits (red lines) at 32 °C, 38 °C, 42 °C and 48 °C from top to bottom. (b) Temperature-dependence of the core radius (open circle) and the micelle radius (solid circle) when the temperature increases from 30 °C to 50 °C. (c) Temperature-dependence of the hard-sphere radius of the micelles. (d) Temperature-dependence of the volume fraction of the micelles.*

6.4 Summary

By solution casting, thick P(S-*b*-MDEGA-*b*-S) films with a thickness of 5 μm are successfully prepared from the PMDEGA- and PS-selective solvents. SAXS measurements

confirm that the core-shell micellar structures formed in solutions are successfully transferred into thick films. In the films prepared from the PMDEGA-selective solvents (water, methanol and ethanol), PS and PMDEGA form the core and the shell, respectively. Whereas in the films prepared from the PS-selective solvents (THF, toluene, benzene, dichloromethane and 1,4-dioxane), the core and the shell are reversed. When the films are immersed in liquid D_2O, in the film prepared from the PMDEGA-selective solvents, the core-shell micellar structure stays unchanged. Only the PMDEGA shell absorbs D_2O and swells. In contrast, in the films prepared from the PS-selective solvents, the core and the shell are reversed due to the selectivity of D_2O. This reversal of the micelles results in two differences of the transition behavior. The first difference observed is the high volume fraction of the swollen micelles after exposure to liquid D_2O for 10 min, meaning that there is additional entanglement between the micelles. This entanglement results in the second difference: the transition region of the film prepared from the PS-selective solvents is significantly broader. Because the transition from the swollen state to the collapsed state is related to hydrogen bonds, the entanglement hinders the attachment and detachment of water to the ether groups, which further influences the transition behavior of the micelles. Besides these two differences, the thick films prepared from the two different selective solvents show the same behavior. Although the swollen PMDEGA shell does not exhibit a pronounced shrinkage when the temperature is heated above the transition temperature, the intermicellar distance abruptly decreases and the volume fraction gradually increases. Furthermore, the final states of the collapsed micelles are similar for the films prepared from the two different selective solvents. This indicates that the PMDEGA based micelles will switch from the swollen state to the collapsed state when the temperature passes the transition temperature. This transition process is not influenced by the degree of entanglement of the chains. Moreover, the collapsed micelles tend to aggregate and to form large domains.

Chapter 7

Summary and outlook

In this thesis, two thermo-responsive polymer PMDEGA and P(S-*b*-MDEGA-*b*-S) are investigated. The focus is on the structure of the thermo-responsive films and an understanding of the corresponding transition behavior. Hence, the conclusion is given to thin PMDEGA and P(S-*b*-MDEGA-*b*-S) films in these two parts, respectively.

As-prepared PMDEGA films exhibit a homogeneous surface as probed with optical microscopy and AFM. Due to the low glass transition temperature (T_g = -50 °C), the PMDEGA chains have high mobility. As a consequence, thin PMDEGA films can show dewetting after storage in ambient conditions. The correlated roughness in the films is not present because of a rearrangement of the chain conformation. Although the surface of the as-prepared PMDEGA films is smooth, in fact the films have a porous structure. Due to the free volume, there are plenty of holes and vacancies. Thus, when the films are mounted in a water vapor atmosphere, the water molecules immediately enter into this free volume of the film. As the water is strongly bound with the PMDEGA chains, it can be understood as structure water, which is not repelled from the swollen films by the transition process when the temperature increases above the LCST.

The swelling capability of thin PMDEGA films depends on the surrounding water vapor pressure, being most sensitive to the pressure range of 3000 Pa - 3169 Pa. A slight decrease of pressure causes a pronounced drop of swelling capability. However, the swelling capability stays unchanged when the vapor pressure is lower than 3000 Pa.

The swelling capability of thin PMDEGA films is significantly smaller as compared to thin PNIPAM films with same thickness, which is attributed to the different chemical structures of PMDEGA and PNIPAM. For PMDEGA, only ether groups can act as the H-acceptor. Therefore, hydrogen bonds can only be formed between the ether groups and water. In contrast, there are not only ether groups (H-acceptor), but also the amide

groups (H-donor) which form hydrogen bonds in PNIPAM. Additionlly, water cages can be formed around isopropyl group on the end of the side chain in PNIPAM.

The swelling process of thin PMDEGA films in water vapor atmosphere is devided into two steps. In the first step, water occupies all free volume in the film, which causes the film thickness to stay constant even if the water content is dramatically increased. In the second step, water starts to form hydrogen bonds with the ether groups in the PMDEGA chains. Thus the film starts to swell and the water content continues to increase. Regarding the transition behavior of thin PMDEGA films, it exhibits a much higher LCST than thin PNIPAM films. Additionally, the LCST of thin PMDEGA films depends on the film thickness: the thinner the film, the higher the LCST. Besides the difference of the LCST, thin PMDEGA films present a much broader transition region when compared to thin PNIPAM films with same film thickness. As there is a large side chain close to the ether groups in PMDEGA, it hinders the detachment of hydrogen bonds in the collapse process. If the temperature suddenly jumps above the LCST, swollen PMDEGA films shows a complex response, containing shrinkage, reorganization and reswelling processes. Surprsingly, even the temperature jumps below the LCST, the complex response of the swollen PMDEGA film is still observed, which is attibuted to the broad transition region discussed above. However, as the final temperature is still below the LCST, the collapsed film slowly recovers to its initially swollen state.

By modification of both ends of the hydrophilic PMDEGA block with hydrophobic PS blocks, the obtained amphiphilic tri-block copolymer P(S-*b*-MDEGA-*b*-S) possesses physical crosslinks, which hinder the rearrangement of the PMDEGA chains in ambient conditions. Therefore, the dewetting of thin P(S-*b*-MDEGA-*b*-S) films is not as severe as in case of thin PMDEGA films. Besides this difference, thin P(S-*b*-MDEGA-*b*-S) films also share some similarities with thin PMDEGA films in the swelling behavior: the swelling capability is sensitive to vapor prssure and the swelling process contains two steps. Due to the introduction of hydrophobic PS blocks, the LCST of thin P(S-*b*-MDEGA-*b*-S) film is lower than thin PMDEGA film with same thickness, whereas the transition region is still very broad.

Moreover, the amphiphilic block copolymer P(S-*b*-MDEGA-*b*-S) has the ability to self-assemble into a micellar structure in solution. By choosing different selective solvents (PMDEGA-selective or PS-selective), the obtained micelles have different core-shell structures in solution. In the PMDEGA-selective solvents, the core consists of PS blocks and the shell is made up of PMDEGA blocks. Whereas in the PS-selective solvents, the core-shell structure is reversed. By solution casting, the different micellar structures are

transfered into thick films. When the films are immersed in D_2O, the micelles in the films prepared from the PMDEGA-selective solvents keep the core-shell structure unchanged, only the shell swells. Even if the temperature is raised above the transition temperature, both the core and the shell stay constant. No pronounced shrinkage of the swollen shell is observed. Only the hard-sphere radius (intermicellar distance) dramatically decreases and the volume fraction gradually increases, indicating that the collapsed micelles tend to approach each other and form large domains. The transition region of thick P(S-*b*-MDEGA-*b*-S) films is broad (40 - 42 °C) as well. However, in case of films prepared from the PS-selective solvents and immersed in D_2O, due to the selective effect of D_2O, the core and the shell are reversed. This reversal process induces additional entanglement of the PMDEGA chains in the shell, causing an even broader transition temperature (36 - 42 °C).

As a consequence, the transition behavior of the PMDEGA based thermo-responsive polymer films is different to the well-investigated PNIPAM films. They do not have a sharp transition region and therefore may not be perfect candidates for appliactions such as thermal switches. In contrast applications such as release of drugs will benefit from a broad transition region. In addition thin PMDEGA and P(S-*b*-MDEGA-*b*-S) films can absorb a large amount of water while the film thickness does not have a pronounced increase. Thus, they may have potential use in water storage and related active cooling of house roofs.

In upcoming projects, it is meaningful to extend the investigation to di-block copolymer P(S-*b*-MDEGA), which can form corona structure in solution. Thus, the film structure obtained and corresponding transition behavior can be studied and compared to thin PMDEGA and P(S-*b*-MDEGA-*b*-S) films investigated in this thesis. Additionally, the responsive behavior of thick P(S-*b*-MDEGA-*b*-S) films to sudden thermal stimuli above or below the transition temperature is still unclear yet. With neutron scattering technique, e.g. small-angle neutron scattering (SANS), the response of thick films can be achieved and compared to the thin films.

Bibliography

[1] T. Tanaka. Collapse of gels and the critical endpoint. *Phys. Rev. Lett.*, 40:820–823, 1978.

[2] H. G. Schild. Poly(N-isopropylacrylamide): experiment, theory and application. *Prog. Polym. Sci.*, 17:163–249, 1992.

[3] A. Suzuki and T. Tanaka. Phase transition in polymer gels induced by visible light. *Nature*, 346:345–347, 1990.

[4] M. Irie. Stimuli-responsive poly(N-isopropylacrylamide) - photoinduced and chemicalinduced phase-transitions. *Adv. Polym. Sci.*, 110:49–65, 1993.

[5] T. Tanaka, I. Nishio, S. T. Sun, and S. Uenonishio. Collapse of gels in an electric field. *Science*, 218:467–469, 1982.

[6] Y. Osada, H. Okuzaki, and H. Hori. A polymer gel with electrically driven motility. *Nature*, 355:242–244, 1992.

[7] B. Jeong and A. Gutowska. Lessons from nature: stimuli-responsive polymers and their biomedical applications. *Trends Biotechnol.*, 20:360–360, 2002.

[8] A. Richter, G. Paschew, S. Klatt, J. Lienig, K. F. Arndt, and H. J. P. Adler. Review on hydrogel-based pH sensors and microsensors. *Sensors*, 8:561–581, 2008.

[9] I. Tokarev and S. Minko. Stimuli-responsive hydrogel thin films. *Soft Matter*, 5:511–524, 2009.

[10] M. A. Cooperstein and H. E. Canavan. Biological cell detachment from poly(N-isopropyl acrylamide) and its applications. *Langmuir*, 26:7695–7707, 2010.

[11] B. Rybtchinski. Adaptive supramolecular nanomaterials based on strong noncovalent interactions. *ACS Nano*, 5:6791–6818, 2011.

[12] A. O. Moughton, M. A. Hillmyer, and T. P. Lodge. Multicompartment block polymer micelles. *Macromolecules*, 45:2–19, 2012.

[13] T. Hellweg, C. D. Dewhurst, W. Eimer, and K. Kratz. PNIPAM-co-polystyrene core-shell microgels: structure, swelling behavior, and crystallization. *Langmuir*, 20:4330–4335, 2004.

[14] K. Akiyoshi, E. C. Kang, S. Kurumada, J. Sunamoto, T. Principi, and F. M. Winnik. Controlled association of amphiphilic polymers in water: thermosensitive nanoparticles formed by self-assembly of hydrophobically modified pullulans and poly(N-isopropylacrylamides). *Macromolecules*, 33:3244–3249, 2000.

[15] E. Akiyama, N. Morimoto, P. Kujawa, Y. Ozawa, F. M. Winnik, and K. Akiyoshit. Self-assembled nanogels of cholesteryl-modified polysaccharides: effect of the polysaccharide structure on their association characteristics in the dilute and semidilute regimes. *Biomacromolecules*, 8:2366–2373, 2007.

[16] M. Yang, C. Liu, Z. Y. Li, G. Gao, and F. Q. Liu. Temperature-responsive properties of poly(acrylic acid-co-acrylamide) hydrophobic association hydrogels with high mechanical strength. *Macromolecules*, 43:10645–10651, 2010.

[17] R. Paris, I. Quijada-Garrido, O. Garcia, and M. Liras. BODIPY-conjugated thermosensitive fluorescent polymers based on 2-(2-methoxyethoxy)ethyl methacrylate. *Macromolecules*, 44:80–86, 2011.

[18] M. Liras, J. M. Garcia-Garcia, I. Quijada-Garrido, A. Gallardo, and R. Paris. Thermo-responsive allyl-functionalized 2-(2-methoxyethoxy)ethyl methacrylate-based polymers as versatile precursors for smart polymer conjugates and conetworks. *Macromolecules*, 44:3739–3745, 2011.

[19] J. C. Gaulding, M. H. Smith, J. S. Hyatt, A. Fernandez-Nieves, and L. A. Lyon. Reversible inter- and intra-microgel cross-linking using disulfides. *Macromolecules*, 45:39–45, 2012.

[20] A. Miasnikova, A. Laschewsky, G. De Paoli, C. M. Papadakis, P. Müller-Buschbaum, and S. S. Funari. Thermoresponsive hydrogels from symmetrical triblock copolymers poly(styrene-block-(methoxy diethylene glycol acrylate)-block-styrene). *Langmuir*, 28:4479–4490, 2012.

[21] A. Nykaenen, M. Nuopponen, P. Hiekkataipale, S. P. Hirvonen, A. Soininen, H. Tenhu, O. Ikkala, R. Mezzenga, and J. Ruokolainen. Direct imaging of nanoscopic plastic deformation below bulk Tg and chain stretching in temperature-responsive block copolymer hydrogels by cryo-TEM. *Macromolecules*, 41:3243–3249, 2008.

[22] M. J. Snowden, M. J. Murray, and B. Z. Chowdry. Some like it hot! Thermosensitive polymers. *Chem. Ind.*, pages 531–534, 1996.

[23] W. X. Song, Q. He, H. Mohwald, Y. Yang, and J. B. Li. Smart polyelectrolyte microcapsules as carriers for water-soluble small molecular drug. *J. Controlled Release*, 139:160–166, 2009.

[24] D. G. Shchukin, D. O. Grigoriev, and H. Mohwald. Application of smart organic nanocontainers in feedback active coatings. *Soft Matter*, 6:720–725, 2010.

[25] S. Schmidt, M. Zeiser, T. Hellweg, C. Duschl, A. Fery, and H. Mohwald. Adhesion and mechanical properties of PNIPAM microgel films and their potential use as switchable cell culture substrates. *Adv. Funct. Mater.*, 20:3235–3243, 2010.

[26] S. Kessel, S. Schmidt, R. Muller, E. Wischerhoff, A. Laschewsky, J. F. Lutz, K. Uhlig, A. Lankenau, C. Duschl, and A. Fery. Thermoresponsive PEG-based polymer layers: surface characterization with AFM force measurements. *Langmuir*, 26:3462–3467, 2010.

[27] F. M. Winnik. Fluorescence studies of aqueous solutions of poly(N-isopropylacrylamide) below and above their LCST. *Macromolecules*, 23:233–242, 1990.

[28] M. Shibayama, T. Tanaka, and C. C. Han. Small angle neutron scattering study on poly(N-isopropyl acrylamide) gels near their volume phase transition temperature. *J. Chem. Phys.*, 97:6829–6841, 1992.

[29] K. C. Tam, X. Y. Wu, and R. H. Pelton. Poly(N-isopropylacrylamide). II. effect of polymer concentration, temperature, and surfactant on the viscosity of aqueous solutions. *J. Polym. Sci., Part A: Polym. Chem.*, 31:963–969, 1993.

[30] E. I. Tiktopulo, V. E. Bychkova, J. Ricka, and O. B. Ptitsyn. Cooperativity of the coil-globule transition in a homopolymer: microcalorimetric study of poly(N-isopropylacrylamide). *Macromolecules*, 27:2879–2882, 1994.

[31] X. H. Wang, X. P. Qiu, and C. Wu. Comparison of the coil-to-globule and the globule-to-coil transitions of a single poly(N-isopropylacrylamide) homopolymer chain in water. *Macromolecules*, 31:2972–2976, 1998.

[32] Y. Maeda, T. Higuchi, and I. Ikeda. FTIR spectroscopic and calorimetric studies of the phase transitions of n-isopropylacrylamide copolymers in water. *Langmuir*, 17:7535–7539, 2001.

[33] R. Kita and S. Wiegand. Soret coefficient of poly(N-isopropylacrylamide)/water in the vicinity of coil-globule transition temperature. *Macromolecules*, 38:4554–4556, 2005.

[34] J. F. Lutz, O. Akdemir, and A. Hoth. Point by point comparison of two thermosensitive polymers exhibiting a similar LCST: is the age of poly(NIPAM) over? *J. Amer. Chem. Soc.*, 128:13046–13047, 2006.

[35] J. Ye, J. Xu, J. M. Hu, X. F. Wang, G. Z. Zhang, S. Y. Liu, and C. Wu. Comparative study of temperature-induced association of cyclic and linear poly(N-isopropylacrylamide) chains in dilute solutions by laser light scattering and stopped-flow temperature jump. *Macromolecules*, 41:4416–4422, 2008.

[36] T. Koga, F. Tanaka, R. Motokawa, S. Koizumi, and F. M. Winnik. Theoretical modeling of associated structures in aqueous solutions of hydrophobically modified telechelic PNIPAM based on a neutron scattering study. *Macromolecules*, 41:9413–9422, 2008.

[37] J. Adelsberger, A. Kulkarni, A. Jain, W. Wang, A. M. Bivigou-Koumba, P. Busch, V. Pipich, O. Holderer, T. Hellweg, A. Laschewsky, P. Müller-Buschbaum, and C. M. Papadakis. Thermoresponsive PS-*b*-PNIPAM-*b*-PS micelles: aggregation behavior, segmental dynamics, and thermal response. *Macromolecules*, 43:2490–2501, 2010.

[38] Y. Maeda, T. Nakamura, and I. Ikeda. Changes in the hydration states of poly(N-alkylacrylamide)s during their phase transitions in water observed by FTIR spectroscopy. *Macromolecules*, 34:1391–1399, 2001.

[39] J. E. Chung, M. Yokoyama, K. Suzuki, T. Aoyagi, Y. Sakurai, and T. Okano. Reversibly thermo-responsive alkyl-terminated poly(N-isopropylacrylamide) core-shell micellar structures. *Colloids Surf., B*, 9:37–48, 1997.

[40] H. Feil, Y. H. Bae, J. Feijen, and S. W. Kim. Effect of comonomer hydrophilicity and ionization on the lower critical solution temperature of N-isopropylacrylamide copolymers. *Macromolecules*, 26:2496–2500, 1993.

[41] V. Y. Grinberg, A. S. Dubovik, D. V. Kuznetsov, N. V. Grinberg, A. Y. Grosberg, and T. Tanaka. Studies of the thermal volume transition of poly(N-isopropylacrylamide) hydrogels by high-sensitivity differential scanning microcalorimetry. 2. thermodynamic functions. *Macromolecules*, 33:8685–8692, 2000.

[42] M. Kano and E. Kokufuta. On the temperature-responsive polymers and gels based on n-propylacrylamides and n-propylmethacrylamides. *Langmuir*, 25:8649–8655, 2009.

[43] W. Wang, K. Troll, G. Kaune, E. Metwalli, M. Ruderer, K. Skrabania, A. Laschewsky, S. V. Roth, C. M. Papadakis, and P. Müller-Buschbaum. Thin films of poly(N-isopropylacrylamide) end-capped with n-butyltrithiocarbonate. *Macromolecules*, 41:3209–3218, 2008.

[44] W. Wang, E. Metwalli, J. Perlich, C. M. Papadakis, R. Cubitt, and P. Müller-Buschbaum. Cyclic switching of water storage in thin block copolymer films containing poly(N-isopropylacrylamide). *Macromolecules*, 42:9041–9051, 2009.

[45] W. Wang, G. Kaune, J. Perlich, C. M. Paradakis, A. M. Bivigou-Koumba, A. Laschewsky, K. Schlage, R. Röhlsberger, S. V. Roth, R. Cubitt, and P. Müller-Buschbaum. Swelling and switching kinetics of gold coated end-capped poly(N-isopropylacrylamide) thin films. *Macromolecules*, 43:2444–2452, 2010.

[46] Q. Zhong, W. Wang, J. Adelsberger, A. Golosova, A. M. Bivigou-Koumba, A. Laschewsky, S. S. Funari, J. Perlich, S. V. Roth, C. M. Papadakis, and P. Müller-Buschbaum. Collapse transition in thin films of poly(methoxydiethylenglycol acrylate). *Colloid. Polym. Sci.*, 289:569–581, 2011.

[47] S. Aoshima and S. Kanaoka. A renaissance in living cationic polymerization. *Chem. Rev.*, 109:5245–5287, 2009.

[48] P. N. Hurter and T. A. Hatton. Solubilization of polycyclic aromatic-hydrocarbons by poly(ethylene oxide-propylene oxide) block copolymer micelles - effects of polymer structure. *Langmuir*, 8(5):1291–1299, 1992.

[49] A. Laschewsky. Molecular concepts, self-organisation and properties of polysoaps. *Adv. Polym. Sci.*, 124:1–86, 1995.

[50] I. R. Schmolka. Gel cosmetics. *Cosmetics & Toiletries*, 99:69–75, 1984.

[51] K. Troll, A. Kulkarni, W. Wang, C. Darko, A. M. Bivigou-Koumba, A. Laschewsky, P. Müller-Buschbaum, and C. M. Papadakis. The collapse transition of poly(styrene-b-(N-isopropylacrylamide)) diblock copolymers in aqueous solution and in thin films. *Colloid and Polymer Science*, 286:1079–1092, 2008.

[52] A. M. Bivigou-Koumba, J. Kristen, A. Laschewsky, P. Müller-Buschbaum, and C. M. Papadakis. Synthesis of symmetrical triblock copolymers of styrene and N-isopropylacrylamide using bifunctional bis(trithiocarbonate)s as RAFT agents. *Macromol. Chem. Phys.*, 210:565–578, 2009.

[53] M. W. Matsen and F. S. Bates. Unifying weak- and strong-segregation block copolymer theories. *Macromolecules*, 29:1091–1098, 1996.

[54] F. S. Bates and G. H. Fredrickson. Block copolymers - designer soft materials. *Phys. Today*, 52:32–38, 1999.

[55] F. S. Bates. Polymer-polymer phase behavior. *Science*, 251:898–905, 1991.

[56] Y. Y. Mai and A. Eisenberg. Self-assembly of block copolymers. *Chem. Soc. Rev.*, 41:5969–85, 2012.

[57] Carsten Tschierske. Amphotropic liquid crystals. *Curr. Opin. Colloid Interface Sci.*, 7:355–370, 2002.

[58] L. F. Zhang and A. Eisenberg. Thermodynamic vs kinetic aspects in the formation and morphological transitions of crew-cut aggregates produced by self-assembly of polystyrene-b-poly(acrylic acid) block copolymers in dilute solution. *Macromolecules*, 32:2239–2249, 1999.

[59] Y. S. Yu, L. F. Zhang, and A. Eisenberg. Morphogenic effect of solvent on crew-cut aggregates of apmphiphilic diblock copolymers. *Macromolecules*, 31:1144–1154, 1998.

[60] D. E. Discher and A. Eisenberg. Polymer vesicles. *Science*, 297:967–973, 2002.

[61] H. W. Shen and A. Eisenberg. Morphological phase diagram for a ternary system of block copolymer PS_{310}-*b*-PAA_{52}/dioxane/H_2O. *J. Phys. Chem. B*, 103:9473–9487, 1999.

[62] P. Lim Soo and A. Eisenberg. Preparation of block copolymer vesicles in solution. *J. Polym. Sci., Part B: Polym. Phys.*, 42:923–938, 2004.

[63] L. F. Zhang and A. Eisenberg. Multiple morphologies of "crew-cut" aggregates of polystyrene-*b*-poly(acrylic acid) block copolymers. *Science*, 268:1728–1731, 1995.

[64] N. S. Cameron, M. K. Corbierre, and A. Eisenberg. 1998 E.W.R. Steacie award lecture asymmetric amphiphilic block copolymers in solution: a morphological wonderland. *Can. J. Chem.*, 77:1311–1326, 1999.

[65] M. W. Matsen and F. S. Bates. Block copolymer microstructures in the intermediate-segregation regime. *J. Chem. Phys.*, 106:2436–2448, 1997.

[66] M. W. Matsen. Self-assembly of block copolymers in thin films. *Curr. Opin. Colloid Interface Sci.*, 3:40–47, 1998.

[67] T. L. Morkved and H. M. Jaeger. Thickness-induced morphology changes in lamellar diblock copolymer ultrathin films. *Europhys. Lett.*, 40:643–648, 1997.

[68] M. J. Fasolka, P. Banerjee, A. M. Mayes, G. Pickett, and A. C. Balazs. Morphology of ultrathin supported diblock copolymer films: Theory and experiment. *Macromolecules*, 33:5702–5712, 2000.

[69] P. Mansky, O. K. C. Tsui, T. P. Russell, and Y. Gallot. Phase coherence and microphase separation transitions in diblock copolymer thin films. *Macromolecules*, 32:4832–4837, 1999.

[70] P. Mansky, T. P. Russell, C. J. Hawker, M. Pitsikalis, and J. Mays. Ordered diblock copolymer films on random copolymer brushes. *Macromolecules*, 30:6810–6813, 1997.

[71] P. Mansky, T. P. Russell, C. J. Hawker, J. Mays, D. C. Cook, and S. K. Satija. Interfacial segregation in disordered block copolymers: effect of tunable surface potentials. *Phys. Rev. Lett.*, 79:237–240, 1997.

[72] H. P. Huinink, J. C. M. Brokken-Zijp, M. A. Van Dijk, and G. J. A. Sevink. Asymmetric block copolymers confined in a thin film. *J. Chem. Phys.*, 112:2452–2462, 2000.

[73] A. Kikuchi and T. Okano. Pulsatile drug release control using hydrogels. *Adv. Drug Deliv. Rev.*, 54:53–77, 2002.

[74] T. Xu, C. J. Hawker, and T. P. Russell. Interfacial interaction dependence of microdomain orientation in diblock copolymer thin films. *Macromolecules*, 38:2802–2805, 2005.

[75] E. Huang, S. Pruzinsky, T. P. Russell, J. Mays, and C. J. Hawker. Neutrality conditions for block copolymer systems on random copolymer brush surfaces. *Macromolecules*, 32:5299–5303, 1999.

[76] E. Huang, P. Mansky, T. P. Russell, C. Harrison, P. M. Chaikin, R. A. Register, C. J. Hawker, and J. Mays. Mixed lamellar films: evolution, commensurability effects, and preferential defect formation. *Macromolecules*, 33:80–88, 2000.

[77] E. S. Gil and S. M. Hudson. Stimuli-reponsive polymers and their bioconjugates. *Prog. Polym. Sci.*, 29:1173–1222, 2004.

[78] S. Reinicke, J. Schmelz, A. Lapp, M. Karg, T. Hellweg, and H. Schmalz. Smart hydrogels based on double responsive triblock terpolymers. *Soft Matter*, 5:2648–2657, 2009.

[79] I. Y. Galaev and B. Mattiasson. "Smart" polymers and what they could do in biotechnology and medicine. *Trends Biotechnol.*, 17:335–340, 1999.

[80] Y. Qiu and K. Park. Environment-sensitive hydrogels for drug delivery. *Adv. Drug Deliv. Rev.*, 53:321–339, 2001.

[81] P. Gupta, K. Vermani, and S. Garg. Hydrogels: from controlled release to pH-responsive drug delivery. *Drug Discovery Today*, 7:569–579, 2002.

[82] A. Chilkoti, M. R. Dreher, D. E. Meyer, and D. Raucher. Targeted drug delivery by thermally responsive polymers. *Adv. Drug Deliv. Rev.*, 54:613–630, 2002.

[83] N. I. Abu-Lail, M. Kaholek, B. LaMattina, R. L. Clark, and S. Zauscher. Micro-cantilevers with end-grafted stimulus-responsive polymer brushes for actuation and sensing. *Sens. Actuators, B: Chemical*, 114:371–378, 2006.

[84] M. Karg, Y. Lu, E. Carbo-Argibay, I. Pastoriza-Santos, J. Perez-Juste, L. M. Liz-Marzan, and T. Hellweg. Multiresponsive hybrid colloids based on gold nanorods and poly(NIPAM-co-allylacetic acid) microgels: temperature- and pH-tunable plasmon resonance. *Langmuir*, 25:3163–3167, 2009.

[85] T. Chen, R. Ferris, J. Zhang, R. Ducker, and S. Zauscher. Stimulus-responsive polymer brushes on surfaces: transduction mechanisms and applications. *Prog. Polym. Sci.*, 35:94–112, 2010.

[86] B. Eichinge and P. J. Flory. Thermodynamics of polymer solutions. part 1. natural rubber and benzene. *Trans. Faraday Soc.*, 64:2035–2052, 1968.

[87] M. Kaholek, W. K. Lee, S. J. Ahn, H. W. Ma, K. C. Caster, B. LaMattina, and S. Zauscher. Stimulus-responsive poly(N-isopropylacrylamide) brushes and nanopatterns prepared by surface-initiated polymerization. *Chem. Mater.*, 16:3688–3696, 2004.

[88] D. Schmaljohann. Thermo- and pH-responsive polymers in drug delivery. *Adv. Drug Deliv. Rev.*, 58:1655–1670, 2006.

[89] L. Klouda and A. G. Mikos. Thermoresponsive hydrogels in biomedical applications. *Eur. J. Pharm. Biopharm.*, 68:34–45, 2008.

[90] S. Mias, J. Sudor, and H. Camon. PNIPAM: a thermo-activated nano-material for use in optical devices. *Microsyst. Technol.*, 14:747–751, 2008.

[91] P. J. Flory. The configuration of real polymer chains. *J. Chem. Phys.*, 17:303–310, 1949.

[92] P. J. Flory. *Principles of polymer chemistry.* Cornell University Press, 1953.

[93] V. Aseyev, H. Tenhu, and F. M. Winnik. Non-ionic thermoresponsive polymers in water. *Adv. Polym. Sci.*, 242:29–89, 2011.

[94] A. Wilkinson A. D. McNaught. *Compendium of chemical terminology.* Blackwell Science, 1997.

[95] A. Y. Grosberg and A. R. Khokhlov. *Statistical physics of macromolecules.* AIP Press, 1994.

[96] I. C. Sanchez. Phase transition behavior of the isolated polymer chain. *Macromolecules*, 12:980–988, 1979.

[97] H. Yamakawa. The radius expansion factor and second virial coefficient for polymer chains below the θ temperature. *Macromolecules*, 26:5061–5066, 1993.

[98] H. Yamakawa, F. Abe, and Y. Einaga. Second virial coefficient of oligo- and polystyrenes near the θ temperature. more on the coil-to-globule transition. *Macromolecules*, 27:5704–5712, 1994.

[99] G. Swislow, S. T. Sun, I. Nishio, and T. Tanaka. Coil-globule phase transition in a single polystyrene chain in cyclohexane. *Phys. Rev. Lett.*, 44:796–798, 1980.

[100] S. T. Sun, I. Nishio, G. Swislow, and T. Tanaka. The coil-globule transition: radius of gyration of polystyrene in cyclohexane. *J. Chem. Phys.*, 73:5971–5975, 1980.

[101] I. Nishio, G. Swislow, S. T. Sun, and T. Tanaka. Critical density fluctuations within a single polymer chain. *Nature*, 300:243–244, 1982.

[102] S. Saeki, N. Kuwahara, M. Nakata, and M. Kaneko. Upper and lower critical solution temperatures in poly (ethyleneglycol) solutions. *Polymer*, 17:685–689, 1976.

[103] G. N. Malcolm and J. S. Rowlinson. The thermodynamic properties of aqueous solutions of polyethylene glycol, polypropylene glycol and dioxane. *Trans. Faraday Soc.*, 53:921–931, 1957.

[104] A. Matsuyama and F. Tanaka. Theory of solvation-induced reentrant phase-separation inpolymer-solutions. *Phys. Rev. Lett.*, 65:341–344, 1990.

[105] J. F. Lutz. Polymerization of oligo(ethylene glycol) (meth)acrylates: toward new generations of smart biocompatible materials. *J. Polym. Sci., Part A: Polym. Chem.*, 46:3459–3470, 2008.

[106] C. Tanford. *The hydrophobic effect: formation of micelles and biological membranes.* Wiley, 1973.

[107] N. T. Southall, K. A. Dill, and A. D. J. Haymet. A view of the hydrophobic effect. *J. Phys. Chem. B*, 106:2812–2812, 2002.

[108] D. Chandler. Interfaces and the driving force of hydrophobic assembly. *Nature*, 437:640–647, 2005.

[109] C. Tanford. *Physical Chemistry of macromolecules*. Wiley, 1966.

[110] J. N. Israelachvili. *Intermolecular and surface forces, 2nd edn.* Academic Press, 1992.

[111] Y. Maeda, T. Nakamura, and I. Ikeda. Changes in the hydration states of poly(N-n-propylmethacrylamide) and poly(N-isopropylmethacrylamide) during their phase transitions in water observed by FTIR spectroscopy. *Macromolecules*, 34:8246–8251, 2001.

[112] Y. Katsumoto, T. Tanaka, H. Sato, and Y. Ozaki. Conformational change of poly(N-isopropylacrylamide) during the coil-globule transition investigated by attenuated total reflection/infrared spectroscopy and density functional theory calculation. *J. Phys. Chem. A*, 106:3429–3435, 2002.

[113] O. Ramon, E. Kesselman, R. Berkovici, Y. Cohen, and Y. Paz. Attenuated total reflectance/Fourier transform infrared studies on the phase-separation process of aqueous solutions of poly(N-isopropylacrylamide). *J. Polym. Sci., Part B: Polym. Phys.*, 39:1665–1677, 2001.

[114] B. Widom, P. Bhimalapuram, and K. Koga. The hydrophobic effect. *Phys. Chem. Chem. Phys.*, 5:3085–3093, 2003.

[115] Y. Okada and F. Tanaka. Cooperative hydration, chain collapse, and flat LCST behavior in aqueous poly(N-isopropylacrylamide) solutions. *Macromolecules*, 38:4465–4471, 2005.

[116] E. I. Tiktopulo, V. N. Uversky, V. B. Lushchik, S. I. Klenin, V. E. Bychkova, and O. B. Ptitsyn. "Domain" coil-globule transition in homopolymers. *Macromolecules*, 28:7519–7524, 1995.

[117] Y. G. Takei, T. Aoki, K. Sanui, N. Ogata, T. Okano, and Y. Sakurai. Temperature-responsive bioconjugates. 1. synthesis of temperature-responsive oligomers with reactive end groups and their coupling to biomolecules. *Bioconjugate Chem.*, 4:42–46, 1993.

[118] Z. L. Ding, G. H. Chen, and A. S. Hoffman. Synthesis and purification of thermally sensitive oligomer-enzyme conjugates of poly(N-isopropylacrylamide)-trypsin. *Bioconjugate Chem.*, 7:121–125, 1996.

[119] H. G. Schild and D. A. Tirrell. Sodium 2-(n-dodecylamino)naphthalene-6-sulfonate as a probe of polymer-surfactant interaction. *Langmuir*, 6:1676–1679, 1990.

[120] S. Furyk, Y. J. Zhang, D. Ortiz-Acosta, P. S. Cremer, and D. E. Bergbreiter. Effects of end group polarity and molecular weight on the lower critical solution temperature of poly(N-isopropylacrylamide). *J. Polym. Sci., Part A: Polym. Chem.*, 44:1492–1501, 2006.

[121] Q. Duan, Y. Miura, A. Narumi, X. Shen, S. Sato, T. Satoh, and T. Kakuchi. Synthesis and thermoresponsive property of end-functionalized poly(N-isopropylacrylamide) with pyrenyl group. *J. Polym. Sci., Part A: Polym. Chem.*, 44:1117–1124, 2006.

[122] Y. Xia, N. A. D. Burke, and H. D. H. Stover. End group effect on the thermal response of narrow-disperse poly(N-isopropylacrylamide) prepared by atom transfer radical polymerization. *Macromolecules*, 39:2275–2283, 2006.

[123] S. Fujishige, K. Kubota, and I. Ando. Phase transition of aqueous solutions of poly(N-isopropylacrylamide) and poly(N-isopropylmethacrylamide). *J. Phys. Chem.*, 93:3311–3313, 1989.

[124] L. D. Taylor and L. D. Cerankowski. Preparation of films exhibiting a balanced temperature dependence to permeation by aqueous solutions - a study of lower consolute behavior. *J. Polym. Sci., Part A: Polym. Chem.*, 13:2551–2570, 1975.

[125] F. M. Winnik, A. R. Davidson, G. K. Hamer, and H. Kitano. Amphiphilic poly(N-isopropylacrylamides) prepared by using a lipophilic radical initiator - synthesis and solution properties in water. *Macromolecules*, 25:1876–1880, 1992.

[126] J. Adelsberger, E. Metwalli, A. Diethert, I. Grillo, A. M. Bivigou-Koumba, A. Laschewsky, P. Müller-Buschbaum, and C. M. Papadakis. Kinetics of collapse transition and cluster formation in a thermoresponsive micellar solution of P(S-*b*-NIPAM-*b*-S) induced by a temperature jump. *Macromol. Rapid Commun.*, 33:254–259, 2012.

[127] Y. Guan and Y. J. Zhang. PNIPAM microgels for biomedical applications: from dispersed particles to 3D assemblies. *Soft Matter*, 7:6375–6384, 2011.

[128] Q. Zhong, E. Metwalli, G. Kaune, M. Rawolle, A. M. Bivigou-Koumba, A. Laschewsky, C. M. Papadakis, R. Cubitt, and P. Müller-Buschbaum. Switching kinetics of thin thermo-responsive hydrogel films of poly(monomethoxy-diethyleneglycol-acrylate) probed with in situ neutron reflectivity. *Soft Matter*, 8:5241–5249, 2012.

[129] J. Adelsberger, A. Meier-Koll, A. M. Bivigou-Koumba, P. Busch, O. Holderer, T. Hellweg, A. Laschewsky, P. Müller-Buschbaum, and C. M. Papadakis. The collapse transition and the segmental dynamics in concentrated micellar solutions of P(S-*b*-NIPAM) diblock copolymers. *Colloid. Polym. Sci.*, 289:711–720, 2011.

[130] R. W. James. *The optical principles of the diffraction of X-rays*. G. Bell And Sons Limited, 1982.

[131] M. Born and E. Wolf. *Principles of Optics: Electromagnetic Theory of Propagation, Interference and Diffraction of Light*. Pergamon Press Ltd, 1993.

[132] F. Abeles. Investigations on the propagation of sinusoidal electromagnetic waves in stratified media. application to thin films. *Ann. de Physique*, 5:596, 1950.

[133] D. W. Berreman. Dynamical theory of X-ray-diffraction in flat, focusung, and distorted crystals by ageless matrix-method. *Phys. Rev. B*, 14:4313–4317, 1976.

[134] J. Lekner. *Theory of Reflection of Electromagnetic and Particle Waves. Developments in Electromagnetic Theory and Application*. Martinus Nijhoff, 1987.

[135] L. G. Parratt. Surface studies of solids by total reflection of X-rays. *Phys. Rev.*, 95:359–369, 1954.

[136] M. Tolan. *X-Ray Scattering from Soft-Matter Thin Films: Materials Science and Basic Research*. Springer Tracts in Modern Physics, 1999.

[137] F. El Feninat, S. Elouatik, T. H. Ellis, E. Sacher, and I. Stangel. Quantitative assessment of surface roughness as measured by AFM: application to polished human dentin. *Appl. Surf. Sci.*, 183:205–215, 2001.

[138] O. Glatter. *Small Angle X-Ray Scattering*. Academic Press, 1982.

[139] R. J. Roe. *Methods of X-ray and Neutron Scattering in Polymer Science*. Oxford University Press, 2000.

[140] P. Lindner and Th. Zemb, editors. *Neutron, X-rays and Light. Scattering Methods Applied to Soft Condensed Matter*. North-Holland, 2002.

[141] D. Posselt, J. S. Pedersen, and K. Mortensen. A SANS investigation on absolute scale of a homologous series of base-catalysed silica aerogels. *J. Non-Cryst. Solids*, 145:128–132, 1992.

[142] J. Daillant and O. Belorgey. Surface scattering of X rays in thin films. part I. theoretical treatment. *J. Chem. Phys.*, 97:5824–5836, 1992.

[143] V. Holy and T. Baumbach. Nonsepcular X-ray reflection from rough multilayers. *Phys. Rev. B: Condens. Matter*, 49:10668–10676, 1994.

[144] T. Salditt, T. H. Metzger, J. Peisl, B. Reinker, M. Moske, and K. Samwer. Determination of the height-height correlation function of rough surfaces from diffuse X-ray scattering. *Europhys. Lett.*, 32:331–336, 1995.

[145] F. J. Hua, X. G. Jiang, D. J. Li, and B. Zhao. Well-defined thermosensitive, water-soluble polyacrylates and polystyrenics with short pendant oligo (ethylene glycol) groups synthesized by nitroxide-mediated radical polymerization. *J. Polym. Sci., Part A: Polym. Chem.*, 44:2454–2467, 2006.

[146] P. Müller-Buschbaum. Influence of surface cleaning on dewetting of thin polystyrene films. *Eur. Phys. J. E Soft Matter*, 12:443–448, 2003.

[147] D. W. Schubert. Spin coating as a method for polymer molecular weight determination. *Polym. Bull.*, 38:177–184, 1997.

[148] D. W. Schubert and T. Dunkel. Spin coating from a molecular point of view: its concentration regimes, influence of molar mass and distribution. *Mater. Res. Innovations*, 7:314–321, 2003.

[149] C. Braun. *Parratt32*. HMI Berlin, 2002.

[150] S. R. Kline. Reduction and analysis of SANS and USANS data using IGOR Pro. *J. Appl. Crystallogr.*, 39:895–900, 2006.

[151] F. Horkay, A. M. Hecht, S. Mallam, E. Geissler, and A. R. Rennie. Macroscopic and microscopic thermodynamic observations in swollen poly(vinyl acetate) networks. *Macromolecules*, 24:2896–2902, 1991.

[152] R. Engels, U. Clemens, G. Kemmerling, H. Noldgen, and J. Schelten. Position-sensitive detectors of the detector group at julich. *Nucl. Instrum. Methods Phys. Res., Sect. A*, 604:147–149, 2009.

[153] S. V. Roth, R. Dohrmann, M. Dommach, M. Kuhlmann, I. Kroger, R. Gehrke, H. Walter, C. Schroer, B. Lengeler, and P. Müller-Buschbaum. Small-angle options of the upgraded ultrasmall-angle X-ray scattering beamline BW4 at HASYLAB. *Rev. Sci. Instrum.*, 77(8), 2006.

[154] P. Müller-Buschbaum, E. Bauer, S. Pfister, S. V. Roth, M. Burghammer, C. Riekel, C. David, and U. Thiele. Creation of multi-scale stripe-like patterns in thin polymer blend films. *Europhys. Lett.*, 73:35–41, 2006.

[155] Y. Yoneda. Anomalous surface reflection of X-rays. *Phys. Rev.*, 131:2010–2013, 1963.

[156] P. Müller-Buschbaum, P. Vanhoorne, V. Scheumann, and M. Stamm. Observation of nano-dewetting structures. *Europhys. Lett.*, 40:655–660, 1997.

[157] P. Müller-Buschbaum. Grazing incidence small-angle X-ray scattering: an advanced scattering technique for the investigation of nanostructured polymer films. *Anal Bioanal Chem.*, 376:3–10, 2003.

[158] R. Cubitt and G. Fragneto. D17: the new reflectometer at the ill. *Appl. Phys. A*, 74:S329–S331, 2002.

[159] A. Nelson. Co-refinement of multiple-contrast neutron/X-ray reflectivity data using MOTOFIT. *J. Appl. Crystallogr.*, 39:273–276, 2006.

[160] V. F. Sears. Neutron scattering lengths and cross sections. *Neutron News 3*, 3:26–37, 1992.

[161] A. R. Hind, S. K. Bhargava, and A. McKinnon. At the solid/liquid interface: FTIR/ATR - the tool of choice. *Adv. Colloid Interface Sci.*, 93:91–114, 2001.

[162] S. G. Kazarian and K. L. A. Chan. Applications of ATR-FTIR spectroscopic imaging to biomedical samples. *Biochim. Biophys. Acta*, 1758:858–867, 2006.

[163] C. S. Brian, editor. *Fundamentals of Fourier Transform Infrared spectroscopy.* CRC press, 1996.

[164] P. Müller-Buschbaum. Dewetting and pattern formation in thin polymer films as investigated in real and reciprocal space. *J. Phys.: Condens. Matter*, 15:R1549–R1582, 2003.

[165] W. Xu, K. S. Siow, Z. Q. Gao, and S. Y. Lee. Novel alternating comblike copolymer electrolytes with single lithium ionic conduction. *Chem. Mater.*, 10:1951–1957, 1998.

[166] P. Müller-Buschbaum, J. S. Gutmann, C. Lorenz, T. Schmitt, and M. Stamm. Decay of interface correlation in thin polymer films. *Macromolecules*, 31:9265–9272, 1998.

[167] Q. Yan and A. S. Hoffman. Synthesis of macroporous hydrogels with rapid swelling and deswelling properties for delivery of macromolecules. *Polymer*, 36:887–889, 1995.

[168] Y. Kaneko, S. Nakamura, K. Sakai, T. Aoyagi, A. Kikuchi, Y. Sakurai, and T. Okano. Rapid deswelling response of poly(N-isopropylacrylamide) hydrogels by the formation of water release channels using poly(ethylene oxide) graft chains. *Macromolecules*, 31:6099–6105, 1998.

[169] E. C. Cho, J. Lee, and K. Cho. Role of bound water and hydrophobic interaction in phase transition of poly(N-isopropylacrylamide) aqueous solution. *Macromolecules*, 36:9929–9934, 2003.

[170] Y. Li and T. Tanaka. Kinetics of swelling and shrinking of gels. *J. Chem. Phys.*, 92:1365–1371, 1990.

[171] T. Tanaka, L. O. Hocker, and G. B. Benedek. Spectrum of light scattered from a viscoelastic gel. *J. Chem. Phys.*, 59:5151–5159, 1973.

[172] T. Tanaka and D. J. Fillmore. Kinetics of swelling of gels. *J. Chem. Phys.*, 70:1214–1218, 1979.

[173] L. D. Landau and E. M. Lifshitz. *Theory of Elasticity*. Butterworth-Heinemann, 1986.

[174] P. Müller-Buschbaum and M. Stamm. Correlated roughness, long-range correlations, and dewetting of thin polymer films. *Macromolecules*, 31:3686–3692, 1998.

[175] R. White. *Chromatography/Fourier Transform Infrared Spectroscopy and its Applications*. 1990.

[176] J. Burke. *Solubility Parameters: Theory and Application.* The Book and Paper Group Annual, 1984.

[177] T. Ueki and M. Watanabe. Polymers in ionic liquids: Dawn of neoteric solvents and innovative materials. *Bull. Chem. Soc. Jpn.*, 85:33–50, 2012.

[178] D. W. Van Krevelen and T. K. Nijenhuis. *Properties of Polymers: Their Correlation with Chemical Structure: their Numerical Estimation and Prediction from Additive Group Contributions.* Elsevier Science, 1990.

[179] M. Al-Hussein, M. A. Ruderer, E. Metwalli, V. Korstgens, U. Vainio, S. V. Roth, R. Dohrmann, R. Gehrke, R. Gebhardt, M. Burghammer, and P. Müller-Buschbaum. Determination of the ordered structure in conjugated-coil diblock copolymers films from a thickness gradient prepared by spin-coated drop technique. *Macromolecules*, 42:4230–4236, 2009.

List of publications

Publications related to the dissertation

- Q. Zhong, E. Metwalli, G. Kaune, M. Rawolle, A. M. Bivigou-Koumba, A. Laschewsky, C. M. Papadakis, R. Cubitt, P. Müller-Buschbaum: Switching kinetics of thin thermo-responsive hydrogel films of poly(monomethoxydiethyleneglycol-acrylate) probed with in situ neutron reflectivity; *Soft Matter* **2012**, *8*, 5241-5249.

- Q. Zhong, W. Wang, J. Adelsberger, A. Golosova, A. M. Bivigou-Koumba, A. Laschewsky, S. S. Funari, J. Perlich, S. V. Roth, C. M. Papadakis, P. Müller-Buschbaum: Collapse transition in thin films of poly(methoxydiethylenglycol acrylate); *Colloid. Polym. Sci.* **2011**, *289*, 569-581.

- Q. Zhong, J. Adelsberger, M. Niedermeier, A. Golosova, A. M. Bivigou-Koumba, A. Laschewsky, S. S. Funari, C. M. Papadakis, P. Müller-Buschbaum: The influence of selective solvents on the transition behavior of poly(styrene-*b*-monomethoxy diethylenglycol-acrylate-*b*-styrene) thick films, submitted.

- Q. Zhong, E. Metwalli, M. Rawolle, G. Kaune, A. M. Bivigou-Koumba, A. Laschewsky, C. M. Papadakis, R. Cubitt, P. Müller-Buschbaum: Structure and thermal response of thin thermo-responsive poly(styrene-*b*-monomethoxydiethylenglycol-acrylate-*b*-styrene) films, in preparation.

Further publications

- M. A. Niedermeier, D. Magerl, Q. Zhong, A. Nathan, V. Körstgens, J. Perlich, S. V. Roth, P. Müller-Buschbaum: Combining mixed titania morphologies into a complex assembly thin film by iterative block copolymer based sol-gel templating; *Nanotechnology* **2012**, *23*, 145602.

- R. Gebhardt, W. Holzmüller, Q. Zhong, P. Müller-Buschbaum, U. Kulozik: Structural ordering of casein micelles on silicon nitride micro-sieves during filtration; *J. Coll. Surf. B* **2011**, *88*, 240-245.

- M. Rawolle, M. A. Ruderer, S. M. Prams, Q. Zhong, D. Magerl, J. Perlich, S. V. Roth, P. Lellig, J. S. Gutmann, P. Müller-Buschbaum: Nanostructureing of titania thin films by combination of micro-fluidics and block copolymer based sol-gel templating; *Small* **2011**, *7*, 884-891.

- A. Diethert, E. Metwalli, R. Meier, Q. Zhong, R. A. Campbell, R. Cubitt, P. Müller-Buschbaum: In-situ neutron reflectometry study of the near-surface solvent concentration profile during solution casting; *Soft Matter* **2011**, *7*, 6648-6659.

- M. A. Ruderer, S. M. Prams, M. Rawolle, Q. Zhong, J. Perlich, S. V. Roth, P. Müller-Buschbaum: Influence of annealing and blending of photoactive polymers on their crystalline structure; *J. Phys. Chem. B* **2010**, *114*, 15451-15458.

- G. Kaune, M. Haese-Seiler, R. Kampmann, J. -F. Moulin, Q. Zhong, P. Müller-Buschbaum: TOF-GISANS investigation of polymer infiltration in mesoporous TiO_2 films for photovoltaic applications; *J. Poly. Sci. Part B* **2010**, *48*, 1628-1635.

- J. Perlich, J. Rubeck, S. Botta, R. Gehrke, S. V. Roth, M. A. Ruderer, S. M. Prams, M. Rawolle, Q. Zhong, V. Körstgens, P. Müller-Buschbaum: Grazing incidence wide angle X-ray scattering at the wiggler beamline BW4 of HASYLAB; *Rev. Sci. Instr.* **2010**, *81*, 105105.

Scientific reports

- Q. Zhong, D. Magerl, V. Körstgens, A. Nathan, A. M. Bivigou-Koumba, A. Laschewsky, J. Perlich, S. V. Roth, C. M. Papadakis, P. Müller-Buschbaum: Internal and surface structure of thermo-responsive PMDEGA films probed with GISAXS and AFM; *HASYLAB, Annual report 2011.*

- Q. Zhong, M. Schindler, A. Nathan, V. Körstgens, A. M. Bivigou-Koumba, A. Laschewsky, S. S. Funari, C. M. Papadakis, P. Müller-Buschbaum: The influence of different solvents on the LCST behavior of thick P(S-*b*-MDEGA-*b*-S) hydrogel films; *HASYLAB, Annual report 2011*

- Q. Zhong, E. Metwalli, G. Kaune, M. Rawolle, C. M. Papadakis, A. M. Bivigou-Koumba, A. Laschewsky, R. Cubitt, P. Müller-Buschbaum: Swelling behavior of novel thermo-responsive poly(styrene-*b*-monomethoxydiethylenglycol-acrylate-*b*-styrene) thin films probed by in-situ neutron reflectivity; *Lehrstuhl für Funktionelle Materialien, Annual report 2011.*

- Q. Zhong, J. Adelsberger, M. Niedermeier, A. Golosova, A. M. Bivigou-Koumba, A. Laschewsky, S. S. Funari, C. M. Papadakis, P. Müller-Buschbaum: Block-selective solvent influence on LCST of tri-block polymer P(S-*b*-MDEGA-*b*-S) film; *HASYLAB, Annual report 2010.*

- Q. Zhong, E. Metwalli, G. Kaune, M. Rawolle, A. M. Bivigou-Koumba, A. Laschewsky, C. M. Papadakis, R. Cubitt, P. Müller-Buschbaum: Kinetics of chain collapse in novel PMDEGA hydrogel films (Exp-No. 9-11-1388); *Experimental Report for the Institut Laue-Langevin (ILL), 2010.*

- Q. Zhong, W. Wang, G. Kaune, M. Rawolle, E. Metwalli, C. M. Papadakis, A. M. Bivigou-Koumba, A. Laschewsky, R. Cubitt, P. Müller-Buschbaum: Switching kinetics of PMDEGA based thermo-responsive hydrogel films probed by in-situ neutron reflectivity; *Lehrstuhl für Funktionelle Materialien, Annual report 2010*

- Q. Zhong, P. Müller-Buschbaum: Characterization of hydrogel film based on PMDEGA; *Lehrstuhl für Funktionelle Materialien, Annual report 2009.*

- Q. Zhong, W. Wang, P. Müller-Buschbaum: Thin films of Poly(Monomethoxy diethyleneglycol acrylate) based homo polymer; *Lehrstuhl für Funktionelle Materialien, Annual report 2008.*

Conference talks

- Q. Zhong, G. Kaune, M. Rawolle, E. Metwalli, A. M. Bivigou-Koumba, A. Laschewsky, C. M. Papadakis, R. Cubitt, P. Müller-Buschbaum: In-situ neutron reflectivity - a tool to probe switching kinetics of PMDEGA based thermo-responsive hydrogel films; *SPP 1259 workshop*, München (Germany), October 2011.

- Q. Zhong, G. Kaune, M. Rawolle, E. Metwalli, A. M. Bivigou-Koumba, A. Laschewsky, C. M. Papadakis, R. Cubitt, P. Müller-Buschbaum: Switching kinetics of PMDEGA

based thermo-responsive hydrogel films probed by in-situ neutron reflectivity; *DPG spring meeting*, Dresden (Germany), March 2011.

- Q. Zhong, W. Wang, G. Kaune, M. Rawolle, E. Metwalli, A. M. Bivigou-Koumba, A. Laschewsky, R. Cubitt, C. M. Papadakis, P. Müller-Buschbaum: In-situ neutron reflectivity as a tool to probe swelling of hydrogel films; *SPP 1259 workshop*, Aachen (Germany), October 2010.

- Q. Zhong, W. Wang, A. M. Bivigou-Koumba, A. Laschewsky, C. M. Papadakis, M. Haese-Seiller, R. Kampmann, P. Müller-Buschbaum: Characterization of PMDEGA based hydrogel film; *4th FRM-II Workshop on Neutron Scattering*, Burg Rothenfels (Germany), June 2009.

Conference poster presentations

- Q. Zhong, E. Metwalli, G. Kaune, M. Rawolle, A. M. Bivigou-Koumba, A. Laschewsky, C. M. Papadakis, R. Cubitt, P. Müller-Buschbaum: Swelling and switching behaviors of novel thermo-responsive P(S-*b*-MDEGA-*b*-S) hydrogel films under vapor atmosphere; *DPG spring meeting*, Berlin (Germany), March 2012.

- Q. Zhong, E. Metwalli, G. Kaune, M. Rawolle, A. M. Bivigou-Koumba, A. Laschewsky, C. M. Papadakis, R. Cubitt, P. Müller-Buschbaum: Switching kinetics of PMDEGA based thermal-responsive hydrogel films probed by in-situ neutron reflectivity; *5th FRM-II Workshop on Neutron Scattering*, Burg Rothenfels (Germany), May 2011.

- Q. Zhong, J. Adelsberger, M. Niedermeier, A. Golosova, A. M. Bivigou-Koumba, A. Laschewsky, C. M. Papadakis, P. Bush, S. Botta, S. S. Funari, P. Müller-Buschbaum: The influence of different solvents on LCST of P(S-*b*-MDEGA-*b*-S) hydrogel films; *FRM II Usermeeting*, Garching (Germany), October 2010.

- Q. Zhong, G. Kaune, M. Rawolle, E. Metwalli, A. M. Bivigou-Koumba, A. Laschewsky, C. M. Papadakis, R. Cubitt, P. Müller-Buschbaum: Characterization of PMDEGA based hydrogel films; *DPG spring meeting*, Regensburg (Germany), March 2010.

- Q. Zhong, W. Wang, A. M. Bivigou-Koumba, A. Laschewsky, C. M. Papadakis, M. Haese-Seiller, R. Kampmann, P. Müller-Buschbaum: Characterization of PMDEGA based hydrogel film; *FRM II Usermeeting*, Garching (Germany), May 2009.

Acknowledgements

I would like to thank Prof. Dr. P. Müller-Buschbaum for giving me the opportunity to finish this thesis under his supervision, for introducing me into this interesting "intelligent hydrogels" project and for providing me invaluable assistance in my work. His scientific insight, advice and encouragement led me to the final success. I am grateful for the discussion with him on scientific and technical issues.

Deutsche Forschungsgemeinschaft (DFG) is gratefully acknowledged for funding the project "intelligent hydrogels" (SPP 1259), which is a cooperative work with Prof. Dr. C. M. Papadakis at Technische Universität München and Prof. Dr. A. Laschewsky at Universität Potsdam. I would like to thank Prof. Dr. C. M. Papadakis for the useful suggestions and discussion during my experiments and data analysis. I also thanks Prof. Dr. A. Laschewsky and A. M. Bivigou-Koumba for the novel thermo-responsive polymers used in my experiements.

The main results in this thesis are gathered from the large facilities in Hamburg and Grenoble, thus I would like to thank the excellent coworkers during the beamtimes: Dr. J. Adelsberger, Dr. A. Golosova, Dr. G. Kaune, Dr. V. Körstgens, Dr. E. Metwalli, Dr. M. Ruderer, Dr. W. Wang, D. Magerl, A. Nathan, M. Niedermeier, S. M. Prams, M. Rawolle, M. Schindler.

I appreciate the local support at the beamlines: Dr. S. Roth, Dr. J. Perlich (HASYLAB, BW4), Dr. R. Cubitt (ILL, D17) and S. S. Funari (HASYLAB A2). Without their preparation and support during the beamtime, the experiments can not be accomplished.

I am also grateful to the help from other chairs at Technische Universität München. Prof. Dr. P. Böni provides the use of X-ray reflectometer at the Lehrstuhl E21. Prof. Dr. T. Bach and Dr. C. Wiegand provide the use of ATR-FTIR spectroscopy at Lehrstuhl

für organische Chemie I.

Special thanks to Dr. W. Wang, who introduces me into the interesting topic of "intelligent hydrogels" at the beginning of my Ph.D thesis and the useful discussion in the scientific issues. I also would like to thank Dr. J. Adelsberger for his excellent experience in small angle scattering and help during the data analysis.

Moreover, I am very thankful to the people who read the manuscript and contributed to its improvement: Dr. E. Metwalli, Dr. V. Körstgens. Dr. M. Philipp, D. Magerl, M. Niedermeier, M. Rawolle, K. Sarkar, M. Schindler.

I also want to thanks the group members I do not mention so far: Dr. G. DePaoli, Dr. Z. Di, Dr. E. M. Herzig, Dr. T. Hoppe, Dr. A. Meier-Koll, Dr. N. Paul, Dr. A. Sepe, Dr. J. Zhang, A. Ammara, C. Birkenstock, P. Douglas, S. Ener, S. Fink, D. M. Gonzalez, S. Guo, M. He, S. Jaksch, D. Müller, A. Naumann, C. Palumbiny, C. Schaffer, B. Su, M. Waletzki, W. Wang, X. Xia, Y. Yuan. I enjoy the wonderful time in our group.

The biggest thank-you goes to my family, my father Xintian and my mother Bo. Thanks for your support to my scientific work in Germany.

Finally, I own individual gratitude to Xu. Thank you for your continuously support and patience when I study abroad.